

2	Getting started: The construction of the immersed annulus	16
3	Introducing braid foliations	21
3.1	Braid foliations of Seifert surfaces for knots	21
3.2	Recognizing destabilizations from the foliation	25
3.3	Recognizing exchange moves from the foliations	27
3.4	Control over the foliation	28
3.5	The 4 graphs	31
4	Braid foliations of the immersed annulus	32
4.1	Braid foliations of $\mathcal{A}_-, \mathcal{A}_+$ and \mathcal{TA}	32
4.2	Construction of the tabs	35
4.3	Microfypes and the foliation of $P(\mathcal{TA})$	37
4.4	The two finger moves	39
4.5	Creating symmetric normal neighborhoods of the clasp arcs	41
4.6	The complexity of the triple (X_-, X_+, \mathcal{TA})	47
4.7	Standardizing the foliation of \mathcal{TA} and $P(\mathcal{TA})$	47
5	Proof of the MTWS.	53
5.1	The role of flypes	54
5.1.1	Constructing the thinly foliated annuli	54
5.1.2	Pushing X_- across \mathcal{S}	58
5.2	The role of exchange moves and handle moves	67
5.3	The proof of parts (a), (b) and (c) of the MTWS	72
5.3.1	Proof of part (a):	73
5.3.2	Proof of part (b):	73
5.3.3	Proof of part (c)	75
5.4	The proof of part (d) of the MTWS.	75
5.4.1	Construction of the templates	75
5.4.2	Finiteness in the foliation of \mathcal{TA}	76
5.4.3	The boundary support $\hat{\mathcal{S}}$ of $X_- \sqcup X_+$, and the formation of moving blocks.	80
5.4.4	Proof of Lemma 5.5 (the Finiteness Lemma):	82
6	Applications to transverse knots	84

1 Introduction

1.1 The problem.

Let \mathcal{X} be an oriented link type in the oriented 3-sphere S^3 or $\mathbb{R}^3 = S^3 - \{\infty\}$. A representative $X \in \mathcal{X}$ is said to be a *closed braid* if there is an unknotted curve $\mathbf{A} \subset S^3 - X$ (the *axis*) and a choice of fibration \mathbf{H} of the open solid torus $S^3 - \mathbf{A}$ by meridian discs $\{H_\theta; \theta \in [0, 2\pi]\}$, such that whenever X meets a fiber H_θ the intersection is transverse. The fact that X is a closed braid with respect to \mathbf{H} implies that the number of points in $X \cap H_\theta$ is independent of θ . We call this number the *braid index* $b(X)$ of X . The braid index $b(\mathcal{X})$ of \mathcal{X} is the minimum value of $b(X)$ over all closed braid representatives $X \in \mathcal{X}$.

Closed braid representations of \mathcal{X} are not unique, and Markov's well-known theorem [3, 13, 24, 25, 32, 38] asserts that any two are related by a finite sequence of elementary moves. One of them is *braid isotopy*, by which we mean isotopy in the complement of the braid axis which preserves transversality between X and fibers of \mathbf{H} . The other two moves are mutually inverse, and are illustrated in Figure 1. Both take closed braids to closed braids. We call them *destabilization* and *stabilization*, where the former decreases braid index by one and the latter increases it by one. The 'weight' w denotes w parallel strands, relative to the given projection. The braid inside the box which is labeled P is an arbitrary $(w + 1)$ -braid. Later, it will be necessary to distinguish between positive and negative destabilizations, so we illustrate both now. The term 'template' will be explained shortly.

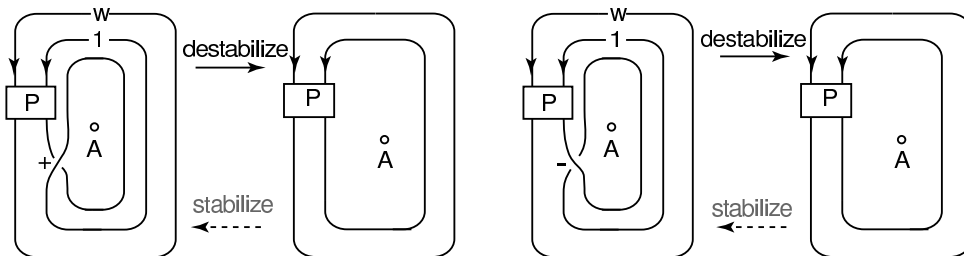


Figure 1: The two destabilization templates

Markov's Theorem: Let X_-, X_+ be closed braid representatives of the same oriented link type \mathcal{X} in oriented 3-space, with the same braid axis \mathbf{A} . Then X_+ may be obtained from X_- by braid isotopy and a finite number of stabilizations and destabilizations.

Markov's Theorem is typical of an entire class of theorems in topology where some form of stabilization and destabilization play a central role. Other examples are:

1. The Reidemeister-Singer Theorem [37] relates any two 2 Heegaard diagrams of the same 3-manifold, by a finite sequence of very simple elementary changes on Heegaard diagrams. The stabilization-destabilization move adds or deletes a pair of simple closed curves a, b in the defining Heegaard diagram, where $a \cap b = 1$ point and neither a nor b intersects any other curve a_i, b_j in the Heegaard diagram.
2. The 'Kirby Calculus' [22] gives a finite number of moves which, when applied repeatedly, suffice to change any surgery presentation of a given 3-manifold into any other, preserving at the same time the topological type of a 4-manifold which the given 3-manifold bounds. The stabilization-destabilization move is the addition-deletion of an unknotted component with framing zero to the defining framed link.

3. Reidemeister's Theorem (see [15]) relates any two diagrams of the same knot or link, by a finite sequence of elementary moves which are known as RI, RII and RIII. The stabilization-destabilization move is RI. It is easy to see that Markov's Theorem implies Reidemeister's Theorem.

These theorems are all like Markov's Theorem in the sense that while the stabilization and destabilization moves are very simple, nevertheless a sequence of these moves, combined with the appropriate isotopy, can have very non-trivial consequences. Here are other examples in which the stabilization move is not used, at the expense of restricting attention to a special example:

4. W. Haken proved that any Heegaard diagram for a non-prime 3-manifold is equivalent to a Heegaard diagram which is the union of two separate Heegaard diagrams, one for each summand, supported on disjoint subsets of the given Heegaard surface. See [36] for a very pleasant proof.
5. Waldhausen [39] proved that any two Heegaard diagrams of arbitrary but fixed genus g for the 3-sphere S^3 are equivalent.

In the course of an effort which we began in 1990 to discover the theorem which will be the main result of this paper (see Theorem 1 below) the authors made several related contributions to the theory of closed braid representatives of knots and links:

- 4'. In the manuscript [10] the authors proved that if X is a closed n -braid representative of a split or composite link, then up to braid isotopy and exchange moves (see Figure 2) X may be assumed to be a split or composite closed braid.

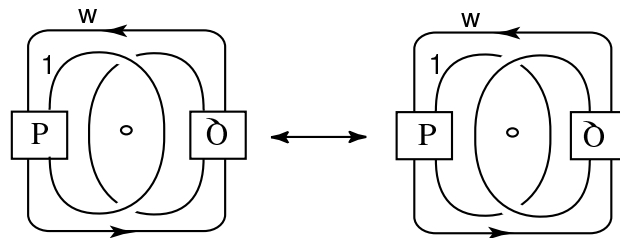


Figure 2: The exchange move template

- 5'. In the manuscript [11] the authors proved that if X is a closed braid representative of the μ -component unlink \mathcal{X} , then a finite sequence of braid isotopies, exchange moves and destabilizations can be found which change X to the identity braid in the braid group B_μ .
- 5''. In a recent manuscript [26] the second author proved that if X is a closed braid representative of an iterated torus link \mathcal{X} , then a finite sequence of braid isotopies, exchange moves and destabilizations suffice to change X to the unique minimum braid-strand representative of \mathcal{X} .
6. In the manuscript [9] the authors discovered that there is another move, the 3-braid flype (see Figure 3) with the property that if X is a closed 3-braid representative of a knot or link type \mathcal{X} which cannot be represented by a 1-braid or 2-braid, then either X has a unique conjugacy class or X has exactly two conjugacy classes, and these two classes are related by a 3-braid flype. They also showed that the exchange move is equivalent to braid isotopy for braid index 3.

The authors also established two fundamental facts which gave strong evidence that a more general result might be true:

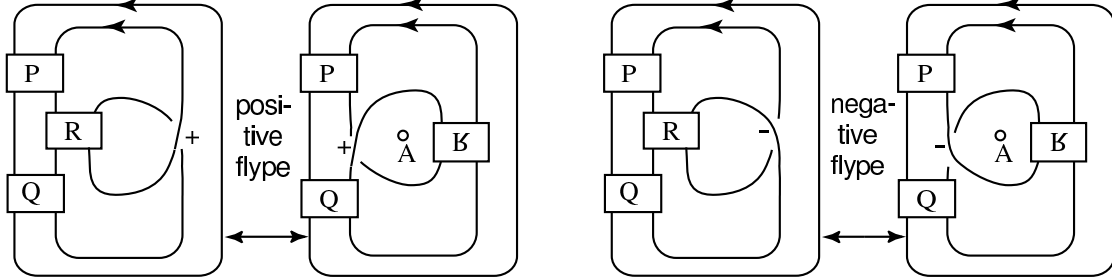


Figure 3: The two 3-braid flype templates

7. In [7] the authors introduced a complexity function on closed braid representatives of \mathcal{X} and proved that, up to braid isotopy, there are at most finitely many conjugacy classes of representatives of minimum complexity.
8. In [12] they proved that if a link type \mathcal{X} has infinitely many conjugacy classes of closed braid representatives of the same braid index, then all but finitely many of them are related by exchange moves.

The goal of this paper is to generalize examples (4'), (5'), (5'') and (6), taking into account (7) and (8), to arbitrary closed braid representatives of arbitrary oriented knots and links. We call our main theorem *Markov's Theorem Without Stabilization* (MTWS), because it is a direct modification of Markov's Theorem, but with his stabilization move replaced by other moves (a finite number for each braid index n representative of a link of braid index m) which allow one to jump from one isotopy class in the complement of \mathbf{A} to another, while keeping the braid index constant or decreasing it.

1.2 The moves

Before we can state our main result, we need to define the 'moves' we will use. Our moves will be described in terms of 'templates', or pairs of block-strand diagrams. Examples are the block-strand diagram pairs which make up the templates in Figures 1, 2 and 3. The 'fixed blocks' in these examples are P and Q . There is also an example of a 'moving block', i.e. the block R in Figure 3). Finally, we have the 'strands that join them' in all three figures. The reader may wish to look ahead to the boxed pairs of block-strand diagrams in Figure 9 for an example of a more complicated and less well-known template.

Definition 1 Block-strand diagram: A *block* B in $S^3 - \mathbf{A}$ is a 3-ball having the structure of $B^2 \times [0, 1]$ such that (i) for any fiber $H_\theta \in \mathbf{H}$ the intersection $H_\theta \cap B$ is either \emptyset or $B^2 \times \{s\}$ for some $s \in [0, 1]$, also and (ii) there exists some $\theta \in [0, 2\pi]$ such that $H_\theta \cap B = \emptyset$. A *block-strand diagram* is a collection $\mathcal{D} = B_1 \cup \dots \cup B_k \cup S_1 \cup \dots \cup S_l$ where $B_1 \cup \dots \cup B_k$ is a collection of pairwise disjoint blocks which are joined up by pairwise disjoint oriented strands $S_1 \cup \dots \cup S_l$ which are transverse to the fibers of \mathbf{H} . Each S_i is homeomorphic to a circle S^1 or interval $[0, 1]$. Also:

- For each block $B_j = B_j^2 \times [0, 1]$: if $S_i \cap B_j \neq \emptyset$, then $S_i \cap B_j = \partial S_i \cap (B_j^2 \times \{0, 1\})$
- For each block B_j there exists an integer m_j (the *braid index* of the block B_j) and a non-empty collection of $2m_j$ strands

$$\{S_{0,j,1}, \dots, S_{0,j,m_j}\}, \{S_{1,j,1}, \dots, S_{1,j,m_j}\} \subset \{S_1, \dots, S_l\}$$

such that $B_j \cap S_{0,j,p} \neq \emptyset$ for all p with $1 \leq p \leq m_j$ and $B_j \cap S_{1,j,q} \neq \emptyset$ for all q with $1 \leq q \leq m_j$.

□

Definition 2 Braiding assignment: A *braiding assignment* to a block-strand diagram \mathcal{D} is a choice of a braid on m_j strands for each $B_j \in \mathcal{D}$. That is, we replace B_j with the chosen braid, so that B_j with this braiding assignment becomes a braided tangle with m_j in-strands and m_j out-strands. In this way a block strand diagram gives us a closed braid representative of a link \mathcal{X} .

Let X be a closed m -braid. We say that X is *carried by* \mathcal{D} if there exists a braiding assignment for the blocks in \mathcal{D} such that the resulting closed braid is braid-isotopic to X . The *braid index* of \mathcal{D} is the maximum braid index of the closed braids carried by \mathcal{D} . \square

Definition 3 Template: A *template* T is a pair of block-strand diagrams $\mathcal{D}, \mathcal{D}'$, both with blocks B_1, \dots, B_k and an isotopy which takes the initial diagram to the final diagram, in such a way that

- for every fixed choice of braiding assignments to the blocks B_1, \dots, B_k the resulting closed braids X, X' represent the same oriented link type \mathcal{X} .

We call \mathcal{D} and \mathcal{D}' the *initial* and *final* block-strand diagrams in the pair. The *moving blocks* (resp. *fixed blocks*) in $\mathcal{T} = (\mathcal{D}, \mathcal{D}')$ are the blocks in \mathcal{D} which are inside (resp. outside) the support of the isotopy. \square

The concept of a block-strand diagram and of a template will be probably be both familiar and new to the reader. When we first began to understand that templates were the appropriate settings for our work on the MTWS we wondered whether our definition was so broad (because the diagrams in question support so many knot and link types) as to be content-free! In this regard, the following fact is fundamental:

Proposition 1.1 *Let \mathcal{D} be a block-strand diagram of braid index n . Assume that every block has braid index less than n . Then there exist n -braids that \mathcal{D} does not carry.*

Proof: Up to conjugation, a block-strand diagram may be described by a word W in the standard elementary braid generators $\sigma_1, \dots, \sigma_{n-1}$ of the n -strand braid group as follows:

$$W = B_1 S_1 B_2 S_2 \dots B_k S_k$$

where each S_i is a fixed braid word on n strands which describes the strands that connect the blocks and each B_j is an arbitrary word which describes the braid carried by the j^{th} block. By hypothesis no block has more than $n - 1$ strands entering or leaving it, so by modifying the S_i 's we may assume without loss of generality that each B_j is a braid on the first q_j -strands, where $q_j < n$. After this modification, the only places where the elementary braid generator σ_{n-1} appears is in the fixed braids S_1, \dots, S_k .

Now let $|S_i|$ be the number of times σ_{n-1} occurs in S_i . The $|S_i|$'s are fixed numbers since we were handed a given block-strand diagram. For an arbitrary conjugacy class $\{C\}$ of n -braids, let $|C|$ be the minimum number of times the generator σ_{n-1} is used, in all possible words which represent $\{C\}$. Our block diagram can only carry closed n -braids C such that (up to conjugacy) $|C| \leq |S_1| + |S_2| + \dots + |S_k|$. But there are closed n -braids X such that $|X|$ is arbitrarily large. \parallel

Our main theorem begins with an arbitrary closed n -braid representative X_- of an arbitrary oriented knot or link type \mathcal{X} in 3-space. Let X_+ be a second such representative, where X_+ has minimum braid index for all closed braid representative of \mathcal{X} . Our goal in this section is to describe some of the templates that we need, and at the same time to describe the building blocks of all of them. Note that we regard braid isotopy, i.e. isotopy in the complement of the braid axis or (equivalently) conjugacy in the braid groups, as a trivial move, sometimes even forgetting to mention it. By Theorem 1 of [29] braids β, β' in the n -string braid group B_n are conjugate if and only if the associated closed braids are isotopic in the complement of the braid axis.

1.2.1 Destabilization

Our two *destabilization* templates were defined in Figure 1. We distinguish the cases of positive and negative destabilization because the strands which join the fixed blocks are different, and so the templates are different. The MTWS does not use the stabilization move. The destabilization templates do not have any moving blocks.

1.2.2 Exchange moves

The *exchange move* was defined by the template in Figure 2. For $n \leq 3$ the exchange move is equivalent to braid isotopy [9], but for $n \geq 4$ and generic choices of the braids P and Q the exchange move cannot be realized by braid isotopy [17]. The exchange move template has two fixed blocks but, like the two destabilization templates, it has no moving blocks.

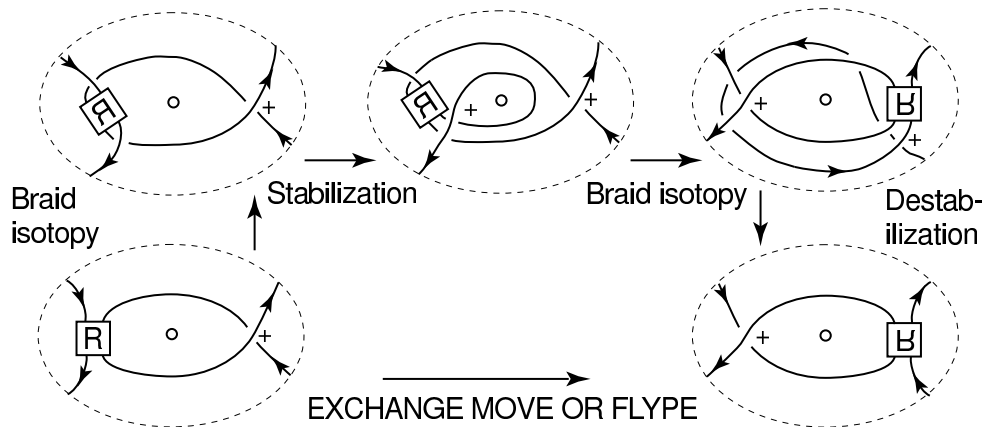


Figure 4: When R is a negative half-twist this 2-step Markov tower can be replaced by an exchange move. When R is an arbitrary braid the move is a positive flype.

By Markov’s Theorem, the left and right braids in the exchange move template of Figure 2 must be related by a sequence of Markov moves. Figure 4 shows such a sequence, in the case when the braid R is a single negative half-twist. The moves used in the sequence are a single stabilization, braid isotopy, and a single destabilization. Thus the exchange move arises in a very natural way in the study of stabilization in the braid groups: it replaces a sequence {stabilization-isotopy-destabilization} by a single braid-index preserving move, the exchange move.

Figure 5 shows how exchange moves, together with braid isotopy, can lead to infinitely many conjugacy classes of closed braid representatives of the same knot or link [11]. Indeed, in [12] the authors proved that if a link has infinitely many conjugacy classes of closed m -braid representatives for any fixed value of m then all but finitely many of them are related by exchange moves. This fact will shape the form of our main theorem. More precisely, our main theorem identifies the finitely many moves which are needed *in addition to* exchange moves, to take one closed n -braid representative of a knot to another of the same braid index.

1.2.3 G-handle moves

We begin with the concept of a handle move over a block-strand tree. Figure 6 shows how we unfold a piece of a closed braid to reveal that it has the structure of a ‘block and strand tree’, and then loop a distinguished subarc of the braid (always of weight 1) over the tree. (These concepts will be defined precisely in Section 5.2. we hope the reader will be patient. Our initial goal is to state our main result.) Notice that, while the unlooping process does not preserve closed braids, we have

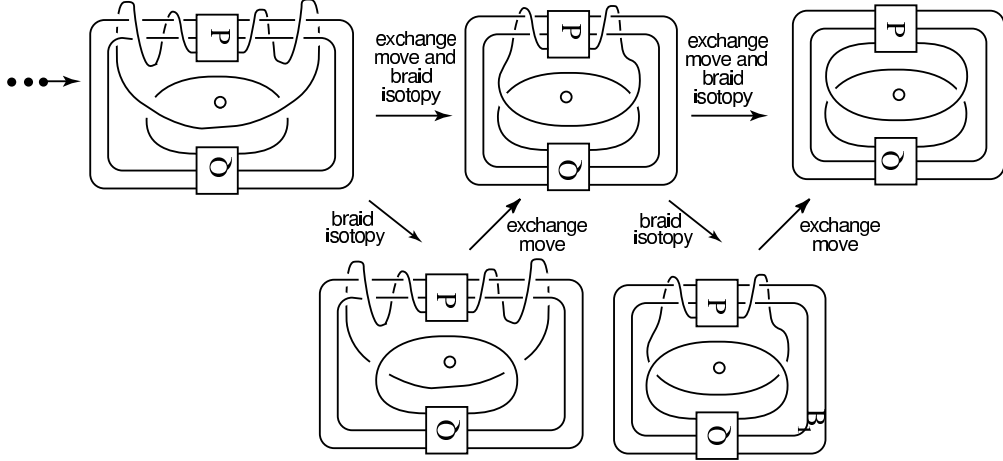


Figure 5: The exchange move can lead to arbitrarily many distinct braid isotopy classes of closed n -braid representatives of a single knot type, $n \geq 4$.

retained the closed braid structure by the device of cutting the braid axis into 4 little ‘axis pieces’. Of course the fibers of \mathcal{H} are arranged radially around these little axis pieces, in a sufficiently small neighborhood, so that when we open up the tree we can retain a local picture of the braid structure. During the looping motion the distinguished strand cuts each axis piece twice.

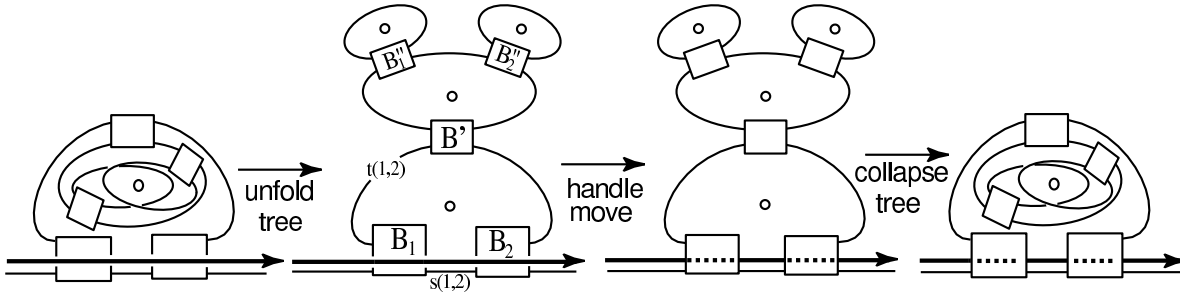


Figure 6: Handle moves over a rooted block-strand tree

The handle moves that we use are realizable as sequences of exchange moves, however that is no longer the case for G-handle moves, and the concept of a handle move over a rooted block and strand tree is needed in order to define G-handle moves. But there is another reason for introducing them: They are very natural, arising during the course of our proof. In the early studies of knot diagrams they were thought to be at the heart of the difficulty in simplifying knot diagrams.

Definition 4 (G-handle move): A G-handle move is an interrelated sequence of handle moves on k distinguished subarcs $\{\alpha_1, \dots, \alpha_k\}$ of the closed braid such that, for each $i \in \{1, \dots, k\}$ the handle move on each α_i cannot be completed before at least part of the handle move on some other α_j is started. \square

The boxed pair of block-strand diagrams in the bottom row of Figure 7 are an example of a template for a G-handle move on a 6-braid. There are 6 braid blocks: A, B, C, D, E, F . Running around the figure clockwise we show how a coordinated sequence of partial exchange moves, each of which can be completed as soon as enough of the other arcs are moved out of the way, achieves the same goal.

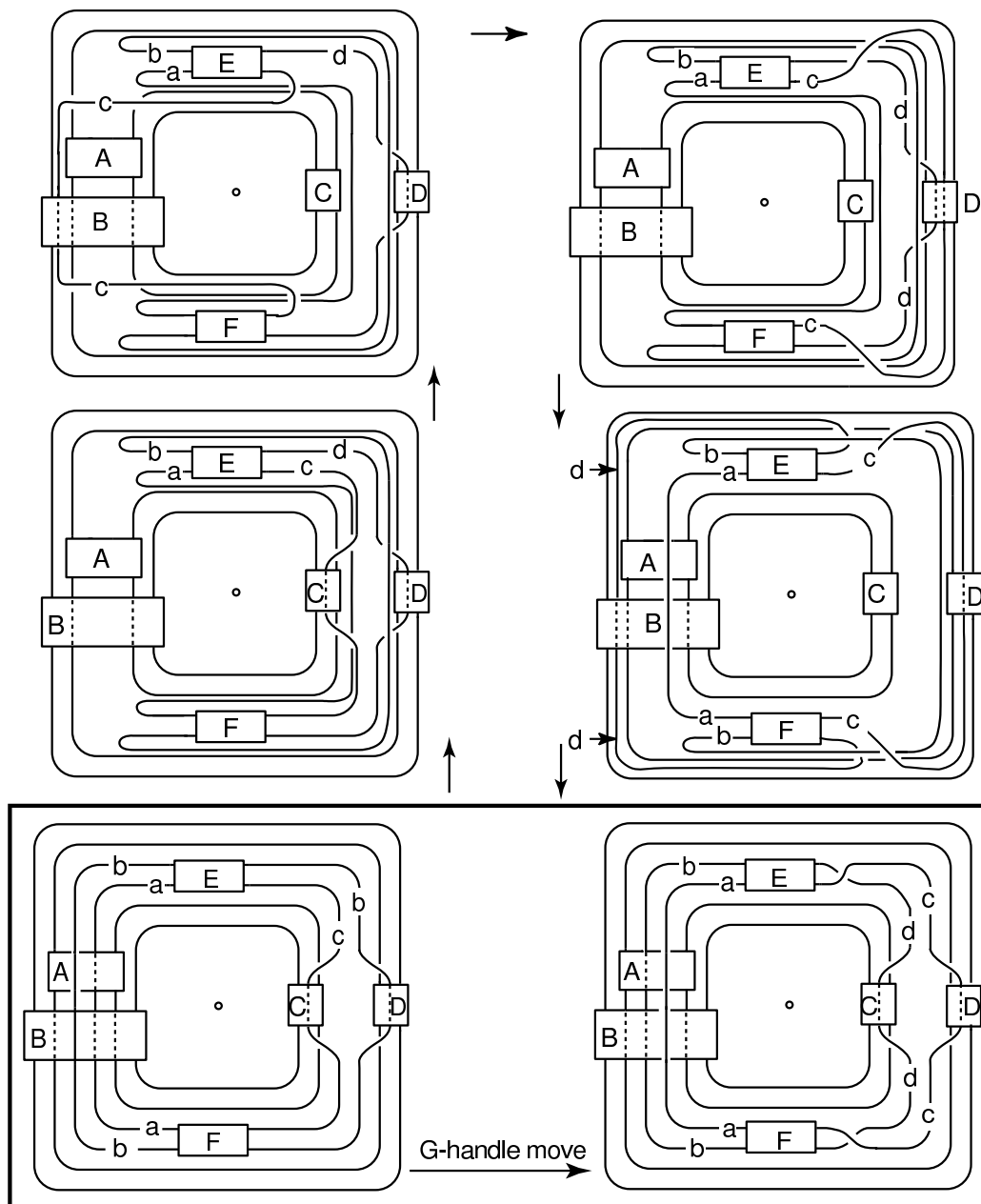


Figure 7: Example of a G-handle move on a 6-braid

In the first passage we have pushed strand a under the braid boxes A and B and across \mathbf{A} , to a position just to the right of braid box C . We have also lifted strand b above the braid boxes A and B and pulled it across \mathbf{A} to a position just to the left of braid box D . Then we begin our handle move on arc c . In the fourth sketch we complete it. In the fifth sketch we begin the handle move on arc d and complete the handle move on arc a . In the final sketch we complete the handle moves on arcs b and d .

Observe that, since exchange moves preserve link type and braid index, it follows that G-handle moves do too.

In the main theorem (Theorem 1) we will prove that for each fixed braid index there is a finite set of templates with the property that if (X_-, X_+) represent the same link and are related by a G-handle move, then there is a template in the set such that, for some braiding assignment to its blocks, the closed braids X_- and X_+ are carried by its initial and final diagrams. An example of a 6-braid template is the one which was given in Figure 7.

1.2.4 Flypes and admissible flypes

We already illustrated the two 3-braid flype templates in Figure 3. There is an obvious way to generalize it to any braid index n , namely declare the strands to be weighted strands. See Figure 8(a), which shows the support of the flype with weighted strands. From now on, the term *flype* will always have this meaning. The *sign* of a flype is the sign of the single crossing (possibly weighted) which is not in the braid box. Both positive and negative flypes are illustrated in Figure 3. They have distinct templates. There is a subtle point: Let X_- and X_+ be the closed braid before and

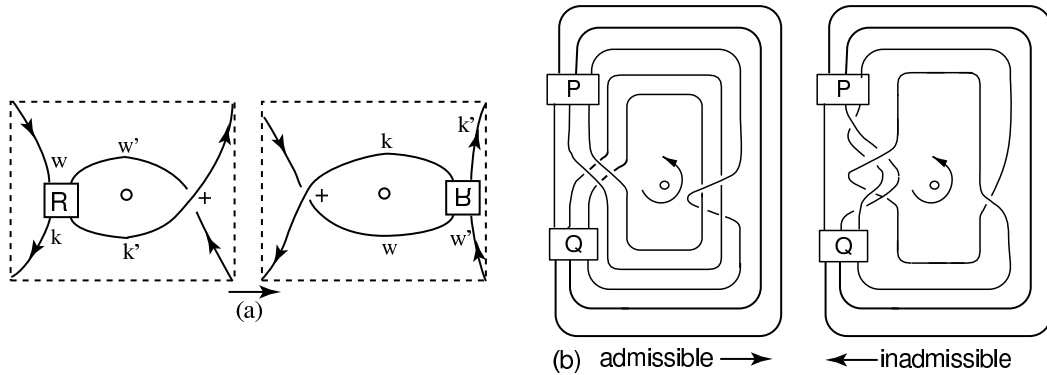


Figure 8: (a)The support of a positive flype with weighted strands. (b) Template for an admissible flype, and an inadmissible flype. Notice the extra twists introduced because of the weighted strands.

after a flype, which we shall consider (for the purpose of describing our moves) as acting left to right. It is supported in a 3-ball B^3 . Observe that the fiber H_θ at $\theta = \pi/2$ intersects $X_- \cap B^3$ in w' points, but intersects X_+ in k points. Observe that $w + w' = k + k'$. We have shown that:

$$(1) \quad b(X_-) - b(X_+) = w' - k = k' - w,$$

Thus flypes with weighted strands are non-increasing on braid index if and only if $w' - k = k' - w \geq 0$. We will refer to a flype which is non-increasing on braid index as an *admissible flype*.

1.2.5 G-flypes

As we noted above, there are flypes which are not admissible because they increase the braid index. Unfortunately, we need to use them too, and our way of handling this issue is to bundle inadmissible flypes into more complicated templates which are always non-increasing on braid index. We call

them, somewhat loosely, G-flypes. They are defined by templates. Each G-flype template will be seen to be built up from a sequence of templates which begins with an inadmissible flype. An example is the boxed pair of 6-braid block-strand diagrams at the bottom of Figure 9. As in the case of Figure 7 the sequence of 7 templates which it replaces can be understood by running around the diagram clockwise. As can be seen, the first step in that sequence is an inadmissible flype which increases the braid index by 1. The existence and finiteness of the set of G-flype templates, for each fixed braid index m , will be established as a major part of the MTWS.

1.3 Statement of results

We are finally ready to state our main result. The statement is fairly complicated because link theory is very complicated! Part (a) deals with the fact, proved in [12] and illustrated in Figure 5 that exchange moves are the unique move that create infinitely many distinct conjugacy classes of closed braid representatives of fixed braid index m of a knot or link. Part (b) (resp. part (c)) deals with the previously unknown role of G-handle moves (resp. G-flypes). Part (d) establishes the finiteness of the set $\mathcal{T}(m)$ of templates that define G-handle moves and G-flypes. The precise enumeration of the templates is a separate matter, outside the scope of this paper, however we have already given examples. These examples will be seen to arise in a natural way in the course of the proof.

Theorem 1 (Markov's Theorem Without Stabilization (MTWS)) *Consider the collection $B(\mathcal{X})$ of all isotopy classes of closed braid representatives of a given oriented link type \mathcal{X} in oriented S^3 . Among these, let $B_{\min}(\mathcal{X})$ be the collection of isotopy classes whose braid index is equal to the braid index of \mathcal{X} . Choose any $X_- \in B(\mathcal{X})$ and any $X_+ \in B_{\min}(\mathcal{X})$. Then additional structures and a complexity function are associated to the braid isotopy class of each $X \in B(\mathcal{X})$, and for each braid index m a set $\mathcal{T}(m)$ of templates is introduced, each determining a move which is non-increasing on braid index, such that the following holds:*

- (a) *There exist $X'_+ \in B_{\min}(\mathcal{X})$ and $X'_- \in B(\mathcal{X})$ and finite sequences of closed braids:*

$$X_+ = X_+^1 \rightarrow \cdots \rightarrow X_+^q = X'_+, \quad \text{and} \quad X_- = X_-^1 \rightarrow \cdots \rightarrow X_-^s = X'_-$$

such that up to braid isotopy each passage in both sequences is a strictly complexity reducing and braid-index preserving exchange move. The lengths q and s of these sequences are unbounded.

- (b) *There is a finite sequence of closed braids:*

$$X'_- = X^1 \rightarrow X^2 \rightarrow \cdots \rightarrow X^r = X'_+$$

with each $X^i \in B(\mathcal{X})$, such that up to braid isotopy each X^{i+1} is obtained from X^i by a single destabilization, G-handle move or flype. Each passage $X^i \rightarrow X^{i+1}$ is strictly complexity-reducing. If the passage $X^i \rightarrow X^{i+1}$ uses a G-handle move, then there is a template $\mathcal{T} \in \mathcal{T}(m)$, where $m = b(X^i) = b(X^{i+1})$, and braiding assignments to the blocks in \mathcal{T} such that the pair (X^i, X^{i+1}) is carried by \mathcal{T} .

- (c) *While the sequence of closed braids in (b) is complexity-reducing, it may use inadmissible flypes and so have steps when it is increasing on braid index. However, the sequence in (b) divides into two subsequences, both non-increasing on braid index, such that:*

- *The initial subsequence $i = 1, \dots, p$ uses only destabilizations, G-handle moves, and admissible flypes. It is therefore non-increasing on braid index.*
- *The entire final subsequence $i = p, \dots, r$ is replaced by the move $X^p \rightarrow X^r$. This move is defined by a single template $\mathcal{T} \in \mathcal{T}(m)$, where $m = b(X^p)$ and where there are braiding assignments to the blocks in \mathcal{T} such that the pair (X^p, X^r) is carried by the initial and final block strand diagrams in \mathcal{T} .*

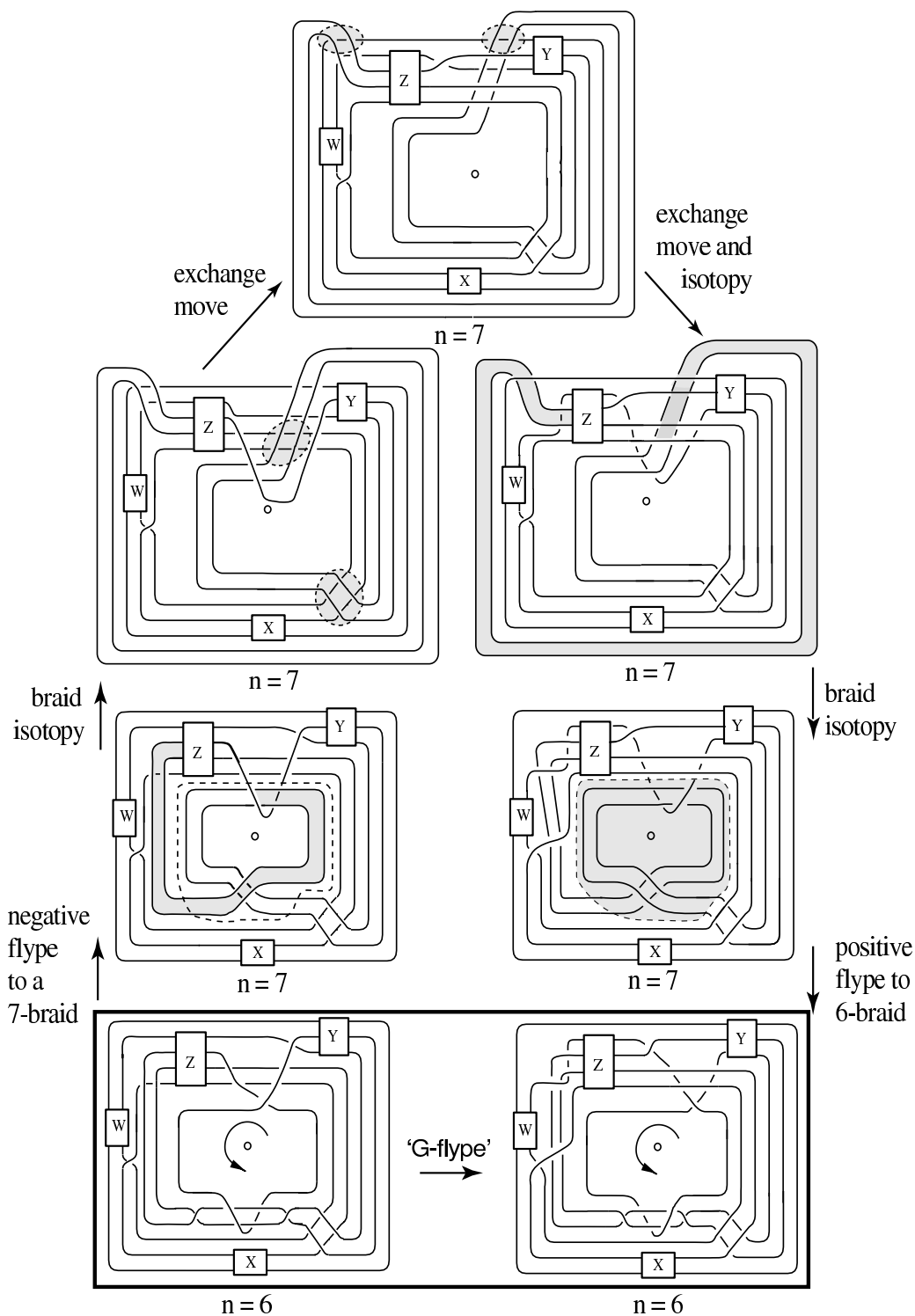


Figure 9: The sequence of flypes and exchange moves describe the isotopy between the two block-strand diagrams in the boxed 6-braid template

- (d) For each fixed m the set $\mathcal{T}(m)$ is finite. The cardinalities begin with $|\mathcal{T}(1)| = |\mathcal{T}(2)| = |\mathcal{T}(3)| = 0$. It is possible that $|\mathcal{T}(4)| = 0$ and $|\mathcal{T}(5)| = 0$. However, $|\mathcal{T}(m)|$ of $\mathcal{T}(m)$ is an increasing function of m for sufficiently high m .

The simplified version of the MTWS which is stated below is implicit in the MTWS. We state it because it may be helpful to the reader:

MTWS, simplified version: Choose any $X_- \in B(\mathcal{X})$ and any $X_+ \in B_{\min}(\mathcal{X})$. Then after an initial sequence of complexity reducing exchange moves which deal with the phenomenon exhibited in Figure 5 we may replace X_-, X_+ with X'_-, X'_+ and find a finite sequence of closed braids:

$$X'_- = X_1 \rightarrow X_2 \rightarrow \cdots \rightarrow X_{k-1} \rightarrow X_k = X'_+$$

such that:

- each passage $X_j \rightarrow X_{j+1}$ is complexity-reducing and non-increasing on braid index,
- X_{j+1} is obtained from X_j by a single destabilization, exchange move, admissible flype or one of the moves defined by a template \mathcal{T} in the finite set $\mathcal{T}(m)$, where $m = b(X_j)$.

There are braiding assignments to the blocks in \mathcal{T} such that the initial and final diagrams of \mathcal{T} carry the pair (X_j, X_{j+1}) . However, the template \mathcal{T} also carries infinitely many other knots and links, for other braiding assignments to its blocks.

The techniques which we introduce to prove the MTWS have consequences which relate to the classification of knots and links which are transversal to the standard tight contact structure on S^3 , up to transversal isotopy. At this writing exactly two invariants of a transversal knot type \mathcal{TK} are known: its topological knot type \mathcal{X} and a self-linking number which is known as the *Bennequin invariant*. For a closed braid representative TX of a transversal knot type \mathcal{TK} the Bennequin invariant may be computed as the difference $\beta(TX) = e(TX) - b(TX)$, where $e(TX)$ is the algebraic crossing number of the closed braid TX and $b(TX)$ is its braid index. In the manuscript [14] a transversal knot type \mathcal{TK} was defined to be *transversally simple* if it is determined, up to transversal isotopy, by its topological knot type and its Bennequin invariant. We address the question: are all knots transversally simple?

Theorem 2 *There exist infinitely many transversal knot types which are not transversally simple. As examples, consider the collection of infinitely many pairs of transversal knots $(\mathcal{TK}_-, \mathcal{TK}_+)$ defined by the pairs of transversal closed 3-braids*

$$TX_- = \sigma_1^{2p+1} \sigma_2^{2r} \sigma_1^{2q} \sigma_2^{-1}, \quad TX_+ = \sigma_1^{2p+1} \sigma_2^{-1} \sigma_1^{2q} \sigma_2^{2r},$$

where $q \neq r$ and $p, q, r > 1$. Then, the transversal knot types \mathcal{TK}_- and \mathcal{TK}_+ associated to each pair belong to the same topological knot type and have the same Bennequin number, but they do not represent the same transversal knot type.

Remark 1: The idea behind the proof of Theorem 2 is to adapt the proof of the MTWS to the transverse setting. We were not able to do that in any sort of generality. Instead, we were able to do it under the very special assumptions that TX_- and TX_+ are transverse closed 3-braids which represent the same transverse knot type, and that transverse knot type has braid index 3. Unfortunately, our proof of Theorem 2 depends upon the full strength of Theorem 1, plus our earlier work on the classification of links which are closed 3-braids in [9]. We wish it did not, because we appreciate that we are asking the reader who is interested primarily in contact structures to digest lots of topology in order to establish the *non-existence* of a transversal isotopy in a very special setting, however it's the best we could do!

We first encountered the examples which are given in Theorem 2 when we studied the problem of classifying knots which are closed 3-braids in the manuscript [9]. We conjectured (privately at that time) that they ought to be counterexamples to the guess that transversal knot types were classified by topological knot type and Thurston-Bennequin number, but we lacked the tools for a proof. We were also unable to find a computable invariant of transversal knot type which could distinguish transverse knots which were not simply the topological knot type and Thurston-Bennequin invariant in disguise.

Remark 2: The proof of the MTWS begins with a construction which is given in Section 2. We have used that construction in two ways: the first is to prove the MTWS in this paper, and the second is to give a new proof of the MT (see [13]). The latter may seem rather uninteresting, since as noted earlier many other proofs exist, however it was the basis for Nancy Wrinkle's thesis, in which she proved the 'Transverse Markov Theorem' (TMT), and that result is new. See [40]. Our earlier attempts to use braid foliation machinery as the basis for a proof of the TMT had failed.

Remark 3: With regard to the MTWS, the cardinality $|\mathcal{T}(m)|$ of $\mathcal{T}(m)$ is an increasing function of m . We do not have a precise description, even for $m = 4$, although that is probably more a matter of the need to stop and say what we know than any fundamental difficulty. For the special case $m = 6$ we have two examples, given in the boxed pairs of block-strand diagrams at the bottom of Figures 7 and 9. Other examples can be obtained from these by replacing the blocks in these templates by other templates and using weighted strands. In principle the techniques in this paper should allow us to say much more about the complications of transverse knot theory.

Conjecture 1 *There exist infinitely many topological knot types which have pairs of closed braid representatives, both of minimal braid index n , but having distinct algebraic crossing number. (Remark: it is an immediate consequence of the main theorem in [12] that for any given knot type at most finitely many distinct algebraic crossing numbers can occur.)*

Conjecture 2 *There exist examples of transversal knot types whose maximum Bennequin number is not realized by a minimum braid index representative of the associated topological knot type.*

Conjecture 3 *We conjecture (weakly) that if \mathcal{X} is a knot type for which the Morton-Franks Williams braid-index inequality fails ([31],[18],[21]), then \mathcal{X} has representatives of minimum braid index with distinct algebraic crossing number.*

We have candidates for Conjectures 1 and 2 above, but were unable to prove that our examples do what we think they do because we lack the needed tools for calculating minimum braid index. The only really effective tool that we know at this time is the Morton-Franks-Williams braid index inequality but unfortunately this inequality is always non-sharp on examples like the ones in the conjecture because it uses the Thurston-Bennequin number of a closed braid in an essential way.

1.4 Plan of the paper

Our proof of Theorem 1 begins in §2, where we set up the topological construction which will be the basis for our work. We will show that there is a very special isotopy that takes us from X_- to X_+ . The trace of the isotopy is an immersed annulus \mathcal{TA} which has a double point set which is the union of a finite number of disjoint clasp arcs. Let $P(\mathcal{TA})$ be the preimage of \mathcal{TA} under the immersion. Each clasp arc γ in \mathcal{TA} lifts to two arcs, γ_+ and γ_- , in $P(\mathcal{TA})$. The component γ_ϵ , where $\epsilon = \pm$, has one endpoint on X_ϵ and one endpoint in the interior of $P(\mathcal{TA})$.

The principle tool in our proof of Theorem 1 is the study of certain 'braid foliations' of \mathcal{TA} and $P(\mathcal{TA})$. Braid foliations were used by the authors in earlier work [7]-[12], but always in the setting

of embedded surfaces. In Section 3 we review the ideas that we need from the literature on braid foliations, and present one new idea which relates directly to immersed surfaces. Readers who are familiar with the literature will probably want to pass quickly over Section 3, referring to it instead, as needed, later in the proof.

We will need to do hard work in Section 4 to arrange things so that γ_+ and γ_- have nice neighborhoods (we call them ‘normal neighborhoods’) on $P(\mathcal{TA})$. Near the end of the section we introduce our complexity function, and develop properties of braid foliations which allow us to standardize the foliation outside the normal neighborhoods.

In Section 5 we get to the heart of the proof. We learn how to translate data in the braid foliation of \mathcal{TA} and the induced foliation of $P(\mathcal{TA})$ into data about the passage from the closed braid X_- to the closed braid X_+ ‘without stabilization’. The templates in $\mathcal{T}(m)$ will be seen to arise naturally, using data in the foliation of $P(\mathcal{TA})$ during the isotopy from X_- to X_+ . Understanding that, we will be able to complete the proof of Theorem 1.

In Section 6 we give the applications to transverse knots, proving Theorem 2.

1.5 Open questions

1. In principle the block diagram pairs in $\mathcal{T}(m)$ can be enumerated, but the actual enumeration is non-routine. We pose this as an open problem for $m = 4, 5$ and any other cases which prove to be computable. A weak conjecture is that for $m = 4$ the only templates that are needed are the destabilization, exchange move and admissible flype templates.
2. Classify links of braid index 4. As a starter, we conjecture that the algebraic crossing number (and so also the Thurston-Bennequin invariant) is a link type invariant for links of braid index 4.
3. An important open problem is to develop new techniques for computing the braid index of a knot or link. Even a collection of ad hoc techniques which are an advance over known methods would be useful.
4. Some knots or links, for example the unlink [11] and iterated torus links [26] have unique closed braid representatives of minimum braid index. On the other hand, there are links of braid index 3 (the ones that admit flypes, see [9]) which do not. We pose the open problem: find general conditions which suffice for a knot or link to have a *unique* closed braid representative of minimum braid index.
5. Use the work in this paper to generalize the results of [14] and [26], finding new classes of transversally simple knots. A deeper question is to investigate the relationship between the work in this paper and the classification of transversal knots.
6. In §1.1 we pointed out analogies between the study of knots via their closed braid representatives and the study of 3-manifolds via their Heegaard diagrams (or equivalently via their ‘Heegaard gluing maps’ in the mapping class group of a closed orientable surface of genus g). In the latter setting equivalence classes of Heegaard splittings are in 1-1 correspondence with double cosets in the mapping class group \mathcal{M}_g modulo the mapping class group \mathcal{H}_g of a handlebody. We pose as an open problem to find moves which (like the moves in $\mathcal{T}(m)$) change the equivalence class of a Heegaard splitting of a 3-manifold without changing its Heegaard genus. A strategy for finding such moves is given in [27], but (lacking an invariant) there is no proof that this strategy actually produces inequivalent splittings. In his PhD thesis [42] Joel Zablów made a relevant contribution in his study of waves in Heegaard diagrams. Is there a tool which plays the role of braid foliations in the situation of Heegaard splittings of 3-manifolds? This seems to be a very interesting area for future investigations.

Acknowledgements: This work has been in progress for many years, so long that it's even difficult for us to remember all the individuals who have made helpful remarks. With apologies for oversights, the first author would like to thank, in particular, Joseph Birman, Kenneth Birman and Oliver Dasbach for not letting her give up. Also, Walter Neumann, Brian Mangum, Joel Zablow, Nancy Wrinkle, Radu Popescu, Tara Brendle and all the other participants in a seminar during the spring of 2001, when she attempted to present the 'whole thing' and they made expert suggestions. Both authors wish to thank Viktor Ginzburg, whose attempts in the early 1990's to use braid foliation machinery to prove the Transverse Markov Theorem (TMT) introduced us to the very interesting work being done on knots in the standard contact structure on \mathbb{R}^3 . The second author wishes to thank Xingru Zhang for his comments on Proposition 1.1.

2 Getting started: The construction of the immersed annulus

In this section we give the basic construction which will allow us to prove Theorem 1. After that we will give a key example. Parts of the construction which will be given in this section were also given in [13] (which was written more or less simultaneously with this paper) where the same ideas were used to give a new proof of Markov's Theorem. They were also used by [40], who has proved a version of Markov's Theorem for transverse knot types.

Since the construction is a little bit tricky we will give it first for the special case when \mathcal{X} is a knot. We will consider how to modify it for the more general case, when \mathcal{X} is a link.

Lemma 2.1 *See Figure 10. Let X_-, X_+ be arbitrary closed braid representatives of the same knot type \mathcal{X} . Assume that X_- and X_+ are geometrically unlinked. Then there is an intermediate closed braid representative X_0 of \mathcal{X} such that the following hold:*

1. X_0 is the braid connected sum of X_- and k copies of closed braid representatives of the unknot.
2. X_- and X_0 cobound an embedded annulus $\mathcal{A}_- \subset \mathbb{R}^3$. (The annulus is the union of the k discs constructed in (1) above, joined up by very thin bands.)
3. X_0 bounds a Seifert surface \mathbf{F} and $X_+ \subset \mathbf{F}$ is a preferred longitude for X_0 . Therefore X_0 and X_+ cobound an embedded annulus $\mathcal{A}_+ \subset \mathbf{F}$.
4. The intersections $\mathcal{A}_- \cap \mathcal{A}_+$ are a finite set of clasp arcs.
5. The clasp arcs may also be assumed to be in braid position, i.e. transverse to the fibers of \mathbf{H} .

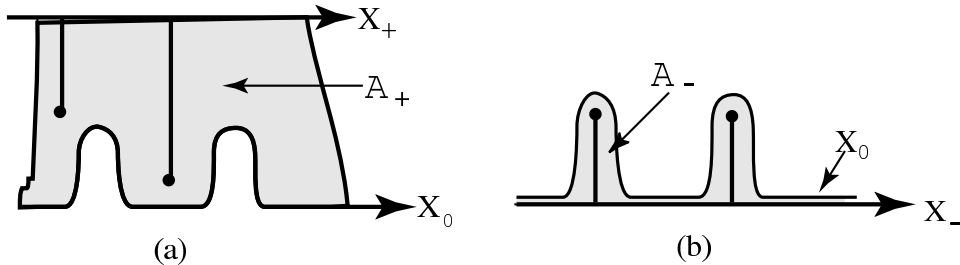
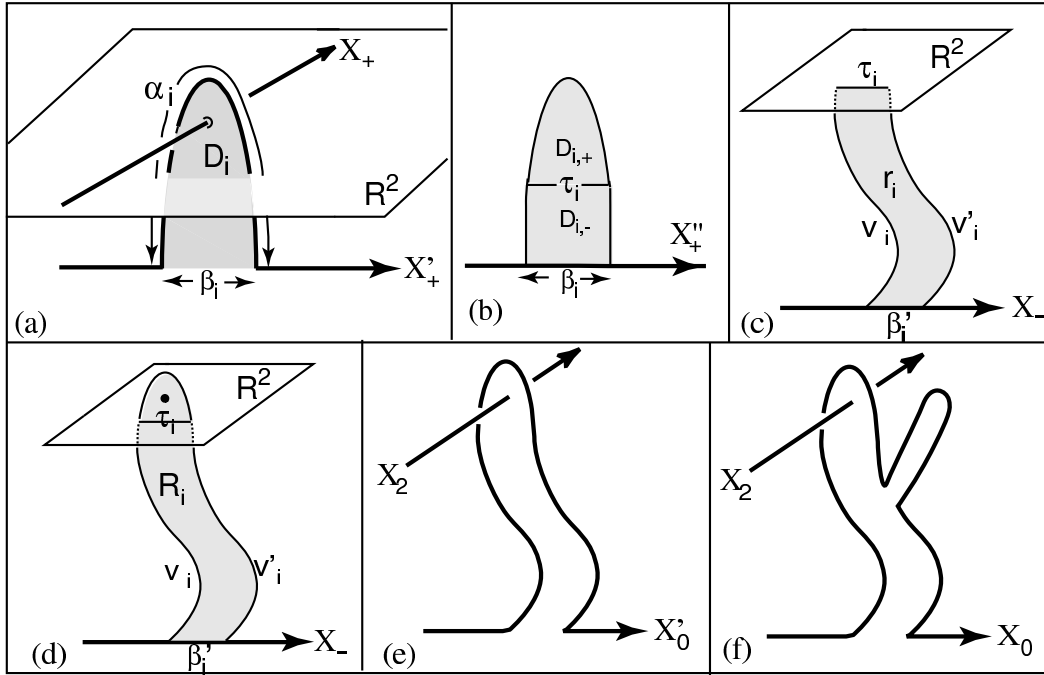


Figure 10: The annuli \mathcal{A}_- and \mathcal{A}_+

Proof: By hypothesis, we are given closed braids X_- and X_+ which represent the same oriented knot type \mathcal{X} in 3-space, and have the same braid axis \mathbf{A} . We may assume without loss of generality

that X_- and X_+ are situated in distinct half-spaces (so that they are geometrically unlinked), with X_+ far above X_- . Our first task is to construct a series of knots X'_+, X''_+, X'_0, X_0 , all representing \mathcal{X} , with X_0 the braid-connected sum of X_- and \mathcal{U}_k . In the construction we will first produce an intermediate representative X'_0 of \mathcal{X} which is the connected sum of X_- and the k -component unlink \mathcal{U}_k . The representatives of \mathcal{U}_k in this intermediate example will in general not be closed braids.

Choose a Seifert surface \mathbf{F}_+ for X_+ . Let $X'_+ \subset \mathbf{F}_+$ be a preferred longitude for X_+ , chosen to lie arbitrarily close to X_+ , in a collar neighborhood of X_+ on \mathbf{F}_+ , so that X'_+ is also a closed braid. The knots X_+ and X'_+ will have algebraic linking number 0, but in $X_+ \cup X'_+$ will not be a split link unless \mathcal{X} is the unknot. Therefore, if we try to push X'_+ below \mathbb{R}^2 it will get stuck, i.e. there will be little hooks where it is forced to cross over X_+ , as in Figure 11(a). Our first change is to modify X'_+ (holding X_+ fixed) to a closed braid which has the same knot type as X'_+ but is geometrically unlinked from X_+ . To do this, choose disjoint discs D_1, \dots, D_k , as in Figure 11(a), such that $X'_+ \cap \partial D_i$ is an arc $\alpha_i \subset \partial D_i$, and such that a push of α_i across D_i to $\beta_i = \partial D_i \setminus \alpha_i$ for each $i = 1, \dots, k$ unlinks X'_+ from X_+ , as in Figure 11(b). Let X''_+ be the knot which is obtained from X'_+ by this ‘unlinking’. By modifying the subarcs β_i of X''_+ a little bit, if necessary, we may assume that β_i is transverse to every fiber H_θ of \mathcal{H} , so that X_+, X'_+ and X''_+ are all closed braids. It will


 Figure 11: Constructing X_0

be convenient to assume that X_+ (resp. X''_+ and X_-) lie in the half-spaces \mathbb{R}^3_+ (resp. \mathbb{R}^3_-), where the two half-spaces are separated by a plane we refer to as \mathbb{R}^2 , also that X'_+ lies in \mathbb{R}^3_- everywhere except for the k hooks where it passes up and over X_+ , intersecting \mathbb{R}^2 twice. See Figure 11(a). Passing to Figure 11(b) we think of each disc D_i , $i = 1, \dots, k$ as a tall thin semi-circular disc which is divided by \mathbb{R}^2 into a semi-circular disc $D_{i,+} \subset \mathbb{R}^3_+$ and a rectangular disc $D_{i,-} \subset \mathbb{R}^3_-$, chosen so that $D_{i,-} \cap X''_+ = \beta_i$, where β_i is the lower edge of the rectangle $D_{i,-}$. Let $\tau_i = D_{i,+} \cap D_{i,-} \subset \mathbb{R}^2$ be the upper edge of the rectangular disc $D_{i,-}$.

Noting that X''_+ and X_- both represent \mathcal{X} , and that both are in \mathbb{R}^3_- , we may find a homeomorphism $g : \mathbb{R}^3_- \rightarrow \mathbb{R}^3_-$ which is the identity on \mathbb{R}^2 with $g(X''_+) = X_-$. Extend g by the identity on

\mathbb{R}_+^3 to a homeomorphism $G : \mathbb{R}^3 \rightarrow \mathbb{R}^3$. Let $r_i = G(D_{i,-})$ and let

$$R_i = G(D_i) = G(D_{i,+} \cup D_{i,-}) = r_i \cup D_{i,+}.$$

Thus $r_i = R_i \cap \mathbb{R}_+^3$. See Figures 11(c) and (d). The facts that (i) G is a homeomorphism which is the identity in \mathbb{R}_+^3 and (ii) if $i \neq j$ then $D_{i,-} \cap D_{j,-} = D_i \cap D_j = \emptyset$ tell us that the r_i 's and the R_i 's are pairwise disjoint embedded discs. By construction $r_i \cap X_+ = \emptyset$, whereas $R_i \cap X_+$ is a single point in the disc $D_{i,+}$, for each $i = 1, \dots, k$. Each r_i joins X_+'' to X_- , meeting X_+'' in the arc β_i and X_- in the arc $\beta_i' = G(\beta_i)$. Each R_i joins X_+ to X_- , meeting X_+ in α_i and X_- in β_i' . The disc r_i has as its boundary the arc $\tau_i \subset \mathbb{R}^2$, the arc $\beta_i' \subset X_-$ and two 'vertical' arcs which we have labeled v_i and v_i' . We will study them later.

Let X_0' be the knot which is obtained from X_- by replacing each $\beta_i' \subset X_-$ by $\partial R_i - \beta_i'$. Then X_0' is constructed from X_- by attaching k pairwise disjoint long thin hooks to X_- . See Figure 11(e). There are two important aspects of our construction:

1. $X_+ \cup X_0'$ has the same link type as $X_+ \cup X_+$. For, by construction, the homeomorphism $G^{-1} : \mathbb{R}^3 \rightarrow \mathbb{R}^3$, being the identity on \mathbb{R}_+^3 , sends $X_+ \cup X_0'$ to $X_+ \cup X_+$.
2. X_0' is the connected sum of X_- and k copies of the unknot, the i^{th} copy being ∂R_i .

Now come several important observations, which we highlight with bullets:

- Since X_+ is a preferred longitude for X_+ , and since $X_+ \cup X_0'$ has the same link type as $X_+ \cup X_+$, it follows that X_0' is also a preferred longitude for X_+ .
- Changing our point of view, we note that X_+ is a preferred longitude for X_0' . We find a Seifert surface \mathbf{F} for X_0' . Holding X_0' and X_+ fixed, we may then isotope the interior of \mathbf{F} until X_+ lies on \mathbf{F} . Let $\mathcal{A}_+ \subset \mathbf{F}$ be the annulus in \mathbf{F} which X_0' and X_+ bound. This annulus is embedded because \mathbf{F} is embedded.
- It may happen that X_0' is a closed braid. This will be the case if the two vertical arcs $v_i \cup v_i' = \partial r_i \setminus \beta_i \cup \beta_i'$ are in braid position, that is are transverse to all fibers of \mathbf{H} , for each $i = 1, \dots, k$. Assume this to be the case, for the moment.
- Let \mathcal{A}_- be the annulus which is obtained from the discs R_1, \dots, R_k by joining them up by in a cycle by bands which are very close to X_- , as in Figure 10 to give an annulus \mathcal{A}_- which has X_- as one of its boundary components. Let $-X_0$ be its other boundary component. The annulus \mathcal{A}_- is embedded because the R_i 's are disjointly embedded.
- We examine the intersections between \mathcal{A}_- and \mathcal{A}_+ . The only part of the construction which we could not control was the construction of $\mathcal{A}_+ \subset \mathbf{F}$. Given two oriented 2-manifolds in an oriented 3-manifold, Sard's theorem [19] tells us we may choose ϵ -close embeddings such that the 2-manifolds intersect transversally. The transversality theorem for compact oriented 2-manifolds with boundary then tells us that each component of the intersection is a compact 1-manifold, i.e. an arc or a simple closed curve. It follows that the intersections are clasps, ribbons and simple closed curves. By our method for constructing the annuli it is clear that an isotopy of \mathcal{A}_- suffices to remove all simple closed curves. As for the ribbon intersections, we can get rid of them by pushing them across the X_+ boundary of \mathcal{A}_+ into $\mathbf{F} \setminus \mathcal{A}_+$. Since $\mathcal{A}_+ \subset \mathbf{F}$, this suffices to eliminate all ribbon intersections between \mathcal{A}_- and \mathcal{A}_+ . By construction, there are exactly k clasp arcs which arise because of the fact that X_+ pierces \mathcal{A}_- once in each disc D_i . There are no other clasp intersections because by construction $X_+ \subset \mathbb{R}_+^3$ and we were very careful to be sure that the construction of \mathcal{A}_- , which took place entirely in \mathbb{R}_-^3 , did not create new intersections. We have proved Lemma 2.1, under the

assumption that the ‘vertical boundaries’ v_i and v'_i of each ribbon r_i are transverse to the fibers of \mathbf{H} .

We next consider the issue: what happens when X'_0 is not a closed braid? Using cylindrical coordinates (ρ, θ, z) in $\mathbb{R}^3 \subset S^3$ a parametrized arc $(\rho(t), \theta(t), z(t))$, $t \in [0, 1]$ is *in braid position* when $d\theta/dt > 0$ for every $t \in [0, 1]$. Call a subarc δ of a knot X *wrongly ordered* if, instead, $d\theta/dt \leq 0$ on δ . Reviewing the construction, we see that the only subarcs of X'_0 which might fail to be transverse to fibers of \mathbf{H} are the parts of the vertical boundaries of the k ribbons r_1, \dots, r_k which are in \mathbb{R}^3_- , since every other subarc is either on X''_+ or on X_- , and both of those are closed braids.

In [1] J.W. Alexander introduced a very simple way to change an arc δ which is not in braid position to one that is. See Figure 12. One finds a disc Δ in 3-space with the properties: (i) $\partial\Delta \cap X = \delta$, also (ii) $\text{int}(\delta) \cap X = \emptyset$, also (iii) if A is the z -axis, then $A \cap \Delta = \{p\}$, a single point in the interior of Δ . Push the interior of δ across Δ to $\delta' = \partial\Delta \setminus \delta$. This changes δ to a transverse arc. Alexander showed that whenever a knot X is not transverse to the fibers of \mathbf{H} it can be divided into small segments which can then be pushed across appropriate Δ -discs, one at a time, to change X to a closed braid. (Remark: in our sketch the Δ -disc looks horizontal, but in general the point where \mathbf{A}

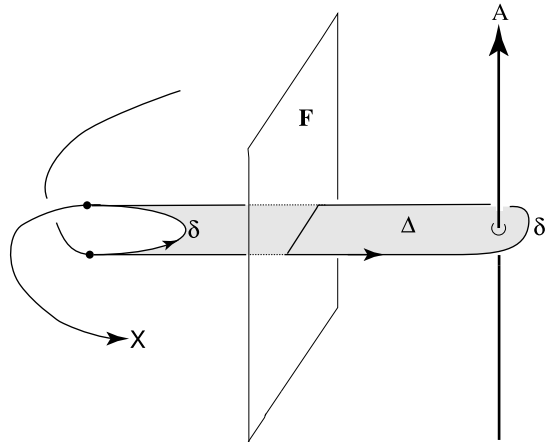


Figure 12: Alexander’s method for modifying arcs to braid position

pierces Δ is arbitrarily far above or below δ .) We assume that we have changed all wrongly ordered subarcs of the union of the vertical arcs in the boundaries of the ribbons $r_1 \cup \dots \cup r_k$ to subarcs that are everywhere transverse to the fibers of \mathbf{H} . We remark that Alexander’s construction is sufficiently loose so that there is no difficulty in assuming that the closed Δ -discs which are used are disjoint from X_+ . Let X_0 be the closed braid which is obtained from X'_0 by Alexander’s isotopy. Assume that the ribbons r_i have also been modified by the addition of the Δ -discs. By an abuse of notation, we continue to use the notation R_1, \dots, R_k for the modified extended ribbons, as illustrated in the passage from Figure 11(d) to (e). They will reappear later in our work in Section 4.

To complete the proof of (1)-(4) of Lemma 2.1 we now need to review all the places in our construction where intersections might be introduced between the modified annulus \mathcal{A}_- and the annulus \mathcal{A}_+ . The only place where we might pick up new intersections are if the Δ -discs happen to intersect the interior of \mathbf{F} . Since $\mathcal{A}_+ \subset \mathbf{F}$, this could introduce ribbon intersections between \mathcal{A}_- and \mathcal{A}_+ . However, we may push all such ribbon intersections across X_+ , off the annulus \mathcal{A}_+ and into $\mathbf{F} \setminus \mathcal{A}_+$, as before, and we now assume that we have done so. This proves statement (4).

It remains to prove statement (5). Let \mathcal{TA} be the *total annulus* $\mathcal{A}_- \cup \mathcal{A}_+$. Let $\Gamma = \gamma_1 \cup \dots \cup \gamma_k$ be the union of the clasp arcs. Then the graph $X_- \cup X_0 \cup X_+ \cup \Gamma$ is embedded in the immersed annulus, which is a subset of \mathbb{R}^3 . We focus now on that graph. By our earlier construction, its subsets X_-, X_0 and X_+ are in braid position, but in general Γ is not in braid position. As in our proof of

(1), we apply Alexander's construction to every wrongly ordered subarc of Γ , doing it so as to avoid intersections with X_- , X_0 and X_+ . The construction allows us to find an orientation-preserving PL homeomorphism $g : S^3 \rightarrow S^3$ which changes Γ to braid position. A classical result of Gugenheim (Theorem 1.5 in [20]) then tells us that we may assume that g is isotopic to the identity. Replacing \mathcal{TA} by $g(\mathcal{TA})$, and using the fact that g leaves X_- , X_0 and X_+ invariant, it follows that we may assume that every subarc of the graph $X_- \cup X_0 \cup X_+ \cup \Gamma \subset \mathcal{TA}$ is in braid position. This completes the proof of Lemma 2.1. \parallel

Proposition 2.1 *A generalization of Lemma 2.1 holds when \mathcal{X} is a μ -component link. In particular, a μ -component link X_0 exists as in Lemma 2.1 and:*

1. *Each component of X_0 is the braid connected sum of X_- and some number of copies of closed braid representatives of the unknot.*
2. *Each component of X_- cobounds with the corresponding component of X_0 an annulus $\mathcal{A}_{-,i}$. The union of these annuli forms an embedded surface $\mathcal{A}_{-,1} \cup \cdots \cup \mathcal{A}_{-,\mu}$.*
3. *The link X_0 bounds an incompressible Seifert surface \mathbf{F} and $X_+ \subset \mathbf{F}$ is a preferred longitude for X_0 . Therefore the subsurface $\mathcal{A}_{+,1} \cup \cdots \cup \mathcal{A}_{+,\mu} \subset \mathbf{F}$ is embedded.*
4. *The intersections $\mathcal{A}_{-,i} \cap \mathcal{A}_{+,j}$ will be a finite collection collection of clasp arcs. The clasp arcs may be assumed to be in braid position.*

Proof: We leave it to the reader to check, step by step, that the basic construction is unchanged. The main new feature is that when we use Alexander's theorem to put the vertical arcs v_i, v'_i into braid position we may introduce intersections between annuli $\mathcal{A}_{-,i}$ and $\mathcal{A}_{+,j}$ associated to distinct components X_i, X_j of \mathcal{X} . \parallel

A key example: The reader is referred to Figure 13. It is a key example, and we will study it in full detail during the course of this manuscript. For present purposes we explain only those features which can be understood now.

In our example \mathcal{X} is a knot and the *total annulus* $\mathcal{TA} = \mathcal{A}_- \cup \mathcal{A}_+$ is a union of two discs which are identified along bands which join the arcs ab and $a'b'$, and also cd and $c'd'$. Thus we initially view \mathcal{TA} via its preimage under the immersion. The black (resp. grey) boundary is X_- (resp. X_+). There is one clasp arc whose two preimages γ_+ and γ_- are shown. The clasp arc γ_ϵ , where $\epsilon = \pm$, has one endpoint on X_ϵ and the other in the interior of the annulus, at the point where $X_{-\epsilon}$ pierces the annulus. We claim that this annulus actually occurs in the passage from the left closed 3-braid in Figure 3 to the right closed 3-braid, in the special case when

$$X_- = \sigma_1^p \sigma_2^{-2} \sigma_1^q \sigma_2^{-1}, \quad X_+ = \sigma_1^p \sigma_2^{-1} \sigma_1^q \sigma_2^{-2}$$

with p and q integers, also $p + q$ odd (so that we get a knot) and absolute value at least 3 (so that, by the work in [9], we know that the flype cannot be replaced by braid isotopy). Notice that in the passage from the left to the right sketch in Figure 3 the isotopy is supported in a 3-ball B^3 whose boundary intersects X_- in 4 points. These are the endpoints of the 2 subarcs of X_- in the bottom middle sketch in Figure 13. The 3-ball B^3 contains in its interior the braid box R (which is our case is a single negative full twist), a little subarc of the braid axis and the single crossing to its right (which in our case is also negative). The signs correspond to the fact that the exponents of σ_2 in the braids which represent X_- and X_+ are both negative. The two long thin bands (which are not illustrated) run along the part of the braid which is outside B^3 . They depend, of course, on the choices of p and q .

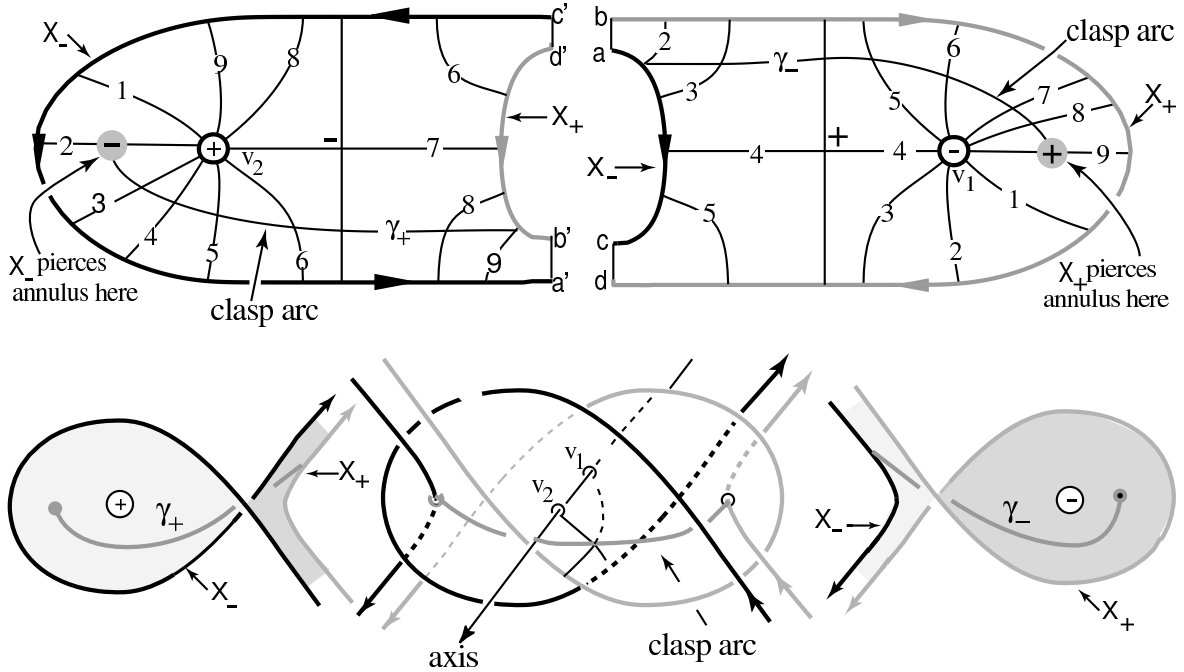


Figure 13: A key example

To visualize the embedding of the annulus in 3-space, first give each of the discs in the top row a half-twist, as in the leftmost and rightmost bottom sketches. Then identify the two half-twisted discs along the clasp arc, as shown in the middle bottom sketch. The passage from X_- (the black boundary) to X_+ (the grey boundary) is realized by a push of X_- across the immersed annulus to X_+ . While the annulus is immersed, there are no self-intersections of the boundary braid as it is pushed across the annulus.

3 Introducing braid foliations

Theorem 1 is about the relationship between two closed braid diagrams which represent the same link. However the work which we do to prove it will not be in the setting of knot diagrams. Rather, we will be working with the immersed annulus \mathcal{TA} , and with certain *braid foliations* of this annulus. Foliated surfaces have been used before, in our earlier papers [7]-[12]. In this section we will review and describe the machinery which we use from these other papers. The reader who has seen these foliations before will be able to omit this section and go directly to Section 4, possibly pausing every now and then to go to this review to refresh his/her memory of details. A more detailed review may be found in the review article [4].

3.1 Braid foliations of Seifert surfaces for knots

We are given a representative X of an oriented link type \mathcal{X} , where X is a closed n -braid with braid axis \mathbf{A} . Let $\mathbf{H} = \{H_\theta; 0 \leq \theta \leq 2\pi\}$ be a choice of disc fibers of the braid axis complement, where H_θ denotes a fiber of \mathbf{H} . The braid axis and the fibers of \mathbf{H} will be seen to serve the role of a coordinate system in 3-space. We will use it to describe the link (and an auxiliary surface which it bounds) via a set of combinatorial data. The fact that X is a closed braid with respect to \mathbf{H} implies that

it intersects each fiber H_θ of \mathbf{H} transversally in exactly n points. The closed braid X is oriented so that it is pointing in the direction of increasing θ at each point of $X \cap H_\theta$.

In order to make this review as simple as possible, we assume that X is a knot, and that it's the boundary of a Seifert surface \mathbf{F} of maximum Euler characteristic. Since X is a closed braid, we know that $\mathbf{A} \cap \mathbf{F}$ is non-empty. After modifying \mathbf{F} we may assume that it admits a special type of singular foliation which was studied and used by the authors in [7]-[12]. The foliation is radial in a neighborhood of each point of $\mathbf{A} \cap \mathbf{F}$ (see Figure 14(a)) and transverse to the boundary in a neighborhood of $\partial\mathbf{F}$ (Figure 14(b)). Notice that in Figure 14 the surface \mathbf{F} is naturally oriented

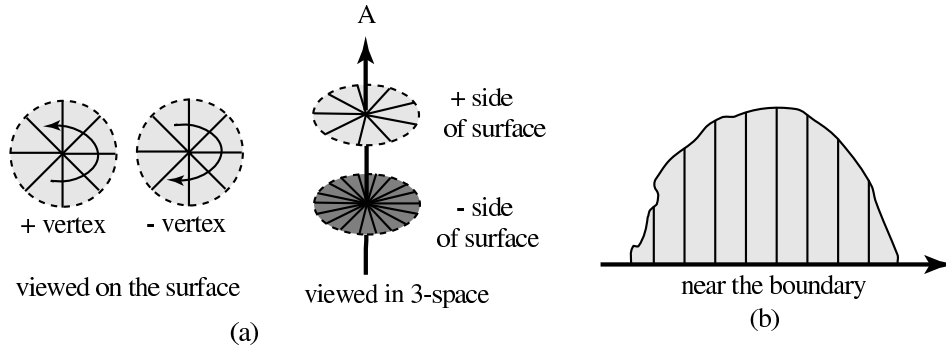


Figure 14: (a)Foliation of surface near a vertex; (b) Foliation of surface near the boundary

by the orientation on X , which is chosen so that the polar angle θ is strictly increasing as we walk along X . A *vertex* in the foliation is a point in $\mathbf{A} \cap \mathbf{F}$. The braid axis \mathbf{A} pierces \mathbf{F} from either the negative or the positive side at each pierce point, and we have indicated this by attaching positive or negative signs to the pierce points on \mathbf{F} . A *leaf* in the foliation is a component of intersection of H_θ with the surface \mathbf{F} . Leaves are *singular* if they contain a singularity of the foliation, otherwise they are *non-singular*. The singularities may be assumed to be finite in number and to occur on distinct fibers of \mathbf{H} . By Morse's classification theorem every singularity may be assumed to result from a local maximum or minimum or a saddle point tangency between \mathbf{F} and a fiber of \mathbf{H} . Non-singular leaves of the foliation, being 1-manifolds, are either arcs or simple closed curves.

A very basic assumption about the leaves of our braid foliations of Seifert surfaces is that they may always be assumed to be arcs. We review the reasons (which go back to [2]). Suppose that there is a scc $\alpha(\theta)$ in $\mathbf{F} \cap H_\theta$ for some non-singular polar angle θ . The fact that \mathbf{F} is pierced non-trivially by the braid axis, and that the foliation is transverse to the boundary, shows that \mathbf{F} cannot be foliated entirely by simple closed curves, so if we follow the sequence of arcs $\alpha(\theta)$ as θ increases or decreases we must arrive at a singularity. Let H_{θ_0} be the singular fiber. The singularity may be assumed to be either be a center or a saddle point, but if it is a center, then by following $\alpha(\theta)$ in the opposite direction we will arrive at another singularity, and that one cannot also be a center because \mathbf{F} is not a 2-sphere, so it must be a saddle point, and the singularity must be a homoclinic point (a singularity which is formed when a generic leaf has a saddle point singularity with itself), as illustrated in Figure 15(a). Note that the singular leaf $\alpha(\theta_0)$ lies in both \mathbf{F} and H_{θ_0} , and necessarily bounds a disc Δ in the latter, we surger \mathbf{F} along Δ .

Now observe that the surgered surface has two components. By assumption \mathbf{F} is incompressible, which implies that one of the two components is a 2-sphere. Discarding it, and smoothing the new \mathbf{F} , we can eliminate the singularity.

It remains to consider the case when the interior of the disc Δ intersects \mathbf{F} . Since s_0 is the only singularity in H_θ , there are no singularities in the interior of Δ . But then each component of $\mathbf{F} \cap \text{int}(\Delta) \subset H_\theta$ must be a scc. Let c be an innermost such scc. Then we can surger \mathbf{F} along c , and then smooth the surgered surface by an isotopy. (We leave it to the reader to draw appropriate pictures). After a finite number of such surgeries we obtain a new surface \mathbf{F}' which has the same

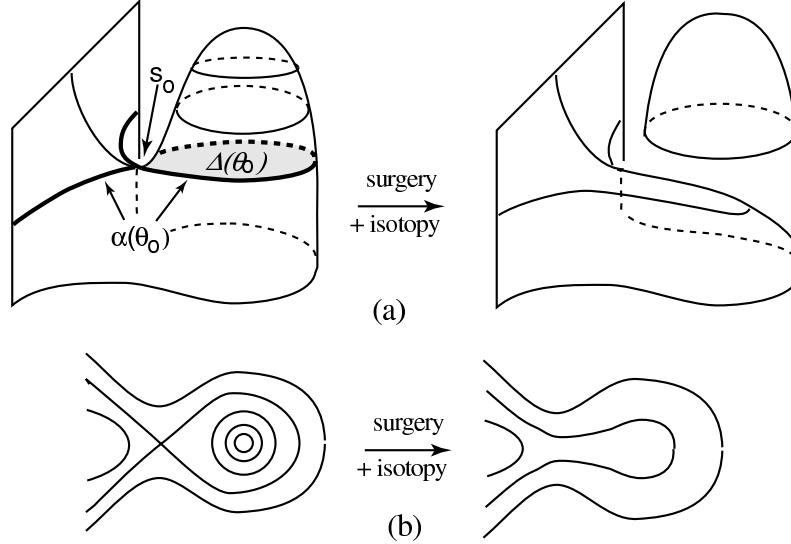


Figure 15: In this sketch the fibers of \mathbf{H} are to be thought of as horizontal planes. (a) Surgering \mathbf{F} along the disc Δ removes the singularity. (b) The change in foliation on \mathbf{F} .

homoclinic point in its foliation, but does not meet the disc Δ . We then do the surgery which is illustrated in Figure 27. In this way all leaves which are scc's can be eliminated.

Now every leaf in the foliation may be assumed to be an arc. The endpoint of a leaf which is an arc could either be at a vertex of the foliation or on the boundary, however we now claim that non-singular leaves which have both endpoints on the boundary do not occur. For, suppose there is a leaf μ which has both endpoints on boundary. Let $N(\mu)$ be a neighborhood of the leaf on \mathbf{F} . Thinking of $N(\mu)$ as a rectangle, it will have a pair of opposite edges on the boundary, and the orientation on these edges will be consistent with the orientation on $N(\mu)$. However, μ also lies in a fiber H_θ of \mathbf{H} , and the boundary of \mathbf{F} is a closed braid. But then, the orientation on one of the edges of $N(\mu)$ will agree with that of the normal to H_θ and (since μ is by hypothesis non-singular) the orientation of the other must disagree with the that of the normal, that is impossible because the boundary curve is a closed braid. It follows from this that the non-singular leaves have two types: those which have both endpoints at a vertex of the foliation (we call them *type b*) and those which have one endpoint on the boundary and the other at a vertex (we call them *type a*). See Figure 16(a). (The sketch in Figure 16(b) will be needed later, when we consider how this is modified in the situation of our annuli \mathcal{A}_- and \mathcal{A}_+).

The foliation may be used to decompose the surface \mathbf{F} into a union of foliated 2-cells, each of which contains exactly one singularity of the foliation. We will sometimes refer to these 2-cells as *tiles* and the resulting decomposition of \mathbf{F} as a *tiling*. Each tile is a regular neighborhood on \mathbf{F} of its singular leaves. The *vertices* of the tiles are the points where the braid axis \mathbf{A} intersects the surface \mathbf{F} . (There are also other vertices on the graph of singular leaves, but we prefer to exclude them when we refer to tile vertices.) The *edges* of the tiles are non-singular leaves of type *a* or *b*. (There are also other tile edges which are subarcs of X , but it will be convenient to ignore those, just as we ignored the vertices which are on X .)

Singularities fall into three types, which we call *aa*, *ab* and *bb*, the notation indicating that just before an *aa*-singularity (respectively *ab*-, *bb*-singularity) the non-singular leaves were both type *a* (respectively types *a* and *b*, respectively both type *b*). We will also sometimes find it helpful to work with foliated neighborhoods of the See Figure 17. The embedding of the tiles in 3-space is determined by the foliation, up to a choice of the order of the vertices on the braid axis (see Theorem

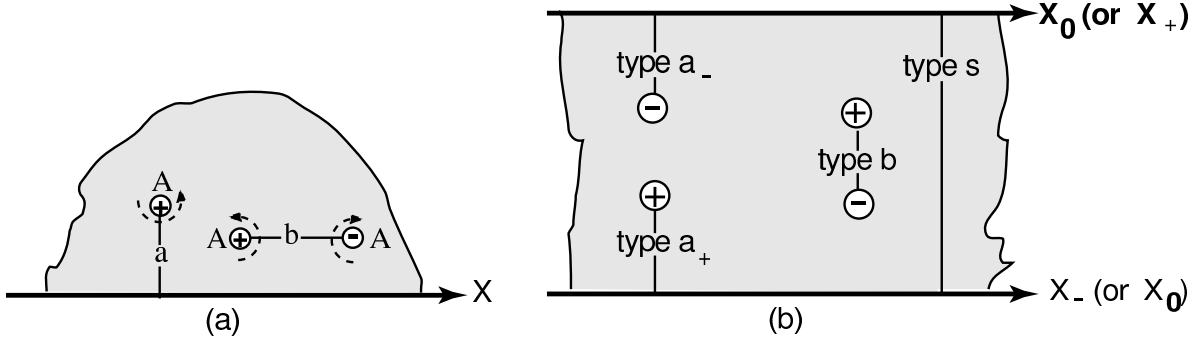


Figure 16: (a) Non-singular leaves in the foliation of \mathbf{F} ; (b) Modifications, in the situation of the annuli \mathcal{A}_- and \mathcal{A}_+ .

4.1 of [4]).

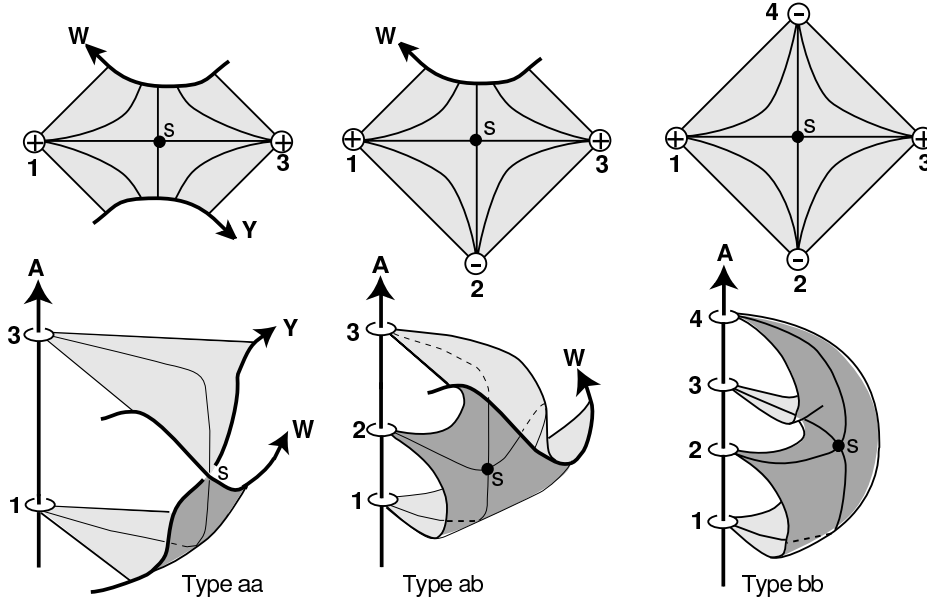


Figure 17: Foliated neighborhoods on \mathbf{F} of singularities of type aa, ab, bb

The singularities also have signs. Let s be a singular point of the foliation of a Markov surface \mathbf{F} for a link X , and let H_θ be the disc fiber which contains s . We say that s is *positive* if the outward-drawn oriented normal to the oriented surface \mathbf{F} coincides in direction with the normal to H_θ in the direction of increasing θ . Otherwise s is *negative*. There are restrictions on the orders and signs of the vertices and singularities, and we shall need the following in our work:

Lemma 3.1 (See Theorem 3.5 of [6]). *Let \mathbf{F} be a surface bounded by a closed braid. Assume that \mathbf{F} supports a foliation which satisfies all of the combinatorial requirements for a braid foliation. Then \mathbf{F} is embeddable in 3-space as a Markov surface only if:*

- (i) *The singularities about each positive (resp. negative) vertex are positively (resp. negatively) cyclically ordered in the fibration, with respect to increasing polar angle θ .*

- (ii) The vertices about each positive (resp. negative) singularity are positively (resp. negatively) cyclically ordered on the oriented braid axis, and

We will also use the following important fact, first proved in [12] and reviewed as Theorem 4.1 of [4]:

Lemma 3.2 *Let X be a closed n -braid, with $X = \partial\mathbf{F}$, where \mathbf{F} is incompressible spanning surface for X which supports a braid foliation. Then the following combinatorial data associated to the foliation of \mathbf{F} determines the embedding of the X up to braid isotopy:*

1. A listing of singularities of type aa and ab on \mathbf{F} . Also, for each singularity, its sign and an identification of its vertices among the cyclically ordered vertices v_i on \mathbf{A} .
2. For each singularity of type aa and ab , an identification of the X -endpoints of its singular leaf among the points p_j on each component of X .
3. For each singularity, the order of the singularity in the cycle s_1, \dots, s_l of fibers around the braid axis \mathbf{A} .

3.2 Recognizing destabilizations from the foliation

In this section we will use braid foliations to give a simple and enlightening proof of Markov's Theorem (the MT) in the special case of the knot. Our proof will have three goals: (i) to show the power of braid foliations via an example, (ii) to establish a result which we will need in Section 4.2 of this paper, and (iii) to show the reader how to recognize when a closed braid representative of a knot or link admits a destabilization, from properties of the foliation of an incompressible Seifert surface bounded by the closed braid. The reader is referred to the first page of this manuscript for the statement of the MT.

Proof of Markov's Theorem in the special case of the unknot: We are given an arbitrary closed n -braid representative X_- of the unknot \mathcal{U} . Since \mathcal{U} is the unknot, we know that $X_- = \partial\mathbf{D}$, where \mathbf{D} is a disc. By our work in Section 3.2 we may assume that \mathbf{D} supports a braid foliation.

The braid index n of X_- is the geometric linking number of X_- with the braid axis \mathbf{A} . Since X_- is transverse to all fibers of \mathbf{H} this geometric linking number coincides with the algebraic linking number $\mathcal{L} = \mathcal{L}(X_-, \mathbf{A})$, and so \mathcal{L} may also be interpreted as the algebraic intersection number of \mathbf{A} with \mathbf{D} . The points of $\mathbf{A} \cap \mathbf{D}$ are the vertices of the foliation, and from this it follows that $n = P - N$, where P and N are the number of positive and negative vertices in the braid foliation of \mathbf{D} . Since $n \geq 1$, it follows that the braid foliation of \mathbf{D} always has at least one positive vertex. Recall that the foliation is the standard radial foliation in a disc neighborhood $N(v)$ of any vertex v . Let $X_+ = \partial N(v)$. Then X_+ is a closed 1-braid representative of \mathcal{U} . We must show that X_- may be modified to $\partial N(v)$ for some choice of positive vertex v , by the moves of the MT, i.e. stabilization and destabilization.

Let us suppose, first, that the foliation contains only positive vertices. Examining Figure 17, we see that since singularities of type ab or bb always require a negative vertex, the singularities in the foliation can only be type aa . Observe that a 'tile' is a neighborhood of its singular leaves, and the foliation gives us, in a natural way, a decomposition of \mathbf{D} into tiles. Since \mathbf{D} is a disc, Euler characteristic considerations tell us that the graph of singular leaves must be a connected tree. Figure 18(a) shows a foliated neighborhood of a vertex of valence 1. As illustrated in sketch (b), the tile signifies the presence of a trivial loop in the closed braid X_- . Removing the singularity, as illustrated, we obtain a new closed braid, with braid index one less than that of the original one. In other words we have just done a *destabilization*. This process will end when there are no more singularities, i.e. when there is precisely one vertex v , and the foliation is radial about that vertex.

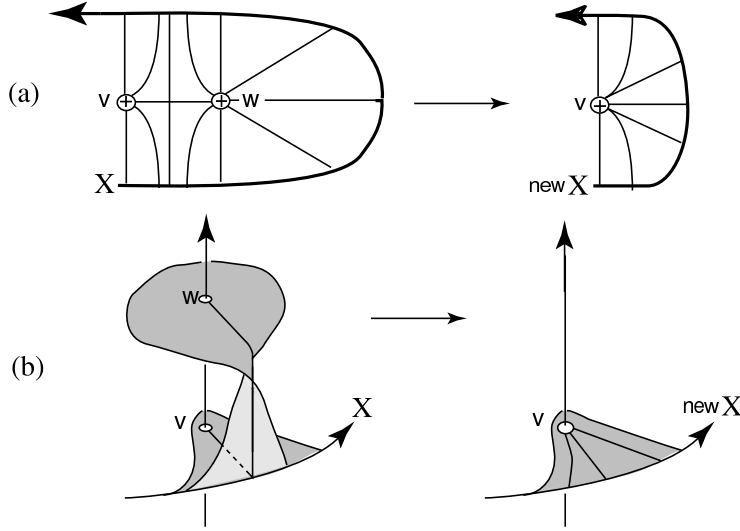


Figure 18: (a) Destabilization along a valence 1 vertex, viewed on the foliated surface; (b) The same move, viewed in 3-space.

That is, X_- will have been changed to the standard 1-braid representative $X_+ = \partial N(v)$ of the unknot.

More generally, there will be both positive and negative vertices in the foliation of \mathbf{D} . We claim that this implies that there must be an ab singularity in the foliation. Clearly, bb or ab singularities, or both, occur. But a bb tile is entirely in the interior of \mathbf{D} , and can only be adjoined to another ab or bb tile, and since only ab tiles have an edge on $\partial\mathbf{D}$ the claim follows. Thus, if there is a negative vertex, then there is an ab singularity.

The top row in Figure 19 shows how, any time there is an ab -singularity in the foliation, we may

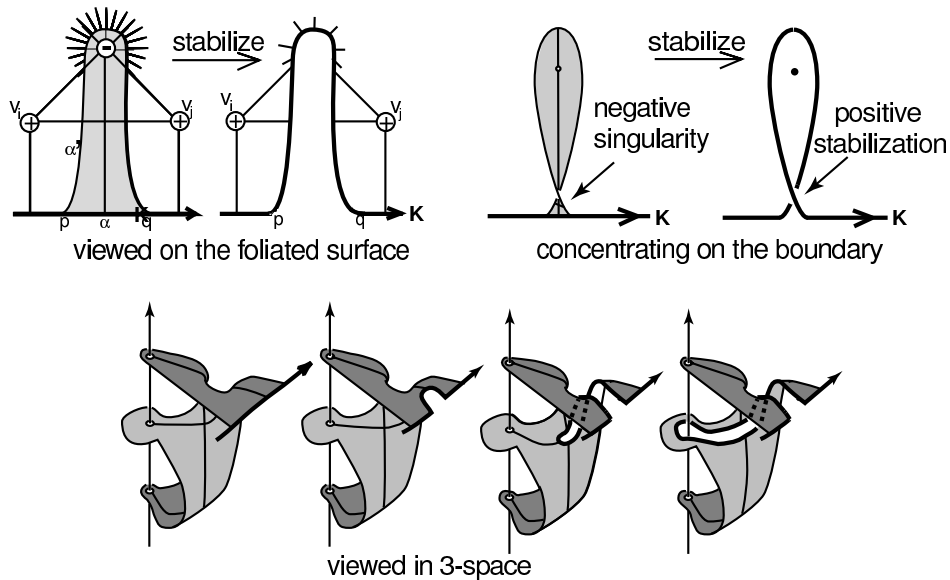


Figure 19: Stabilization along an ab -tile, viewed from three perspectives

push X_- across the singularity and its associated negative vertex, in a neighborhood of the separating leaf which meets X_- , to a new position which is again everywhere transverse to the foliation. It follows that after we do this move we will have a new closed braid representative, say X^* , of the unknot. Notice that after stabilizing, a bb singularity may have become an ab singularity. The middle row of pictures shows why the move *increases* the braid index from n to $n + 1$, while *decreasing* the number N of negative vertices from N to $N - 1$. The bottom row shows our stabilization move on the embedded surface in 3-space. If one looks carefully one can see the half-twist which has been introduced in the course of the push. We note that the pictures of ab -tiles in the bottom row of Figure 19 are deformations of the picture in Figure 17: we stretched out the top sheet to make visible a neighborhood of the singular leaf.

Inducting on the number N of negative vertices, the proof of the MT in the special case of the unknot is complete. \parallel

Remark : In the course of the proof, we have learned, from an example, how to recognize from the foliation of \mathbf{F} when X_- admits a destabilization: it admits a destabilization precisely when the foliation has a vertex of valence 1, as in Figure 18(a).

3.3 Recognizing exchange moves from the foliations

Exchange moves were discussed briefly in §1 to this paper, as moves on block diagrams for closed braids. We now show how to recognize, from the foliation of \mathbf{F} , when $X = \partial\mathbf{F}$ admits an exchange move.

Definition 5 (Essential and inessential b-arcs): A b -arc in the foliation is *inessential* if it joins a pair of vertices x, y in the foliation, where x and y are adjacent in the natural ordering of vertices along \mathbf{A} . A collection of b -arcs joining vertices x_1y_1, \dots, x_ky_k may be nested, i.e the ordering of their vertices may be y_1, \dots, y_k and then x_k, \dots, x_1 , in which case we say that x_k and y_k are *innermost*. If x_k and y_k are innermost, and separated on \mathbf{A} by a positive vertex z , then we say that the b -arcs in the family are all *essential*. \square

Lemma 3.3 *Suppose that the foliation of \mathbf{F} has a vertex v of valence 2. Suppose further that the adjacent singularities have opposite sign. Then the closed braid $X = \partial\mathbf{F}$ admits an exchange move. After the move, there is a surface \mathbf{F}' , isotopic to \mathbf{F} , with a decomposition containing two fewer vertices and two fewer singularities than the decomposition of \mathbf{F} .*

Proof: There are two cases to consider:

The bb exchange move: In this case the non-singular leaves which have an endpoint at v are all type b . The left and right sketches show the changes in 3-space. The changes in the braid projection can be understood by looking down the axis onto a plane orthogonal to the braid axis. The foliation does not change at all after a bb exchange move, however there is a change in the order of the vertices along the braid axis. The ‘pocket has been emptied’ and after the exchange move, the empty pocket can be collapsed by pushing every b -arc $\beta(\theta)$ across its disc $\Delta(\theta)$, as in Figure 21. (That is the reason we say that arcs like $\beta(\theta)$ are inessential b -arcs.) The passage from the left to right sketches in Figure 21 shows the change in the foliation, after the removal of all inessential b -arcs.

The ab exchange move: In this case there are non-singular leaves of both type a and type b which have an endpoint at v . See the left sketch in Figure 22(a). The change in the foliation of \mathbf{F} is very easy to understand in this case. One pushes the subarc $\alpha \subset X$ across the shaded disc in the left sketch in (a) to α' . The foliation tells us how to arrange that α' is in braid position, so that we know the move takes closed braids to closed braids. Passing to Figure 22(b), we examine the

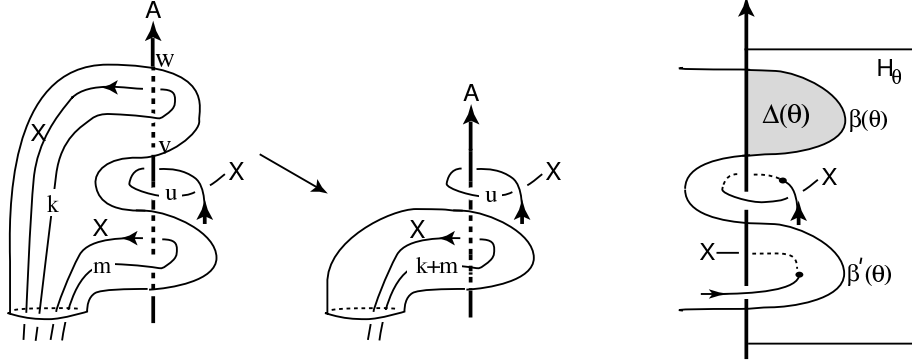


Figure 20: The type bb -exchange move, followed by an isotopy of \mathbf{F}

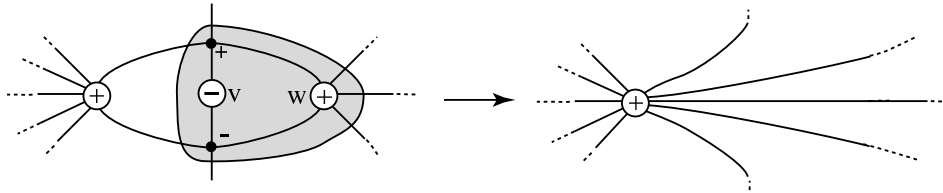


Figure 21: Changes in foliation after the removal of inessential b -arcs

move in 3-space. For full details, consult [4]. The shaded disc in the left sketch in (a) has boundary $\alpha \cup \alpha'$, and the disc is pierced twice by the braid axis at v and w . From this it is easy to see that its imbedded image form a ‘pouch’ like the one which is illustrated in Figure 22(b). The pouch is pierced twice by the braid axis, at w and v . We may assume without loss of generality that all of the b -arcs which have an endpoint at v are essential, hence the link X must encircle the subarc vw of the braid axis which is inside the pouch. After the exchange move the shaded disc will have vanished. Peering down the braid axis (as we did in Figure 2 we see that the projection has changed in the predicted manner.

Notice that we have described how three of the moves of the MTWS can be detected in the foliation of an embedded surface by inspecting the valences of vertices: destabilization and the bb and ab exchange moves. The main work ahead of us is to do the same for G-flypes and G-handle moves, in the setting of immersed annuli. After we do that we will be able to prove the MTWS.

3.4 Control over the foliation

Braid foliations are not unique, and in this section we describe some of the ways we have discovered to modify them. This is an essential part of the argument in the proof of the MTWS, because vertices of valence 1 and 2 may not be present initially, but after a change in foliation they may be present.

The foliation of \mathbf{F} depends upon the choice of half-planes H_θ in the fibration of $\mathbb{R}^3 - \mathbf{A}$. A *change in foliation* is the choice of a new set of half-planes $\mathbf{H} = \{H_\theta; 0 \leq \theta \leq 2\pi\}$. Equivalently, one may fix the fibers of \mathbf{H} and the link, and move the surface, and we shall move back and forth freely between these two viewpoints. The changes which we shall make are always very controlled and very local. In particular they do not change the braid, and the change in foliation which occurs is supported in one or two well-specified tiles. The question of when such changes are possible has been studied in earlier papers by the author, and we will use those results as needed here. We will describe three separate but related changes in foliation.

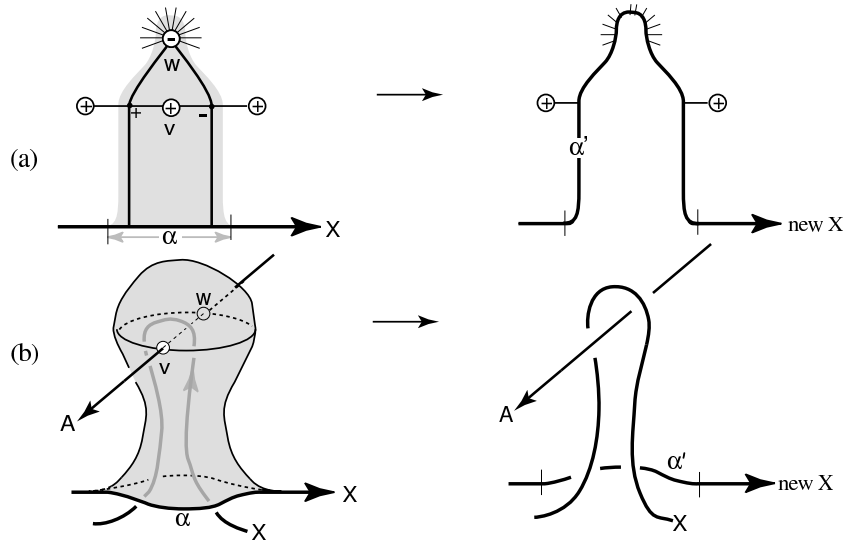


Figure 22: The type ab exchange move. The left and right sketches in (a) (resp. (b)) show the configurations on the foliated surface \mathbf{F} (resp. in 3-space). The braid changes can be understood by looking at the projection onto a plane orthogonal to the braid axis.

	BEFORE	AFTER
CASE 1		or
CASE 2		or
CASE 3		or

Figure 23: The first change in foliation: two singularities of the same sign have associated vertices v, w which share a common b -arc vw

Lemma 3.4 First change in foliation: *The resulting changes in $\partial\mathbf{F}$ correspond to defining relations in the braid group, using the presentation of [5] and the ‘boundary word’ methods of [6]. Let s_1 and s_2 be singularities of the same sign ϵ in tiles T_1 and T_2 , where T_1 and T_2 intersect in a common b-arc vw . Then after a change in fibration which is supported on a neighborhood $N(\alpha)$ in $T_1 \cup T_2$ of an arc α which joins the two singular points, the foliation of $T_1 \cup T_2$ changes in one of the two ways which are shown in the three cases illustrated in Figure 23. In particular, the valence of the vertices v and w decreases as a result of the change.*

Proof: See Theorem 2.1 of [4] for a proof of the Lemma. \parallel

Lemma 3.5 Second change in foliation: *A variation on Lemma 3.4: The conclusions of Lemma 3.4 still hold when the support of the change in foliation is the union of two surfaces \mathbf{F}_1 and \mathbf{F}_2 which meet transversally along a common arc, or if both have boundary and they are smoothly joined along subarcs of the boundary.*

Proof: The proof of the lemma in the new situation is identical to that in the old situation. In both cases the change in foliation is realized by an isotopy of the surface in which one of the two singularities is pushed past the other one. For details see [4]. The only new feature is that we are focusing on a subset of the surface which was considered in the old situation. \parallel

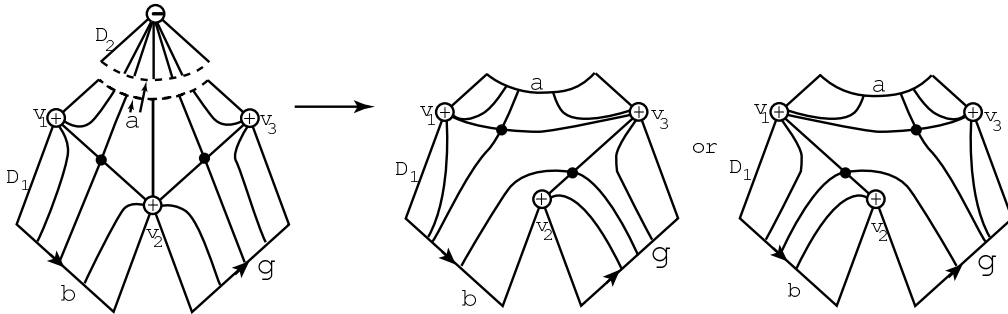


Figure 24: The second change in foliation (a variation on the first change). Two tiles of the same sign share a common b-arc edge, case (3)

We will need one more change in foliation which is similar to that of Lemma 3.4, except that it holds without restriction as to the signs of the two singularities which are involved. The reader may find Figure 25 helpful in understanding what it says.

Lemma 3.6 Third change in foliation: *Let γ be an arc which is located in a foliated disc N which is a subset of a foliated surface. Assume that the foliation of N contains exactly two singular points s_1 and s_2 , of either the same or opposite signs. Assume that s_1, s_2 are adjacent in the fibration. Let l_i be the singular leaf through $s_i, i = 1, 2$. Let H_{θ_i} be the fiber of \mathbf{H} which contains $s_i, i = 1, 2$. Suppose that there is a disc Δ in 3-space, such that:*

- (i) The interior of Δ has empty intersection with \mathbf{F} .
- (ii) $\partial\Delta = \alpha \cup \gamma$.
- (iii) $\Delta \cap N = \gamma$ and $\Delta \cap H_{\theta_2} = \alpha$.
- (iv) $\gamma \cap l_1 = s_1$ and $\gamma \cap l_2 = \{p\}$, where p is a point.

Then after a change in fibration which is induced by pushing N along Δ , changing the order of s_1 and s_2 , we may assume that $\gamma \cap l_1 = s_1$ and $\gamma \cap l_2 = \emptyset$. Moreover, the change in the foliation of \mathbf{F} may be assumed to be supported on an arbitrarily small neighborhood on N of the subarcs $[s_1, p] \subset \gamma$ and $[p, s_2] \subset l_2$. There could also be several singularities s_1, s_2, \dots, s_k , with associated neighborhoods,

and if the conditions are met for each of them in turn then the disc Δ may be used to push s_1 past many singularities, one at a time.

Proof: Figures 25(a) shows the foliated disc N before and after the change which we propose to make. The arrows which are attached to the leaves indicate the direction of increasing θ . Using the foliation of N , and knowing the signs of the singularities, one may construct an embedding of N in 3-space, and we have done so in Figure 25(b) in the case when the signs of the singularities at s_1 and s_2 are different. (The other case is similar). In Figure 25(b) fibers of \mathbf{H} are to be thought of as horizontal planes, and the direction of increasing θ is bottom to top. The auxiliary disc Δ , is also illustrated. The move which we make to realize the change in foliation in Figure 25(a) is to push N down along the disc Δ . To understand how this changes the foliation of N , we have labeled certain endpoints on ∂N with numbers 1,2,3,4,5,6. There are non-singular leaves which we call 12, 34, 56, each with arrows directed inward (to illustrate the direction n of increasing θ) and joining 1 to 2, 3 to 4 and 5 to 6 respectively. In the left picture the first singularity occurs when leaf 12 approaches leaf 34, but in the right picture the first singularity occurs when leaf 12 approaches leaf 56. ||

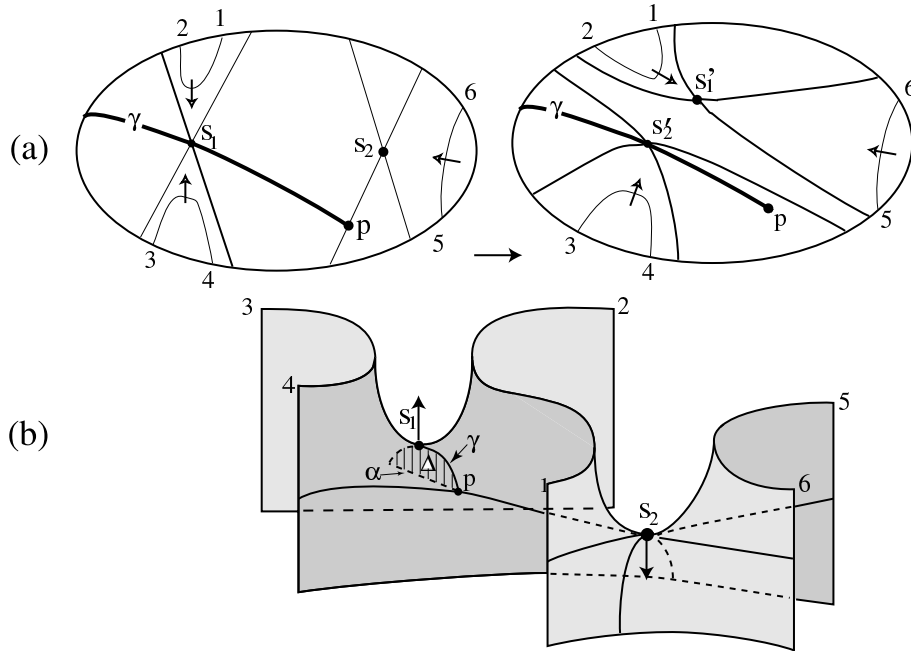


Figure 25: Sketch (a) shows the third or ‘ Δ -disc’ change in foliation. Sketch (b) shows N , embedded in 3-space, before the change, illustrating the position of Δ . The move is a push downward of s_1 along Δ .

3.5 The 4 graphs

One expects the singular leaves to contain essentially all of the key information about our foliation in the complement of the clasp arcs. That’s true, but in addition more is true: Our singularities and vertices have signs, and there is additional information in those signs. For this reason, we will make use of four subgraphs of the graph of the singular leaves, denoted $G_{+,+}, G_{+,-}, G_{-,-}, G_{-,+}$. See Figure 26. Similar graphs appeared in Bennequin [2], in connection with his studies of the characteristic foliation of surfaces by knots. In the graph $G_{\epsilon,\delta}$ the subscript ϵ (resp. δ) is the sign of the vertices (resp. singularities) in our subgraphs. The graphs $G_{+,+}, G_{+,-}, G_{-,-}, G_{-,+}$

were studied in Lemma 3.8 and Theorem 3.1 of [4]. That work will be reviewed and extended later in this paper. See, in particular, Sections 4.6 and 4.7, later in this paper.

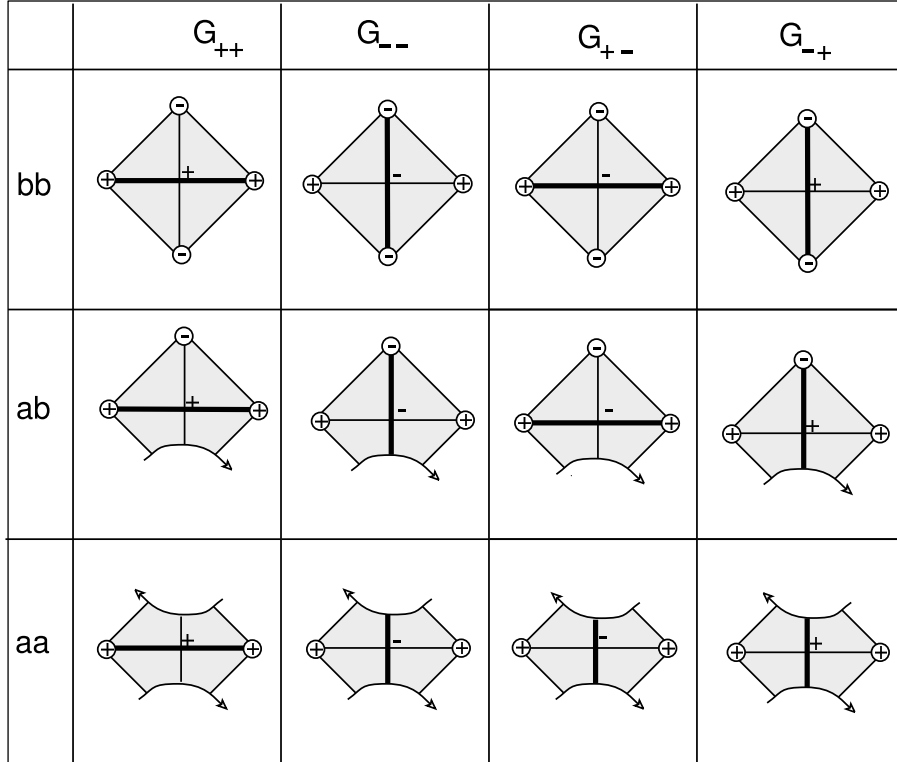


Figure 26: The thick edges are in the graphs $G_{+,+}$, $G_{-,-}$, $G_{+,-}$, $G_{-,+}$

4 Braid foliations of the immersed annulus

During this part of our work, as in §2, there will be no loss in generality in assuming (most of the time) that \mathcal{X} is a knot. When we get to the proof of the MTWS, in the next section, we will return to the general case, when \mathcal{X} is a link.

Our work begins with the two closed braid representatives X_- and X_+ of \mathcal{X} . In §2 we presented a topological construction which gave us an intermediate closed braid X_0 , two embedded annuli \mathcal{A}_- and \mathcal{A}_+ , and an immersed annulus $\mathcal{TA} = \mathcal{A}_- \cup \mathcal{A}_+$ whose self-intersection set was a collection $\Gamma = \{\gamma^1, \dots, \gamma^k\}$ of finitely many clasp arcs. We showed that we could assume that each clasp arc is in braid position, i.e. its intersections with the half-planes $\{H_\theta, \theta \in [0, 2\pi]\}$ are always transverse. (Remark: there is no natural choice of orientation on γ^i .) See Lemma 2.1. In this section we study the braid foliations on \mathcal{TA} . The key point which will allow us to apply the machinery of §3 is that both annuli are embedded. The really new feature is the presence of the clasp arcs. The assumption that X_+ has minimum braid index among all closed braid representatives of \mathcal{X} has not been used up to this point, but in this section it will begin to play a role in the argument.

4.1 Braid foliations of \mathcal{A}_- , \mathcal{A}_+ and \mathcal{TA}

The foliation which is of interest to us now is the foliation of $\mathcal{A}_- \cup \mathcal{A}_+$ which is induced by intersections of these annuli with the family of half-planes $\{H_\theta, \theta \in [0, 2\pi]\}$ which fiber $\mathbb{R}^3 \setminus \mathbf{A}$. The closed braids

X_-, X_0, X_+ are all oriented so that they point in the direction of increasing θ at each point of intersection with an H_θ . We choose an orientation on the annulus \mathcal{A}_- in such a way that it induces the given orientation on its boundary component X_- . Notice that this means that the orientation on X_0 does not agree with that induced by the chosen orientation on \mathcal{A}_- . Similarly, we choose an orientation on the annulus \mathcal{A}_+ in such a way that it induces the given orientation on its boundary component X_0 , which implies that the orientation on X_+ does not agree with that induced by the chosen orientation on \mathcal{A}_+ .

As in the situation of Seifert surfaces, the foliation may be assumed to be radial in a neighborhood of each point of $\mathbf{A} \cap \mathcal{A}_\pm$ (see Figure 14(a)) and transverse to the boundary in a neighborhood of $\partial\mathcal{A}_\pm$ (Figure 14(b)). The braid axis \mathbf{A} pierces \mathcal{A}_\pm from either the negative or the positive side at each pierce point, and we have indicated this by attaching positive or negative signs to the pierce points on \mathcal{A}_\pm . As before, leaves in the foliation are *singular* if they contain a singularity of the foliation, otherwise they are *non-singular*. The singularities may be assumed to be finite in number and to occur on distinct fibers of \mathbf{H} .

We now show that, as in the situation of Seifert surfaces, we may assume that there are no leaves in the foliation of $\mathcal{TA} = \mathcal{A}_- \cup \mathcal{A}_+$ which are simple closed curves. See Figure 27 There are three new

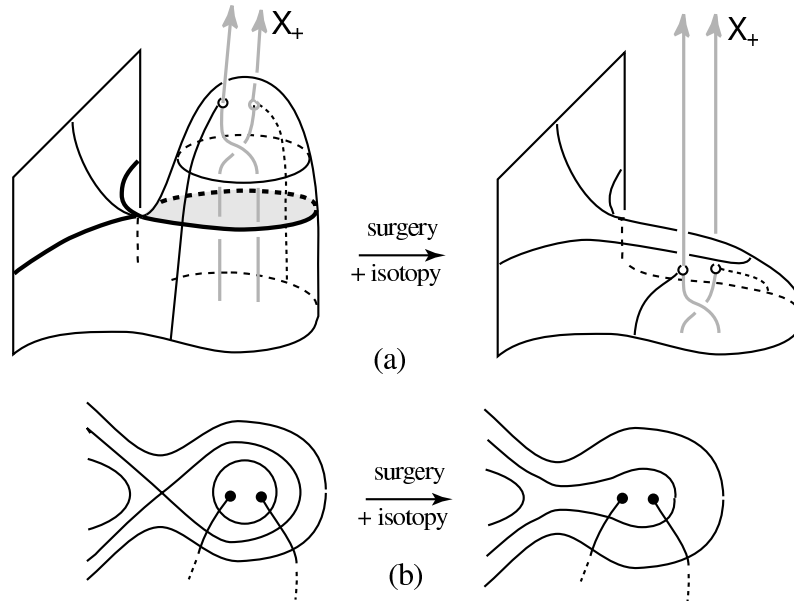


Figure 27: The elimination of a homoclinic singularity and associated simple closed curves in the presence of clasp arcs

issues to settle. (i) Our closed braid X_0 lies in both the boundary of \mathcal{A}_- and the boundary of \mathcal{A}_+ , separating \mathcal{TA} , and the first question we ask is whether X_0 could intersect a disc which is foliated by simple closed curves? The answer is ‘no’, because if there is a disc in \mathbf{F} which is foliated entirely by scc’s, then X_0 would necessarily be tangent to one of the scc’s, say c , but c is a leaf in the foliation and so lies entirely in one of the half-planes H_{θ_c} , however X_0 is transverse to every half-plane H_θ . Thus, if simple closed curves occur, they are either in \mathcal{A}_- or \mathcal{A}_+ . (ii) For exactly the same reason, a clasp arc in braid position cannot cross a region which is foliated by simple close curves, because by Lemma 2.1 every clasp arc is in braid position. (iii) Finally, we consider the possibility that a clasp arc has a pierce point inside a region which is foliated by simple closed curves. However, Figure 27 shows that exactly the same ‘surgery and isotopy’ that we used in Figure 15 works here too.

We have learned that we may assume that every leaf is an arc. The situation is a little bit more complicated than it was in the case of Seifert surfaces. Consult Figure 16(b). There are

now 5 possible types of non-singular arcs in the foliation of \mathcal{A}_- and \mathcal{A}_+ : (i) arcs which have both endpoints at vertices (type b); (ii) arcs which have one endpoint at a positive vertex (type a_+), (iii) arcs which have one endpoint at a negative vertex (type a_-), (iv) Arcs which have one endpoint on one boundary component and the other on the opposite boundary component (type s); and (v) arcs which have both endpoints on the same boundary component. As for type (v), the exact argument that we used in the case of Seifert surfaces applies, because X_-, X_0, X_+ are all closed braids, so type (v) does not occur.

An exhaustive list of the singularities which could, in principle, occur in the foliation of \mathcal{A}_- and \mathcal{A}_+ are types $a_+a_+, a_+b, a_+s, a_+a_-, a_-a_-, a_-b, a_-s, sb, ss,$ and bb , where the notation is consistent with that used in §3. However, we have:

Lemma 4.1 *Singularities of type ss do not occur in either \mathcal{A}_- or \mathcal{A}_+ . Singularities of type a_-a_- and a_-s do not occur in \mathcal{A}_+ .*

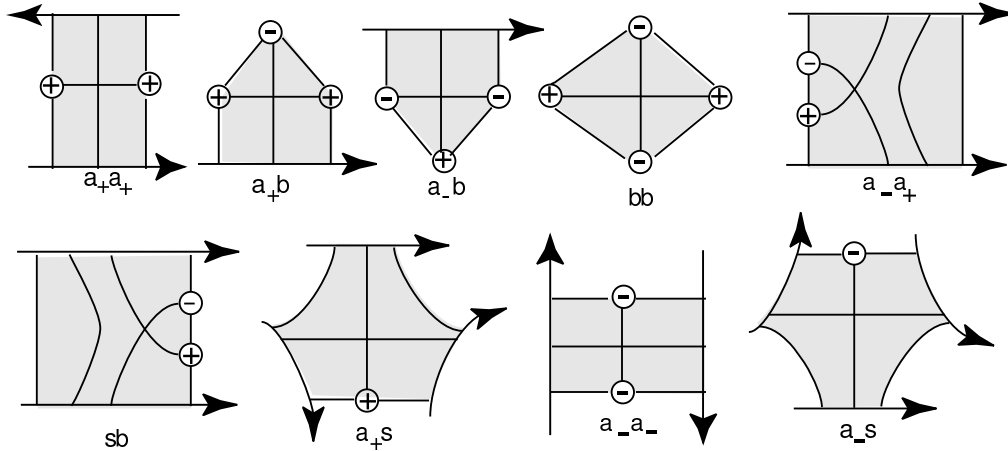


Figure 28: Possible tile types in the foliation of \mathcal{A}_- and \mathcal{A}_+ . However, types a_-a_- and a_-s do not occur in \mathcal{A}_+ .

Proof: To see that singularities of type ss do not occur, note that a type s leaf separates \mathcal{A} and the flow near the two boundary points is always in the direction of the orientation on the boundary components. However, both boundary components are closed braids, so there is no way for two such leaves to approach one-another as the foliation evolves.

We now prove that singularities of type a_-a_- and a_-s do not occur in the annulus \mathcal{A}_+ . Suppose that a singularity of either type a_-a_- or a_-s occurs. Notice that there is an arc, α , contained in the singular leaf which has both of its endpoints on X_+ and which, together with one of the two subarcs β of $X_+ - (X_+ \cap \partial\alpha)$ forms a simple closed curve C which bounds a disc $D \subset \mathcal{A}_+$. Since C bounds a disc it represents the unknot. Now observe that if we perturb the points of α slightly along X_+ we may change α to an arc α' which is transverse to fibers of \mathbf{H} . Thus, after an arbitrarily small perturbation, we may change C to $C' = \alpha' \cup \beta$, where C' is a closed braid and where $\beta \subset X_+$ is a subarc of the closed braid X_+ . Let b be the braid index of C' . The fact that C' is everywhere transverse to fibers of \mathbf{H} guarantees that $b \geq 1$. But then, we may reduce the braid index of X_+ by at least one without changing its knot type by replacing β by α' . However that is impossible because by hypothesis the braid index of X_+ is minimal. \parallel

4.2 Construction of the tabs

Our next goal is to change the discs R_1, \dots, R_k which we constructed in Section 2 (See Figure 11) to special foliated discs which we call ‘tabs’. A *tab* in the foliated annulus \mathcal{A}_- is a linearly ordered sequence of tiles in \mathcal{A}_- , the *initial tile* being type a_-a_- with one vertex of valence 1 and the other of valence 2, the intermediate ones being a_-a_- tiles with both vertices of valence 2, and the final one being a single a_-s tile. See Figure 29 for an example. We now show that we may replace each

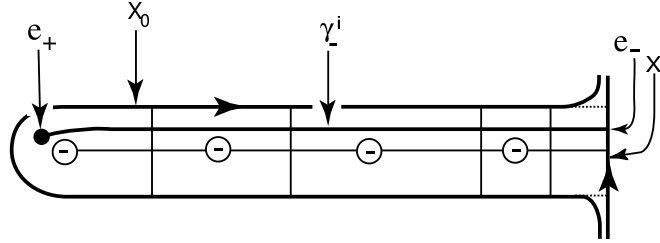


Figure 29: Example of a tab.

R_i by a tab which is pierced once by X_+ in its end-tile. The tab contains the preimage γ_-^i of a clasp arc. This arc runs parallel to the chain of singular leaves through the negative vertices in the tab. The main result in this section is:

Lemma 4.2 *After some number of modifications of X_0 we may assume that each R_i is a tab. Moreover, we may assume that each clasp arc in a tab crosses at least one singular leaf.*

Proof: We focus on a single R_i . It is a subset of the embedded annulus \mathcal{A}_- , and it contains one of the components of the preimage of a single clasp arc γ_-^i in its interior. We shall think of R_i as a topological disc which is bounded by 2 arcs: a subarc $x_0 = x_0^i \subset X_0$, a subarc $x_- = x_-^i \subset X_-$ and two s -arcs which join the former to the latter. After tilting the s -arcs a little bit ∂R_i will be a closed braid. Using the methods described in §3 we may further assume that R_i supports a braid foliation. We will use the ideas in the proof of Markov’s Theorem for the special case of the unknot, given in Section 3.2, only what we will be doing here is to simplify the foliation in \mathcal{A}_- at the expense of pushing singularities into \mathcal{A}_+ . For example, when the proof which motivates our work removes a singularity by stabilization along an ab tile, we will instead be moving the boundary X_0 between \mathcal{A}_- and \mathcal{A}_+ across an ab -tile which has a subarc of X_0 in its boundary, pushing the singularity in this tile from \mathcal{A}_- to \mathcal{A}_+ .

The arc $\gamma_-^i \subset R_i$ has one of its endpoints at a point e_+ in the interior of R_i , and its other endpoint at a point $e_- \in X_-$. In between, it winds around the vertices of the foliated disc R_i , staying transverse to the leaves of the foliation. We may assume without loss of generality that the point e_+ where X_+ pierces the interior of R_i is not on a singular leaf. Therefore e_+ belongs to a non-singular leaf of type s, a_+, a_-, b .

Let $\alpha^i \subset R_i - \gamma_-^i$ be a simple path that starts at e_+ and ends at a point $e_0 \in X_-$. Without loss of generality we may assume that $\gamma_-^i \cup \alpha^i \subset R_i$ is a simple path transverse to the foliation of R_i and having endpoints $e_- \cup e_0 \in X_-$. (If not, we can always apply Alexander’s braiding argument to α^i .)

Let $R'_i \subset R_i$ be the foliated subdisc that $\gamma_-^i \cup \alpha^i$ splits off in R_i . We are now in position to re-choose γ_-^i and α^i in R_i so that R'_i has the foliation of a tab and e_- is contained in the end-tile vertex of valence one. This re-choosing is achieved through, first, stabilization of $\gamma_-^i \cup \alpha^i$. If the induced foliation of R'_i contains a positive vertex v then this sub-foliation must also contain a singular leaf that has its endpoint on $\gamma_-^i \cup \alpha^i$ and is adjacent to v . We can then stabilize $\gamma_-^i \cup \alpha^i$ along this singular leaf (see Figure 19 with the modification that the parity of the vertices is reversed). We can easily assume that e_- is away from all singular leaves so, after a sequence of ab -stabilizations as in Figure 19, we may assume that $\gamma_-^i \cup \alpha^i$ splits off a subdisc $R'_i \subset R_i$ where the induced foliation of R'_i contains only positive vertices.

Now the foliation of R'_i is either a tab (as we would like it to be) or its graph of singular leaves is a tree. In the latter case, since e_- can be adjacent to only one positive vertex, either γ^i_- or α^i intersect a singular leaf in the foliation of R'_i twice. We then can find a valence one vertex, as in Figure 18(a), with either γ^i_- or α^i in its boundary. After a ‘destabilization’ (which has the effect of moving the singularity in the aa tile which is in \mathcal{A}_- into \mathcal{A}_+) we can eliminate this positive vertex from \mathcal{A}_- and also from R'_i . Iterating this procedure, we alter $\gamma^i_- \cup \alpha^i$, until R'_i is changed to a tab. ||

Simplified notation and simplified tile types: From this point on we will be dealing mainly with the immersed annulus $\mathcal{TA} = \mathcal{A}_- \cup \mathcal{A}_+$, with its boundary components X_- and X_+ . Having standardized the tabs, we will not have any more use for X_0 . Therefore an a -arc always means an arc of type a_+ or a_- . This allows the following simplification: Let $\epsilon = \pm$. Then an a_ϵ -arc has one endpoint on a vertex of sign ϵ and the other endpoint on $X_{-\epsilon}$.

The symbol $P(\mathcal{TA})$ denotes the *pre-image annulus*, with additional structure. It is foliated, its foliation being the pullback of the foliation on \mathcal{TA} under the immersion. We may also pull back the k clasp arcs to k pairs of arcs on $P(\mathcal{TA})$. This foliated annulus, marked to indicate the $2k$ preimages of the clasp arcs, is $P(\mathcal{TA})$.

We claim that from now on tiles of type a_-a_- and a_-s do not occur. This is a consequence of our hypothesis that the braid index $b(X_+)$ of X_+ is minimal. For, a tile of type a_-a_- or a_-s contains a separating leaf. This separating leaf together with a subarc of X_+ bounds a disc. If we modify \mathcal{TA} by cutting off the disc, we will have reduced $b(X_+)$. However, that is impossible because $b(X_+)$ is minimal.

Example: An example is given in Figure 30. It illustrates the foliated annulus $P(\mathcal{TA})$ which is the preimage of the immersed annulus \mathcal{TA} associated to the boxed sketches at the bottom of Figure 9. In the pages which follow we will return to study many aspects of this example. The features which can be understood now include the following:

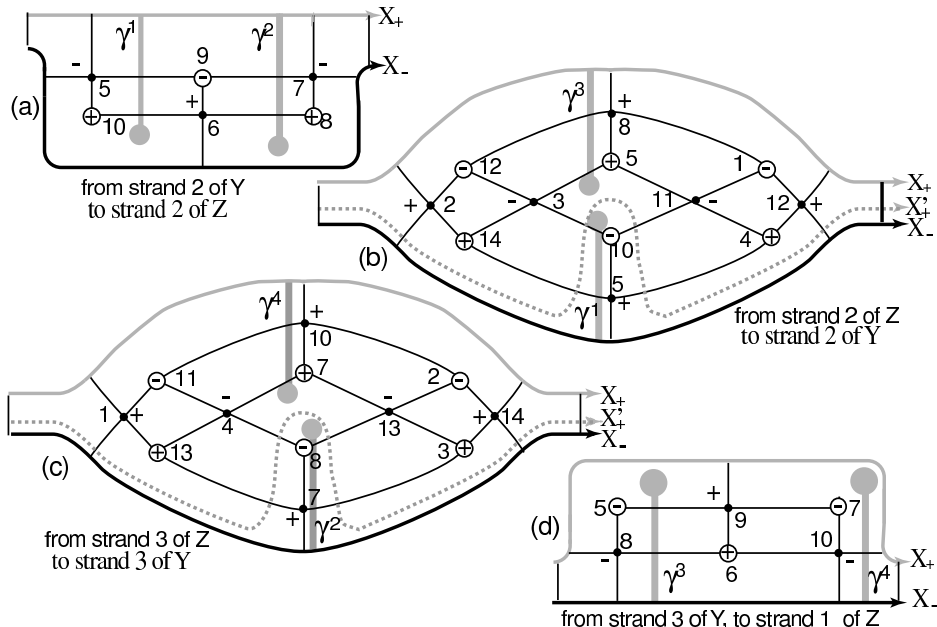


Figure 30: The foliation of $P(\mathcal{TA})$, in the situation of the 6-braid template of Figure 9

- The figure shows 4 foliated discs, each of which begins and ends in a band of s -arcs. There are tiles of type $a_\epsilon b$, bb and sb .
- The vertices (resp. singularities) are labeled to show their signs and their cyclic order on the axis \mathbf{A} (resp. in the fibration \mathbf{H}). There are 4 clasp arcs, labeled $\gamma^1, \gamma^2, \gamma^3, \gamma^4$ and each appears twice. They have been pushed into a union of singular leaves, a matter which will be discussed later in this section.
- The label ‘from Y, strand 2’ on sketch (a) means that the X_- boundary of the band of s -arcs at the left of the disc in (a) came from the second braid strand out of block Y in Figure 9. Following this braid strand in Figure 9 we see that after it leaves the foliated disc it necessarily becomes the second braid strand into block Z, in both the before and after block-strand diagrams in the template. The labels on the other 3 discs have similar meaning. The dotted thick grey arcs and thr labels X'_+ will be explained later.

4.3 Microflypes and the foliation of $P(\mathcal{TA})$.

In this section we begin to establish a connection between the foliation of $P(\mathcal{TA})$ and the embedding of X_- and X_+ in 3-space. The work that we do here will be essential to an understanding of the proof of the MTWS.

Definition 6 (Microflypes and Microblocks): A *micro-flype* is a flype (consult Figure 3) in which the braid in the braid box R consists of exactly one full twist of either sign on two strands. By our definition of a flype, all strands must have weight 1. The *sign pair* of a microflype is the pair (α^*, β^*) where α^* is sign of the half-twist which is outside the braid box and β^* is the sign of the full twist which is inside the braid box. The sign of the flype which is determined by a microflype of sign pair (α^*, β^*) is α^* . The sign α^* is the same as the sign of the associated flype, as defined in the Introduction to this paper. We will refer to a block which has braid index 2 and contains exactly one full twist as a *microblock*. \square

For example, the microflype which is illustrated in the bottom middle sketch in Figure 13 has sign $(-1, -1)$. As we shall see, microflypes with their associated microblocks are the building blocks of more general flypes.

We will show that when the total annulus \mathcal{TA} is a union of one a_+s and one a_-s tiles, joined up by two bands foliated entirely by s -arcs, where the signs of the singularities on the two tiles disagree and where the two discs intersect along exactly one clasp arc as in Figure 13, then its boundary braids admit a microflype. This microflype (which was already discussed in §2 and illustrated in Figure 13), but now we have a new tool (the braid foliations of \mathcal{TA}) and are in a position to give full details.

Going back to Figure 13 we are ready to discuss the braid foliation of this very simple foliated annulus. The signs of the two vertices are determined by the fact that an a_ϵ leaf has one endpoint on a vertex of sign ϵ and the other on $X_{-\epsilon}$. This implies that the flow is counterclockwise about the vertex in the left tile and clockwise about the vertex in the right tile. The fact that the two clasp arcs in $P(\mathcal{TA})$ are identified in \mathcal{TA} implies that the θ -coordinates of the leaves in the two tiles must be matched up as shown, where the number i means that the leaf lies in the fiber H_{θ_i} . The top sketch shows the foliated annulus, and the bottom 2 sketches show the embedding of the boundary curves in 3-space. In the right sketch we give a highly symmetric view of the embedded boundary, under the assumption that the clasp arcs have been pushed into the singular leaves. In a few moments we will prove that this is always possible.

Call a puncture point p on a clasp arc positive or negative according as the orientation of X_ϵ at p agrees or disagrees with the orientation of the outward drawn normal to the surface at p . We claim that the puncture endpoints in the right and left tiles must have opposite signs. The reason is that one endpoint of the clasp arc lies on X_+ and the other lies on X_- . Thus the sign of the puncture on

the right tile determines that on the left tile. In Figure 31 we have illustrated the case when the left puncture is negative and the right puncture is positive, but the opposite choices are also possible.

There is also a choice for the signs of the two singularities. Let α, β be the signs of the pair (singularity, puncture) on the right tile, and let α' be the sign of the left singularity. There are 8 possible sign choices for the triplet (α, β, α') .

Lemma 4.3 *The signs of the singularities in the two tiles which meet at a clasp arc disagree. In particular, $\alpha' = -\alpha$. The possible sign choices (α, β) for the pair (singularity, puncture) are $(-, -), (-, +), (+, -), (+, +)$.*

Proof: The first thing to notice is that there is a symmetry, vis: If one reflects the surface in a plane through the axis and changes the orientation of the new surface so that its boundary is a closed braid, the effect on the foliation will be to reverse the cyclic order in the fibration and change the signs of the singularities. The effect on the boundary braid is to replace it by its mirror image, and the effect on (α, β, α') is to replace them by $(-\alpha, -\beta, -\alpha')$. But then, up to symmetry we have four cases to investigate: $(\alpha, \beta, \alpha') = (-, -, +), (-, +, +), (+, -, +)$ and $(+, +, +)$.

The case $(\alpha, \beta, \alpha') = (-, -, +)$ is illustrated in Figures 13 and 31. To verify that \mathcal{TA} exists as an

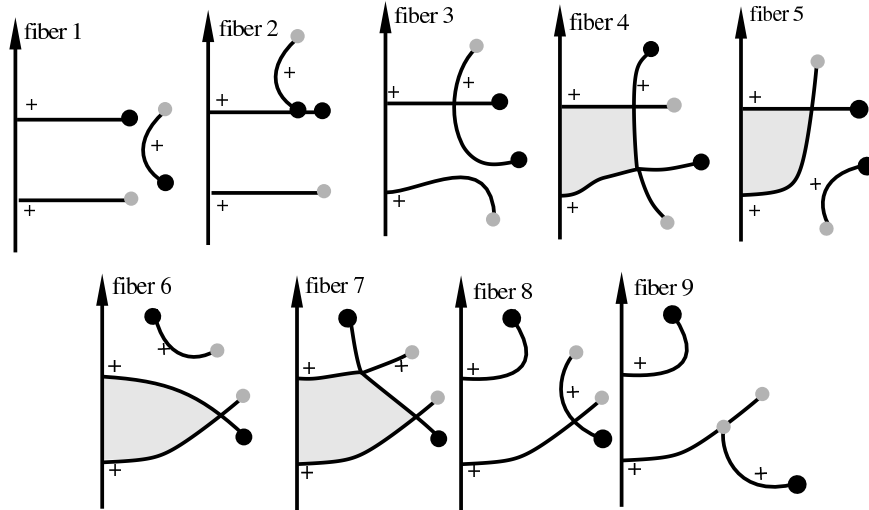


Figure 31: The H_θ sequence for the foliated annulus in Figure 13, in the case when $(\alpha, \beta) = (-, -)$

immersed surface with a single clasp singularity, and to show that its boundary admits a microftype, we investigate the arcs and curves in $\mathcal{TA} \cap H_\theta$ as θ is varied between 0 and 2π . For that it suffices to study $\mathcal{TA} \cap H_\theta$ at selected fibers (chosen so that $\mathcal{TA} \cap H_\theta$ only changes by isotopy in between the selected fibers). At θ_1 we see two a -arcs and the two points where \mathcal{TA} meets the braid axis, i.e. the two vertices. The top vertex is the positive one (from the right tile) and the bottom is the negative one. Notice that the positive vertex is joined by an a -arc to X_- and the negative vertex by an a -arc to X_+ . These braids intersect the fiber in gray and black dots. The same two vertices, with the same signs, occur at every θ_i . The fiber at θ_1 also shows a little s -arc which runs between X_- and X_+ , illustrated as a second pair of gray and black dots. In general there could be many s -arcs in every fiber.

The clasp arc begins at θ_2 and ends at θ_9 . At θ_2 the s -arc has just begun to intersect the a -arc. We also see it a little bit later, just before the singularity at θ_3 . The connectivity changes at θ_4 and the new s -arc migrates to a position where we can visualize the second singularity, at θ_7 , and continue to complete the cycle. There are no forced unwanted self-intersections in \mathcal{TA} , and we have,

in effect, constructed \mathcal{TA} as an immersed surface in 3-space, with exactly two singularities and one clasp type self-intersection.

We return to Figure 13 for a 3-space view of the immersed tiles in \mathcal{TA} . The two black arcs are the two subarcs of X_- in Figure 13. The first subscript indicates that both are subarcs of X_- . The two tiles are twisted in a neighborhood of the clasp arc. Away from the clasp arc the surface \mathcal{TA} is embedded.

Notice the topological symmetry in the H_θ sequence, too: $\mathcal{TA} \cap H_{\theta_4}$ and $\mathcal{TA} \cap H_{\theta_7}$ are topologically identical, as are $\mathcal{TA} \cap H_{\theta_5}$ and $\mathcal{TA} \cap H_{\theta_6}$. Also, $\mathcal{TA} \cap H_{\theta_8}$ and $\mathcal{TA} \cap H_{\theta_+}$ are topologically equivalent up to a horizontal reflection, and the same is true for $\mathcal{TA} \cap H_{\theta_0}$ and $\mathcal{TA} \cap H_{\theta_2}$, whereas $\mathcal{TA} \cap H_{\theta_1}$ is symmetric under the same reflection. Putting this another way, the H_θ sequence for case (iii) can be obtained from that for case (i) by reversing the sense of the fibration.

The H_θ sequence in Figure 31 actually tells us more. Let's ask what happens in the case when $(\alpha, \beta, \alpha') = (+, -, +)$? Examining Figure 31, but changing the sign of the singularity at θ_7 , we see that the H_θ sequence will be unchanged as we proceed through the fibers at $\theta_1, \theta_2, \dots, \theta_6$, but as we approach θ_7 we encounter a problem. We are required to have a positive singularity in H_{θ_7} , but the negative sides of the surface are not accessible to one-another without creating a new self-intersection. The case $(+, -, +)$ is thus impossible. But then, so its symmetric image, i.e. $(-, +, -)$.

We turn next to Figure 32, which illustrates the case $(\alpha, \beta, \alpha') = (-, +, +)$. Once again the H_θ -

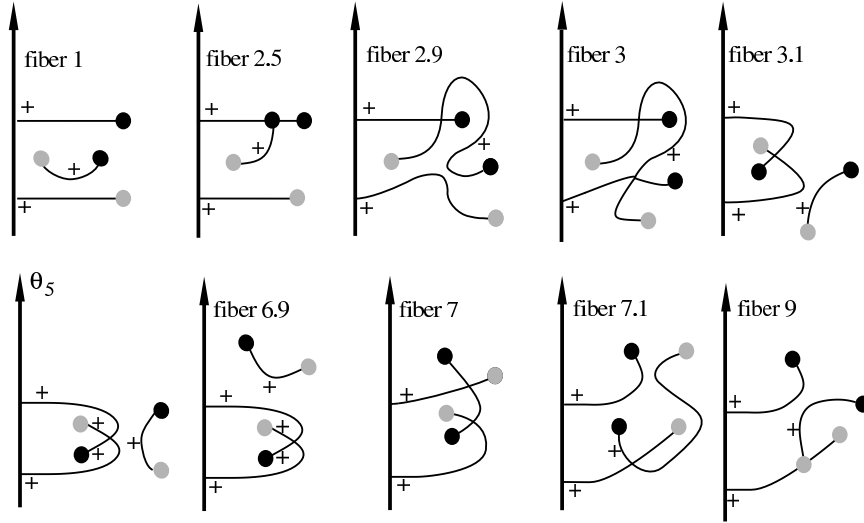


Figure 32: The H_θ -sequence for the case $(\alpha, \beta) = (-, +)$

sequence shows that \mathcal{TA} can be realized as an immersed surface with exactly one clasp intersection. The argument is exactly like the one we used in the previous case, even though the details of the pictures are different. We also learn that the cases $(\alpha, \beta, \alpha') = (+, +, +)$ and $(-, -, -)$ are impossible, for reason just like the ones we used to show that the cases $(+, -, +)$ and $(-, +, -)$ are impossible.

The signs α and β are of course the same as α^* and β^* , introduced in Definition 6. In particular, this shows that α is the sign of the flype, as defined in §1.2.4. The proof of the Lemma is complete. ||

4.4 The two finger moves

We need tools that will allow us to modify neighborhoods of the clasp arcs in \mathcal{TA} in a controlled manner, keeping track of the foliation on the two branches and making sure that no new self-

intersections are introduced. The ‘finger moves’ will help us to do that.

Consult Figure 33. The first column in Figure 33 shows foliated neighborhoods N of a subarc of

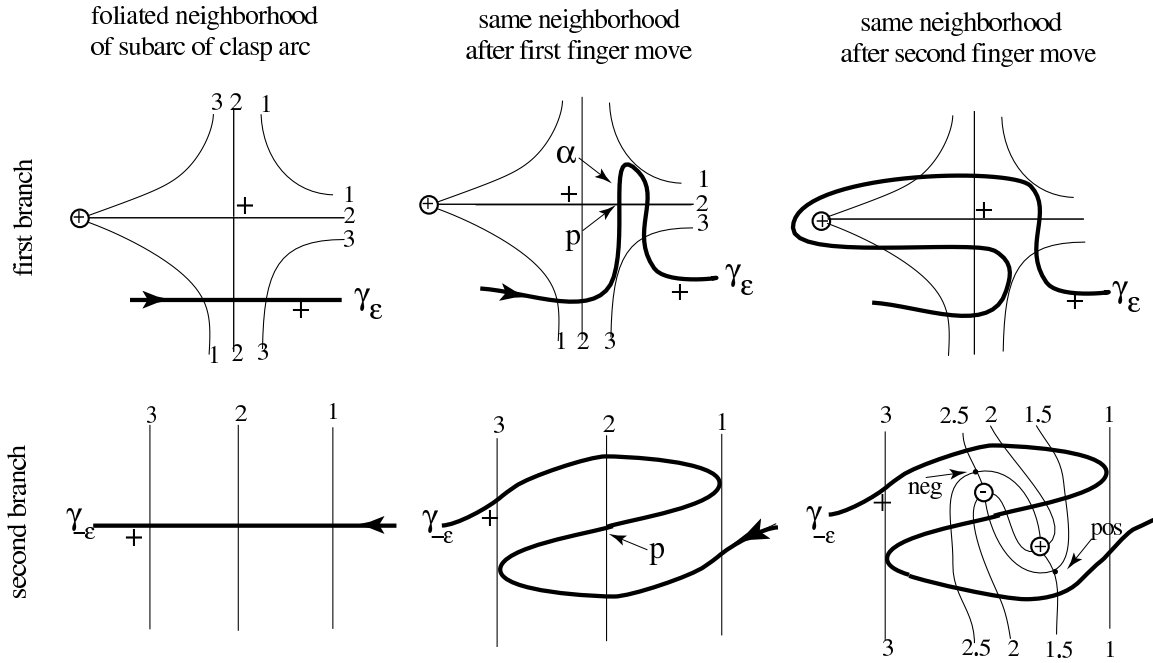


Figure 33: Controlled local changes in the clasp arc in a neighborhood of a singularity

one of the clasp arcs. We give separate pictures of the two foliated branches, N_1 (the *first branch*) and N_2 (the *second branch*). They intersect transversally. By hypothesis the clasp arc (and so also its preimages γ_+ and γ_-) is transverse to the leaves of \mathbf{H} . We have oriented the clasp arc (arbitrarily).

We are interested in modifying the position of one of the clasp arcs in a neighborhood of a singular leaf on one of two branches \mathcal{A}_1 or \mathcal{A}_+ . Since singular leaves correspond to places where one of the two branches is tangent to a fiber of \mathcal{H} , and since the two branches intersect transversally along a clasp arc, we may assume that there is a neighborhood of the singular point in which the other branch is foliated without singularities. The neighborhood has been chosen so that N_2 is foliated without singularities, but N_1 contains a singularity, together with the vertex endpoint of one of the branches of the singular leaf. There are two sign choices: the sign of the vertex and the sign of the singularity. We have chosen these to be $(+, +)$, but in a moment we will consider the 4 possible sign choices. There are also little “+” signs next to the two components of the clasp arcs. They indicate which side of N_2 (resp. N_1) is the positive side, at γ_ϵ (resp. $\gamma_{-\epsilon}$).

Selected fibers H_{θ_i} have labels $i = 1, 2, 3$. The labels on the fibers and the way that γ intersects them and the little + signs next to γ_1 and γ_2 completely determine the position of N in 3-space, relative to the coordinate system provided by the fibers of \mathbf{H} . We are ready to describe our two controlled changes in the clasp arc, and the corresponding changes in the foliation of N_1 and N_2 and in the way that γ_ϵ and $\gamma_{-\epsilon}$ intersect the leaves in the foliation.

Definition 7 (The two finger moves):

1. Our *first finger move*, illustrated in the middle row of Figure 33, pushes γ across the horizontal branch of the singular leaf in the first branch, creating two points where it is not transverse to the fibers of \mathbf{H} , one on fiber 1 and the other on fiber 3. This move is always possible, because it occurs within an arbitrarily small neighborhood of the singularity. The corresponding change

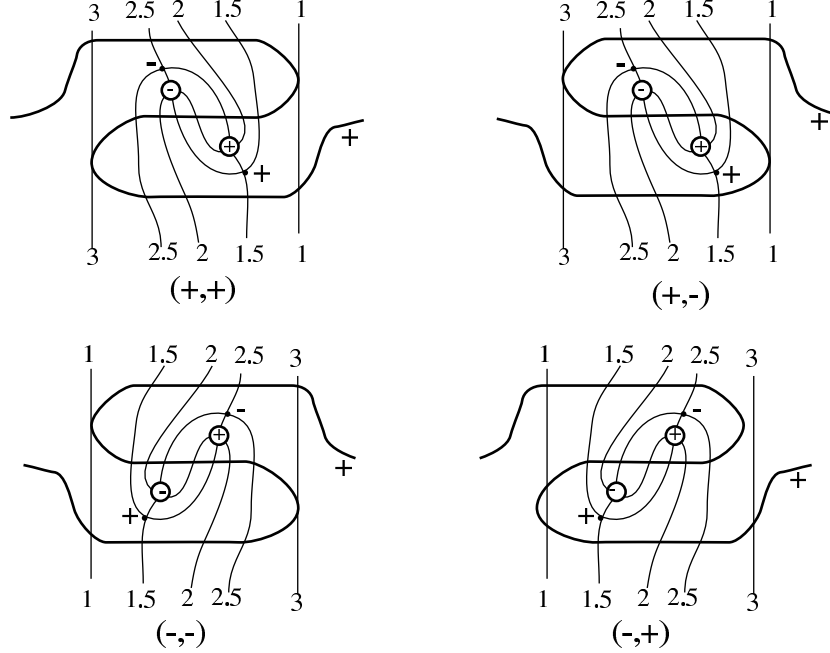


Figure 34: Local changes after the first and second finger moves, for the 4 possible choices of the signs of the pair (vertex,singularity)

in the second branch can be understood by noticing that before the change γ_1 intersected fibers 1,2,3 transversally in that order. After the change there are two points of tangency with fibers of \mathbf{H} , the first with fiber 3 and the second with fiber 1. This explains the doubling back of $\gamma_{-\epsilon}$ after the first finger move.

2. Let α denote the subarc of the clasp arc which is between the two points of non-transversality, and let $p \in \alpha \cap \text{fiber } 2$ be the point which is closest to the singularity on γ_ϵ . The *second finger move*, illustrated in the right column of Figure 33, pushes a neighborhood $N(p)$ of p on α across the singularity and across the vertex, staying within a neighborhood of the singular leaf. The foliation on the first branch is unchanged. The foliation of the second branch changes in an arbitrarily small neighborhood of p on the second branch. Two new vertices of opposite parity and two new singularities of opposite parity are created, as illustrated in the bottom row sketch. \square

The two finger moves are always possible because of their local nature and because of our control over the geometry. We have illustrated the case when the singularity and vertex are both positive. The other three cases differ from this one by local symmetries. See Figure 34 for the local changes with the four possible sign choices for the pair (vertex,singularity).

4.5 Creating symmetric normal neighborhoods of the clasp arcs

Our goal in this section is to obtain more symmetric descriptions of the foliation and the H_θ -sequences, by showing that we may push the clasp arc into the union of two fibers. We start with a definition. See Figure 35 for an example:

Definition 8 (Tab neighborhood pair): Let $\gamma \subset \mathcal{TA}$ be a clasp arc. Let γ_ϵ be either of its preimages in $P(\mathcal{TA})$. Then $\mathcal{T}(\gamma_\epsilon) \subset P(\mathcal{TA})$ is a *tab neighborhood* of γ_ϵ in $P(\mathcal{TA})$ if

- $\partial\mathcal{T}(\gamma_\epsilon) = \alpha \cup \beta$ where $\alpha \subset X_\epsilon$ and β is an arc that is transverse to the foliation of $P(\mathcal{TA})$.
- $\mathcal{T}(\gamma_\epsilon)$ contains a simple path, l_ϵ , which is contained in singular leaves. Moreover, l_ϵ starts on X_ϵ , ends at a vertex of sign ϵ , and contains all k singularities and k vertices of $\mathcal{T}(\gamma_\epsilon)$.
- The arc $\gamma_\epsilon \subset \mathcal{T}(\gamma_\epsilon)$ is the only clasp arc which intersects $\mathcal{T}(\gamma_\epsilon)$. It is everywhere transverse to the leaves in the foliation of $P(\mathcal{TA})$. The arc γ_ϵ intersects each of the k singular leaves in the induced foliation of $\mathcal{T}(\gamma_\epsilon)$ exactly once.

If $\gamma \subset \mathcal{TA}$ is a clasp arc in the total annulus, then (γ_+, γ_-) is a *clasp arc pair* and the pair of neighborhoods $(\mathcal{T}(\gamma_+), \mathcal{T}(\gamma_-))$ in $P(\mathcal{TA})$ is the associated *tab neighborhood pair*. \square

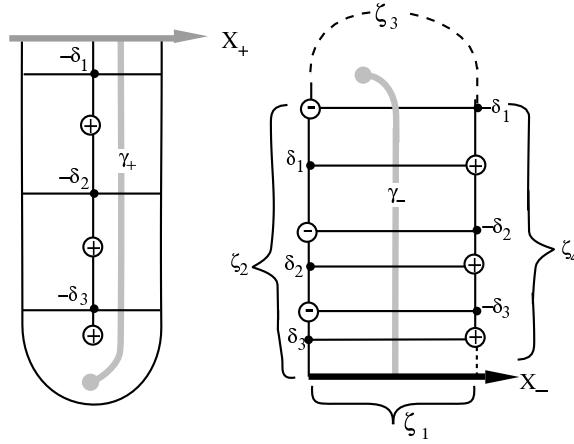


Figure 35: Tab neighborhood pair in $P(\mathcal{TA})$

Lemma 4.4 *We may assume that for each pair of clasp arcs $(\gamma_+, \gamma_-) \subset P(\mathcal{TA})$ there exists a tab neighborhood pair $(\mathcal{T}(\gamma_+), \mathcal{T}(\gamma_-))$. The combinatorial structure of the tab neighborhood pair is as follows:*

- (1) $\mathcal{T}(\gamma_\epsilon)$ contains only vertices of parity $-\epsilon$. The foliation of $P(\mathcal{TA})$ restricted to $\mathcal{T}(\gamma_\epsilon)$ has $k-1$ singularities of type $a_{-\epsilon}a_{-\epsilon}$ followed by one singularity of type $a_{-\epsilon}s$. The latter (by definition belongs to the ‘end tile’. Moreover, considering only this restricted foliation, $\mathcal{T}(\gamma_\epsilon)$ is pierced once by $X_{-\epsilon}$ in its unique end-tile.
- (2) Traversing $\gamma_\epsilon \subset \mathcal{T}(\gamma_\epsilon)$ starting at X_ϵ , if $\{\delta_1, \delta_2, \dots, \delta_k\}$ is the sequence of parities of the singular leaves that γ_ϵ crosses then the corresponding sequence of parities as we traverse $\gamma_{-\epsilon} \subset \mathcal{T}_{\gamma_{-\epsilon}}^{ab}$, starting at the pierce-endpoint, will be $\{-\delta_1, -\delta_2, \dots, -\delta_k\}$.
- (3) Let $e_+e', e'e'', \dots, e' \dots' e_- \subset \gamma_+ \subset \mathcal{T}(\gamma_+)$ be a subdivision of the clasp arc into k subarcs such that each subarc crosses one singular leaf. Then the corresponding induced subdivision given by the immersion \mathcal{TA} of $\gamma_- \subset \mathcal{T}(\gamma_-)$ also has each subarc crossing one singular leaf.

Proof: The underlying strategy for proving the lemma is to make repeated use of the first and second finger moves. Consult Figure 36, which shows the changes we will make as they appear on the tab, and Figure 37, which depicts the corresponding changes on the annulus.

By Lemma 4.2 we know that γ_+ already is contained in a tab neighborhood which we now call $\mathcal{T}(\gamma_+)$. Moreover, Lemma 4.2 tells us that γ_+ is transverse to the leaves of the foliation of $\mathcal{T}(\gamma_+)$, so a sufficiently small foliated neighborhood of γ_- in $P(\mathcal{TA})$ we will also have γ_- transverse to the

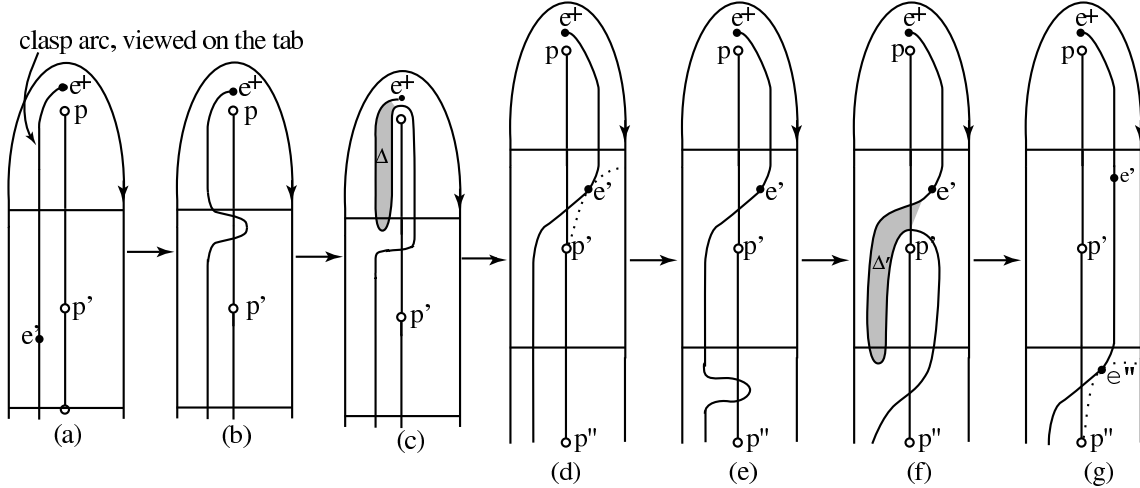


Figure 36: Local changes, as they appear on a typical tab

leaves of the foliation. Some of these leaves intersecting γ_- may be singular. We have labeled them l_1, \dots, l_t in Figure 37. The first change we introduce is to perform the first finger move on a small subarc of γ_+ which is just below the singular leaf in the end-tilde of $\mathcal{T}(\gamma_+)$ across the singular leaf, as in the passage of Figure 36(a) \rightarrow 36(b) and 37(a) \rightarrow 37(b). We next perform the second finger move

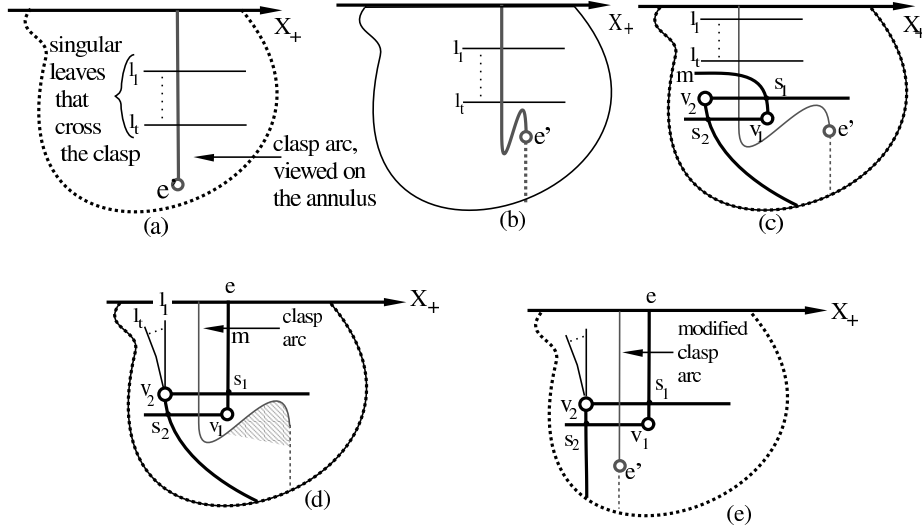


Figure 37: Local changes, depicted on the annulus

as shown in the passage Figure 36(b) \rightarrow 36(c) and the corresponding alteration 37(b) \rightarrow 37(c). It will be helpful to label the two new vertices and singularities introduced by this second finger move as v_0 and v_1 (the vertices) and s_0 and s_1 (the singularities). This second finger move creates a Δ -disc in the tab $\mathcal{T}(\gamma_+)$ whose interior is necessarily embedded because it is on a tab-neighborhood of γ_+ and there is only one clasp arc on each such tab-neighborhood. We use it to do the change in foliation which is given by Lemma 3.6 and Figure 25, where the notation has been chosen so that s_1 in Figure 36(c) and Δ in Figure 37(c) correspond to s_1 and Δ in Figure 25. The singularity s_2 of Figure 25 is not shown on 37(c), also the singularity s_0 of Figure 37(c) is similarly not part of the geometry of

Figure 25. After a series of such changes in fibration the singular leaf which is labeled m in Figure 37(c) will have exchanged order with the leaves l_1, \dots, l_t as illustrated in 37(d). After that the clasp arc can be tightened, resulting in the picture we see in 37(e).

The condition on the signs of the vertices in (1) follows from the fact that a the vertex endpoint of a leaf of the foliation of $P(\mathcal{TA})$ which begins at X_ϵ necessarily has sign $-\epsilon$. But then, the tiles which make up $\mathcal{T}_{\gamma_\epsilon}^{ab}$ are all type $a_{-\epsilon}a_{-\epsilon}$ and never type $a_\epsilon a_\epsilon$.

The point e' in Figure 36(d) is defined to be the point where the deformed clasp arc is tangent to a fiber of \mathbf{H} . Figures 36(b) \rightarrow 36(e) \rightarrow 36(f) \rightarrow 36(g) shows how the argument can be iterated. If there are k tiles on $\mathcal{T}(\gamma_+)$, then after k iterations—finger move 1 followed by finger move 2 followed by a Δ -disc change of fibration—we will have created a tab neighborhood for γ_- . Since we have not moved γ_+ outside of $\mathcal{T}(\gamma_+)$ and since after the final iteration of our Δ -disc change of fibration γ_+ will be transverse to the foliation, we will have created a tab neighborhood pair for (γ_+, γ_-) .

We shall use the sequence ‘finger move 1 followed by finger move 2 followed by a Δ -disc change of fibration’ often enough so that the shorthand notation $FF\Delta$ is appropriate. Our $FF\Delta$ move establishes condition (3). We refer the reader back to the discussion in §4.4, where we introduced the two finger moves, to verify that the parity information of condition (2) is satisfied. \parallel

The next definition introduces a concept which will play a central role in our proof of Theorem 1. The reader may find it helpful to consult Figure 38 as we proceed through the definition of a ‘normal neighborhood’ of a clasp arc in $P(\mathcal{TA})$.

Definition 9 (Normal neighborhood): Let $\gamma_\epsilon \subset \mathcal{T}(\gamma_\epsilon) \subset P(\mathcal{TA})$ be a clasp arc and its associated tab neighborhood, where the latter contains contains k singularities. A neighborhood $N(\gamma_\epsilon)$ of γ_ϵ is a *normal neighborhood* if the following conditions hold:

1. $\gamma_\epsilon \subset \mathcal{T}(\gamma_\epsilon) \subset N(\gamma_\epsilon)$ and $N(\gamma_\epsilon)$ intersects no other clasp arcs.
2. $\partial N(\gamma_\epsilon) = \varphi_1 \cup \varphi_2 \cup \varphi_3 \cup \varphi_4$ where:
 - (a) $\varphi_1 \subset X_\epsilon$.
 - (b) φ_2 is a path contained in one arc of type $a_{-\epsilon}$ and k singular leaves.
 - (c) φ_3 is transverse to the foliation of $P(\mathcal{TA})$.
 - (d) φ_4 is a path contained in k singular leaves and one arc of type b (or type a_ϵ , in the special case when the puncture point on γ_ϵ is near $X_{-\epsilon}$).
3. As a result of condition (2) $\partial N(\gamma_\epsilon)$ contains k vertices of sign $-\epsilon$ (on φ_2) and k vertices of sign ϵ (on φ_4). Each vertex on φ_2 or φ_4 is adjacent to two singular leaves on $\partial N(\gamma_\epsilon)$ and one singular leaf in $\text{int}(N(\gamma_\epsilon))$.
4. $\text{int}(N(\gamma_\epsilon))$ contains k vertices of sign ϵ and k vertices of sign $-\epsilon$ and $2k$ singularities. One vertex of of sign $-\epsilon$ (the ‘end-tile’ vertex of $\mathcal{T}(\gamma_\epsilon)$) is adjacent to three singular leaves of $N(\gamma_\epsilon)$. One vertex of sign ϵ is adjacent to three singular leaves and arcs of type a_ϵ . All other interior vertices are adjacent to four singular leaves.
5. Traversing $\varphi_1 \subset X_\epsilon \cap \partial N(\gamma_\epsilon)$, beginning at the point $\varphi_1 \cap \varphi_4$, we pass through the endpoint of a type $a_\epsilon b$ singular leaf, and end at the X_- endpoint of an a_ϵ leaf. \square

Assume that we are given the tab neighborhood pair $(\mathcal{T}(\gamma_+), \mathcal{T}(\gamma_-))$. Then $(N(\gamma_\epsilon), N(\gamma_{-\epsilon}))$ is a *normal neighborhood pair* associated to the tab neighborhood pair $(\mathcal{T}(\gamma_+), \mathcal{T}(\gamma_-))$ if each $N(\gamma_\pm)$ is a normal neighborhood associated to $\mathcal{T}(\gamma_\pm)$.

Proposition 4.1 *For each clasp arc pair $(\gamma_+, \gamma_-) = (\gamma_+^i, \gamma_-^i)$ we may assume that there is a normal neighborhood pair $(N(\gamma_+), N(\gamma_-))$. Moreover, let $\{\delta_1, \dots, \delta_k\}$ be the sequence of parities of the*

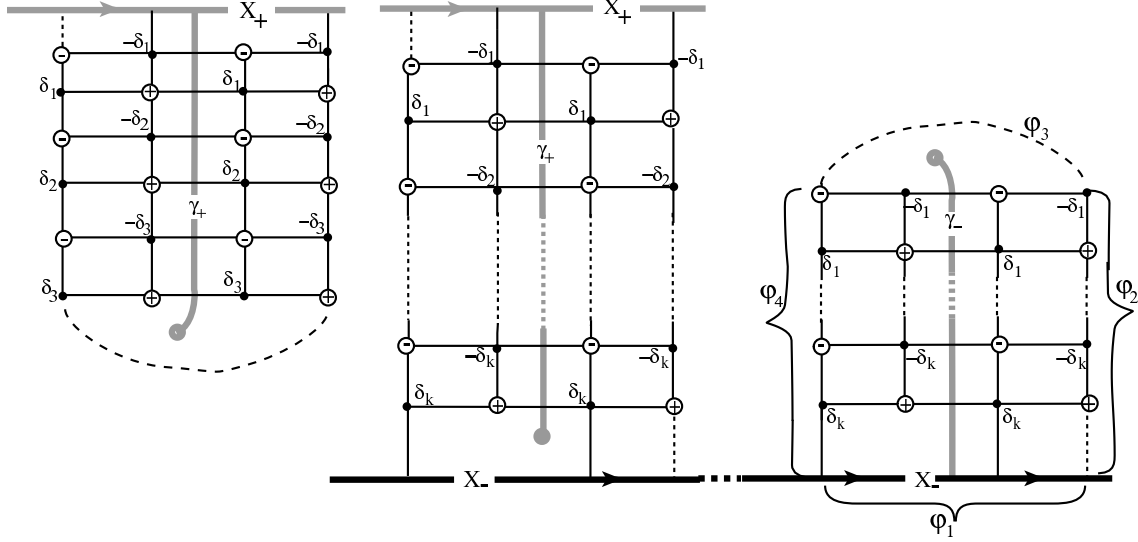


Figure 38: Normal neighborhoods of γ_+ and γ_- in $P(\mathcal{TA})$, up to reflection about a vertical axis. The arc γ_+ ends in the interior of $P(\mathcal{TA})$ in the left sketch and near X_- in the middle case. The right sketch shows $N(\gamma_-)$, which begins on X_- , in both cases.

singular leaves crossed by γ_ϵ . Then $N(\gamma_\epsilon)$ contains disjoint paths $\varrho_1, \dots, \varrho_{2k}$ where: each ϱ_i is contained in the singular leaves of $N(\gamma_\epsilon)$ and contains two vertices and two singularities; traversing γ_ϵ starting at X_ϵ the clasp arc transversally intersects each ϱ_i once and the sequential order of intersection corresponds to the index ordering of the ϱ_i 's; and, for $1 \leq i \leq k$, the singularities in ϱ_{2i-1} have parity δ_i and the singularities in ϱ_{2i} have parity $-\delta_i$.

Proof: The strategy for proving our proposition is to apply the procedure of Lemma 4.4 so as to put a tab neighborhood “inside” a tab neighborhood. To see how this strategy is carried out we first observe that an iterated FF Δ move will always place γ_- inside a foliated neighborhood \tilde{N}_{γ_-} satisfying the following conditions:

- (i) $\partial\tilde{N}_{\gamma_-} = \zeta_1 \cup \zeta_2 \cup \zeta_+ \cup \zeta_4$ with all vertices and singularities of \tilde{N}_{γ_-} contained on $\zeta_2 \cup \zeta_4$.
- (ii) ζ_2 is a path contained in one a_- -arc and k -singular leaves and ζ_4 is a path contained in one a_+ - or b -arc and k -singular leaves.
- (iii) ζ_+ is transverse to the foliation of $P(\mathcal{TA})$.
- (iv) $\zeta_1 \subset X_-$.
- (v) Starting at X_- and traversing ζ_2 we would have the singularity parity sequence $\{\delta_1, \dots, \delta_k\}$ and traversing ζ_4 starting at X_- we would have the singularity parity sequence $\{-\delta_1, \dots, -\delta_k\}$. (Here we assume the parity sequence in $\mathcal{T}(\gamma_+)$ starting at X_+ is $\{-\delta_k, \dots, -\delta_1\}$.)

Figure 38 illustrates our \tilde{N}_{γ_-} neighborhood for the case where $k = 3$. By repeating the procedure of Lemma 4.4 to the (γ_+, γ_-) we can replicate another \tilde{N} neighborhood inside the \tilde{N}_{γ_-} of Figure 38 to produce the normal neighborhood of Figure 38. This places γ_- inside a normal neighborhood $N(\gamma_-)$. Since $N(\gamma_-)$ contains a tab neighborhood $\mathcal{T}(\gamma_-)$ which belongs to a tab neighborhood pair, we can interchange the roles of γ_- and γ_+ to produce a corresponding normal neighborhood for γ_+ . (The main point is that the application of our FF Δ procedure does not move γ_- outside the tab

neighborhood that is nested inside $N(\gamma_-)$). The combinatorics of the normal neighborhoods follows. ||

Now that we have the ability to position any clasp arc pair in a normal neighborhood pair, we wish to allow ourselves the flexibility to be able to push each clasp arc into a finite union of leaves. See Figure 39(c). To accomplish this repositioning, in the general situation which we now face, we

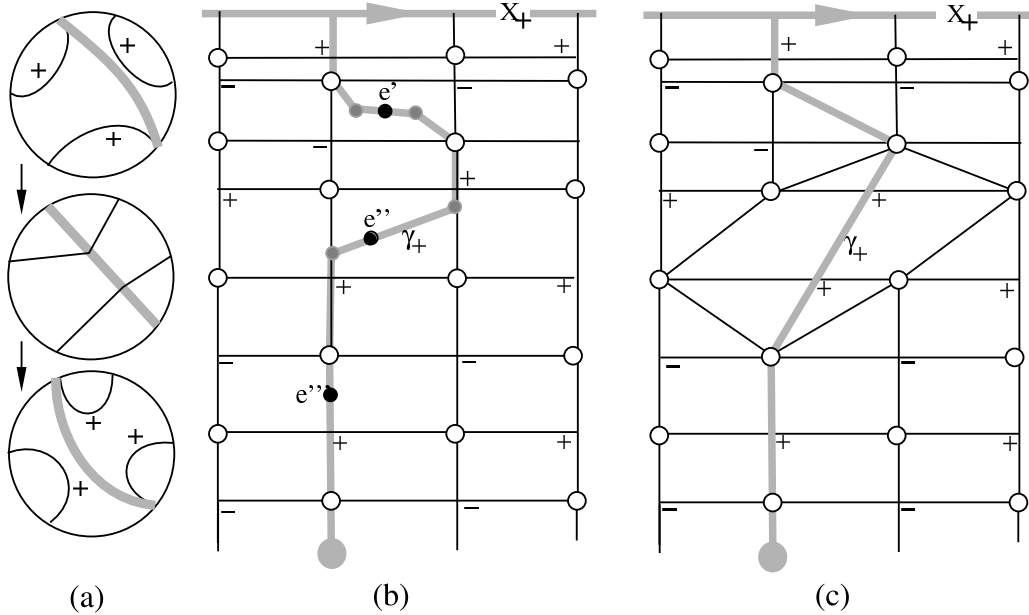


Figure 39: Positioning the clasp arc γ_+ into a finite number of disc fibers

will need to allow for the possibility of singular leaves that contain two singular points as opposed to one. These two-singularity tiles arise naturally from the change of fibration in case (1) of Figure 23. For, as we perform the change of fibration isotopy in Figure 23, case (1), we must pass through a tile having six sides and a two-singularity singular leaf. (This is explained carefully in [4]). The two singular points will always have common parity. Once we allow the use of such tiles in the foliation of $P(\mathcal{TA})$ we can establish the following proposition.

Proposition 4.2 *We may assume that each clasp arc pair is positioned in a finite union of leaves in its normal neighborhood pair.*

Proof: Our procedure for creating normal neighborhood for a clasp arc pair (γ_+, γ_-) creates the conditions necessary for pushing the associated clasp intersection arc into the singular leaves. To see this let us review our construction of the normal neighborhood. Starting with the tab neighborhood pair that is constructed in Lemma 4.4 we observe that each of the subarcs $e^+e', e'e'', \dots, e' \dots' e^- \subset \gamma_+ \subset \mathcal{T}(\gamma_\epsilon)$ in Figure 35 has a single tile neighborhood that corresponds to the foliation of the tiles in Figure 31 and 32 of §4.3. So except for a neighborhood around each $e', e'', \dots, e' \dots'$ in γ_ϵ , we can push γ_ϵ into a finite number of leaves, and the parity of each of these singular leaves is the same as the parity of the pierce end-point of γ_ϵ . Figure 39(b) illustrates an example of a clasp arc having a positive pierce end-point that has been partially pushed into singular leaves. Figure 39(c) illustrates that with the introduction of singular leaves that have two singular points (Figure 39(a)) it is possible to push our clasp arc into a finite union of leaves by pushing the remaining arc neighborhoods of the points $e', e', \dots, e' \dots'$ into leaves of the foliation. ||

4.6 The complexity of the triple (X_-, X_+, \mathcal{TA})

Armed with the results in Proposition 4.1 and 4.2 we are ready to introduce our complexity function. By Proposition 4.1 we know that each clasp arc pair is contained in a normal neighborhood pair. By Proposition 4.2 we may assume that each clasp arc has been pushed into a union of singular leaves. By the methods used in the proof of Lemma 4.2 we know that each clasp arc may be assumed to contain at least one singularity of the foliation, i.e. it is not contained in a collar annular neighborhood which has an induced foliation by only s -arcs or a_+ arcs. Subject to these restrictions, we define the *complexity* $C(X_-, X_+, \mathcal{TA}) = (n_1, n_2, n_3)$ to be a lexicographically ordered 3-tuple, where:

n_1 is the number of singular points contained in clasp arcs, when clasp arcs are positioned to be contained in the finite union of leaves of $P(\mathcal{TA})$.

n_2 is the number of vertices in the tiling of $P(\mathcal{TA})$ that are not in normal neighborhoods.

n_3 is the number of singular points in the foliation of $P(\mathcal{TA})$ that are not in normal neighborhoods.

An example may be helpful. Referring back to Figure 30, let's compute the complexity of \mathcal{TA} . Since the discs in (a) and (d) are contained entirely in normal neighborhoods they contribute only to n_1 . So $n_1 = 8, n_2 = 8, n_3 = 8$. The realization of the motion of X_- across the thinly foliated annulus of Figure 30 was given in the introduction to this paper, in Figure 9. The sequence of motions consisting of an inadmissible flype, two exchange moves (actually four, because each uses weighted strands) and an admissible flype is exhibited by running around the diagram clockwise in Figure 9. At this time we have not yet made the complete connection between the braid motion and the foliation, even in this simple example, however it will be possible to explain it anyhow. The motion begins with an inadmissible flype, which is indicated in Figure 30 as a push of X_- across part of the annulus to the two dotted arcs in discs (b) and (c). This motion is matched by a related motion in regions (a) and (d). It reduces n_1 from 8 to 4. In Figure 9 it can be seen as the inadmissible flype which changes the braid index of the block-strand diagram from a 6-braid to a 7-braid. After this motion, two ab exchange moves become possible. Using our earlier explanation of ab exchange moves, in Figure 18 the reader should be able to see them in discs (b) and (c) of Figure 30. This reduces n_2 and n_3 to 0. After the exchange moves the new X_- is in the position for another flype, bringing n_1 down to zero. Thus the entire motion (which is an example of a G-flype) reduces complexity and is non-increasing on braid index.

4.7 Standardizing the foliation of \mathcal{TA} and $P(\mathcal{TA})$

We turn our attention to the standardization of the foliation of \mathcal{TA} and $P(\mathcal{TA})$ in the complement of the normal neighborhoods of the clasp arcs. A vertex is said to be *near* X_ϵ if it is the endpoint of a leaf of type $a_{-\epsilon}$ in the foliation of $P(\mathcal{TA})$. An *interior vertex* is a vertex which is not near either X_- or X_+ . If v is an interior vertex, we define $link(v)$ be the closure of the union of all b-arcs which meet v .

We introduce further terminology. Specify two closed braids X, X' to be *exchange-equivalent* if they are equivalent under the exchange moves which were defined in Lemmas 3.3. This is an equivalence relation on the collection of all closed n -braid representatives of a single link type. We now make the assumption that the exchange-equivalence class of X_- does not contain a representative which bounds a Markov surface having an a_+a_+ tile with a vertex of valence 1. Call such an exchange-equivalence class an *irreducible* class. Call a class which is not irreducible a *reducible* class. Note that this does not rule out the possibility that there are flypes which either reduce braid index of X_- or take a member of an irreducible class to a reducible class. We mention this because it differs from our assumption on X_+ , namely that its braid index is minimal for all closed

braid representatives of its link type. Of course that assumption implies that X_- does not admit a destabilization.

We will be working with the 4 graphs $G_{+,+}, G_{+,-}, G_{-,-}$ and $G_{-,+}$ which were introduced in Section 3.5 of this paper. See, in particular, Figure 26. Given a subdisc $\Delta \subset P(\mathcal{TA})$ and a clasp arc γ_ϵ we say that γ_ϵ intersects Δ *transversally* if when γ_ϵ is positioned in a finite number of singular leaves each component of $\gamma \cap \Delta$ is contained in a component of $\Delta \cap G_{\epsilon,\delta}$. In particular, inside Δ , γ_ϵ is never pushed into an a_ϵ - or b -arc and no singular leaf having two singularities is created when γ_ϵ is positioned in a finite number of singular leaves.

If v is an interior vertex we define $link(v)$ to be the closure of the union of all b -arcs which meet v . If v is a non-interior vertex we define $link(v)$ to be the closure of the union of all b -arcs and a_ϵ -arcs which meet v .

Definition 10 (Good disc): We say that $link(v)$ is *good* if it does not contain the puncture end-point of a clasp arc and if every clasp arc which intersects it, intersects it transversally. More generally, a subdisc of $P(\mathcal{TA})$ is *good* if it does not contain the puncture end-point of a clasp arc and if any clasp arc that intersects it does so transversally. \square

Our initial goal is to place restrictions on the foliation of $P(\mathcal{TA})$, under the assumptions that (X_+, X_-, \mathcal{TA}) is minimal and that we are working in regions which are good.

Our next result is an adaptation of Lemma 3.5 of [4] to $P(\mathcal{TA})$. To reiterate our assumptions on the triple (X_+, X_-, \mathcal{TA}) , we assume that the closed braid X_- belongs to an irreducible exchange-equivalence class. Also, the closed braid X_+ is of minimal braid index. Moreover (so that the graphs $G_{\epsilon,\delta}$ are well defined in $P(\mathcal{TA})$) we assume that the clasp arcs are positioned in the normal neighborhoods to be transverse to the foliation of $P(\mathcal{TA})$. When our discussion is not centered on $G_{\epsilon,\delta}$ this transversality assumption can be replaced by the assumption that the clasp arcs are contained in a finite number of leaves of the foliation.

We will use the symbol $N(\gamma_\epsilon)$ for a normal neighborhood of the clasp arc γ_ϵ and the symbol \mathcal{N} for $\bigcup_{\gamma_\epsilon} N(\gamma_\epsilon)$.

Lemma 4.5 *Let (X_+, X_-, \mathcal{TA}) be of minimal complexity. We may assume the behavior of the $G_{\epsilon,\delta}$ graphs in $P(\mathcal{TA})$ satisfy the following conditions:*

1. $G_{\epsilon,\delta} \cap G_{-\epsilon,-\delta} = \emptyset$.
2. *Every singular point and every vertex in the foliation of $P(\mathcal{TA})$ is in $G_{+,+}$ or $G_{-,-}$ (and also in $G_{+,-}$ or $G_{-,+}$.)*
3. $G_{\epsilon,\delta}$ has no interior isolated vertex v .
4. $G_{\epsilon,\delta} \setminus (G_{\epsilon,\delta} \cap \mathcal{N})$ has no interior endpoint vertex v .
5. $G_{\epsilon,\delta}$ contains no closed loop l which bounds a good disc $\Delta \subset P(\mathcal{TA})$.
6. *There is no closed loop l which is the union of an edgpath $\mathcal{E}_1 \subset G_{\epsilon,+}$ and an edgpath $\mathcal{E}_2 \subset G_{\epsilon,-}$ which bounds a good disc $\Delta \subset P(\mathcal{TA}) \setminus \mathcal{N}$.*
7. *Let E_1, E_2, E_3 be connected arcs, with $E_1 \subset G_{\epsilon,\epsilon}$, $E_2 \subset G_{\epsilon,-\epsilon}$, $E_3 \subset X_\epsilon$. Then there is no closed loop $l = E_1 \cup E_2 \cup E_3$ or $E_2 \cup E_3$ or $E_1 \cup E_3$ which bounds a good disc Δ on $P(\mathcal{TA})$.*

Remarks: Our definition of the complexity 3-tuple (n_1, n_2, n_3) and of a good disc has been chosen so that, if we can achieve the modifications of parts (5), (6) and (7) of the Lemma, then our task will be to seek ways to modify X_- so that we can use the Lemma to reduce n_1 if a good disc exists inside the normal neighborhoods, and to reduce n_2 and n_3 if a good disc exists outside the normal neighborhoods. These ideas will be developed in detail in Section 5 below.

Proof: The proof is a straightforward generalization of the proof of Lemma 3.8 of [4] to our immersed annuli. The key fact which makes it possible to carry over arguments used in [4] is the concept of a good disc. Comparing with [4] we note that some of the statements have been simplified because of our assumption that the complexity is minimal. The change in notation from that in [4] has to do with the fact that in [4] all of the boundary components of \mathcal{F} were oriented in a fashion which was consistent with the orientation on \mathcal{F} , whereas one of the boundary components on each of our annuli is ‘wrongly oriented’.

1. Follows directly from the definition of the graphs.
2. Follows directly from the definition of the graphs.
3. Notice that the $link(v)$ of any vertex is an embedded disc. Thus, this is a statement about all embedded discs that are links of an interior vertex. We can therefore appeal to the proof which was given in [4]. We repeat it here, because later we will need it under somewhat different conditions and it will be helpful to see the details worked out. We are given a vertex $v \in G_{\epsilon, \delta}$. If we can prove that singular points of both signs necessarily occur in $link(v)$, then it will follow that v cannot be an isolated vertex. Let v_1, v_2, \dots, v_r be the vertices in $link(v)$, ordered so that their cyclic order on the oriented braid axis \mathbf{A} is v, v_1, v_2, \dots, v_r . That is, v_1 is the first vertex which is encountered if one starts at v and travels along the oriented braid axis \mathbf{A} in the positive direction. The vertices v_1, \dots, v_r all have sign $-\epsilon$ because v is an interior vertex of sign ϵ , therefore each pair v, v_i are opposite endpoints of a b -arcs in every non-singular fiber. The vertices v_1, \dots, v_r also have a second order, in the flow around v . Traveling around v in the direction of increasing polar angle, let $v_0 \in \{v_1, \dots, v_r\}$ be the vertex which occurs just before v_1 , and let s be the singular point in $link(v)$ which is between v_0 and v_1 . Choose a non-singular fiber H_{θ_1} which contains a b -arc β_1 joining v to v_1 . The arc β_1 divides H_{θ_1} into two half-discs, which we call $H_{\theta_1}^+$ and $H_{\theta_1}^-$, where the signs are chosen so that $H_{\theta_1}^+$ is the half-disc of H_{θ_1} which meets the side of \mathcal{F} which has sign ϵ . The fact that the order of the vertices on \mathbf{A} is v, v_1, \dots, v_r then implies that the vertices v_2, \dots, v_r are all on the $\partial H_{\theta_1}^{-\epsilon}$ part of \mathbf{A} .

The sign of a singularity has natural meaning when it is examined in a sequence of fibers of \mathbf{H} , namely: when the singularity has sign ϵ the sides of $\mathcal{F} \cap H_\theta$ of sign $-\epsilon$ approach one-another on H_θ just before the singularity and then split apart in a new way. This means that, if we follow the flow around v , the first singularity occurring after β_1 must have sign ϵ , for if not β_1 would surger with a b -arc having an endpoint on $\partial H_{\theta_1}^\epsilon$, but since v_2, \dots, v_r are on $\partial H_{\theta_1}^{-\epsilon}$, this is impossible. Now, s is the singular point in $link(v)$ which occurs between v_0 and v_1 . Thus, if β_0 and β_1 are b -arcs joining v to v_0 and v_1 , respectively, then β_0, s, β_1 have that order in the fibration. When viewed on a sequence of fibers of \mathbf{H} , we see that the singularity at s results in the creation of the b -arc β_1 , and that just before this singularity occurs there is a non-singular fiber H_{θ_0} containing the b -arc β_0 . The fact that v has sign ϵ forces v_0 to have sign $-\epsilon$, because v and v_0 are the two endpoints of a b -arc. This means that the oriented axis \mathbf{A} intersects the $-\epsilon$ side of \mathcal{F} first at v_0 . It follows that v_1 must be on the $-\epsilon$ side of H_{θ_0} split along β_0 . But then, the sign of the singularity at s must be $-\epsilon$. This proves assertion (3).

We interrupt the argument briefly to establish the modifications we will need to use exchange moves and changes of fibration of (see §3.3 and §3.4) in the presence of clasp arcs. Our arguments will use the complexity function $C(X_-, X_+, \mathcal{TA})$. In this regard we note: if the tab neighborhood of a clasp arc can be altered so that it contains fewer singular points, then n_1 can be reduced. The procedure that we used to change the tab neighborhoods to normal neighborhoods can then be applied to produce a new triple (X_-, X_+, \mathcal{TA}) with reduced complexity. With this in mind, the descriptions of our exchange moves and changes in foliation will be from the point of view of alterations to the tab neighborhoods.

Exchange Moves. Assume that v is a vertex of valence 2 in the tiling of $P(\mathcal{TA})$, and that the singularities s_+, s_- in $link(v)$ have opposite parity. Assume that $link(v)$ is good. If $link(v)$ has empty intersection with the clasp arcs, then we may use the standard exchange moves of §3.3 to reduce complexity. This will reduce n_2 and n_3 of our complexity measure, but by hypothesis complexity is minimal. Therefore we may assume that there is a clasp arc γ which intersects $link(v)$. By definition of a good disc we know that $link(v)$ does not contain the puncture endpoint of a clasp arc. Since we have two types of exchange moves, i.e. type bb and type ab , we have two possible situations to deal with. In both cases, the elimination of a valence 2 vertex will be seen to reduce $C(X_-, X_+, \mathcal{TA})$.

- (bb)^{*} *Eliminating an interior valence 2 vertex, v , when $link(v)$ is good.* See Figure 20. By our definition of a good disc, if there is a clasp arc γ that transversally intersects $link(v)$ then the tab neighborhood of γ must contain only one of the two singularities of $link(v)$, say s_+ , and the two vertices $u, w \in link(v)$ with $u \neq v, w \neq v$. We can then position γ so that inside its tab neighborhood it is transverse to the foliation and $\gamma \cap link(v) = \emptyset$. Using the standard (bb) exchange move, followed by the elimination of inessential b -arcs, we can eliminate v , reducing complexity.
- (ab)^{*} *Eliminating a non-interior valence-2 vertex w , when $link(w)$ is good.* See Figure 22. If there is a γ transversally intersecting $link(v)$ then the tab neighborhood of γ must contain one of the singular points of $link(v)$ and the single vertex w of $link(v)$ that is not v . As before, we can position γ to be transverse to the foliation of its tab neighborhood and have $\gamma \cap link(v) = \emptyset$. We can then position γ so that inside its tab neighborhood it is transverse to the foliation and $\gamma \cap link(v) = \emptyset$. Now, eliminating v through the use of the standard ab exchange move will eliminate one vertex and singularity from the tab neighborhood of γ . This will reduce complexity.

Change of Foliation. Referring to Figure 23, we have the following three cases.

- C_1 *One of the two singularities is contained in a tab neighborhood of a clasp arc.* After the change in fibration, the path of the clasp arc is unchanged. For example, if $\epsilon = +$ and the symmetric clasp arc contains s_1 (resp. s_2) in each of the three cases in Figure 23 then we have a change of fibration that takes us to the first (resp. second) choice of the two possible change of fibrations.
- C_2 *Both s_1 and s_2 are contained in a single tab neighborhood as consecutive singularities of a clasp arc.* After the change of fibration, the path of the clasp arc contains one fewer singularity, so $C(X_-, X_+, \mathcal{TA})$ is reduced. In particular, if $\epsilon = +$ and we have a symmetric clasp arc then the resulting change of fibration is the second choice in all three cases of Figure 23 and the clasp arc contains the two right-most positive vertices and the right-most singular point in these choices. If $\epsilon = -$ and we have a symmetric clasp arc then the resulting change of fibration is the left (first) choice in all three cases of Figure 23 and the clasp arc contains the two left-most negative vertices and the left-most singular point in these choices. (The related situation for skew-symmetric clasp arcs is obvious.)
- C_3 *The two singularities are contained in disjoint tab neighborhoods of different clasp arcs.* The path of the two clasp arcs is unchanged by the change in foliation. For example, if $\epsilon = +$ and the bottom singularity was contained in a symmetric clasp arc for all three beginning tilings in the sequences in Figure 23 then the resulting change of foliation is the second (right) choice in all three cases.

The groundwork has been laid and we are now ready to prove the remaining assertions in Lemma 4.5.

4. To prove (4), suppose that v is an interior endpoint vertex of $G_{\epsilon,\delta}$ that is not in \mathcal{N} . By (3) above v cannot be an isolated vertex, so v is the endpoint of at least one edge e of $G_{\epsilon,\delta} \setminus (G_{\epsilon,\delta} \cup \mathcal{N})$. The fact that v is an endpoint vertex implies that every vertex in $\text{link}(v)$ except v and the other vertex endpoint of e is in $G_{-\epsilon,-\delta}$. Using changes in foliation (either those in Figure 24, or C_1, C_2, C_3), we reduce the valence v until it is of valence 2. The singularities must have opposite signs $(+, -)$, for if not v would not be an endpoint vertex, also v has type (b, b) or (a, b) . But then, we may eliminate it by either the classical bb or ab exchange moves of Lemma 3.3, or by moves $(bb)^*$ or $(ab)^*$. But that is impossible, because of our assumption of minimum complexity.
5. Suppose that one of the graphs $G_{\epsilon,\delta}$ contains a closed loop l which bounds a good disc Δ on the immersed annulus. Without loss in generality we may assume that l is innermost. Since every vertex and every singularity in the foliation is in either $G_{\epsilon,\delta}$ or $G_{-\epsilon,-\delta}$ it follows that these two graphs meet the interior of Δ in a union of isolated vertices and tree components. By (4) we may assume that there are no tree components. Thus the only possibility is a collection of isolated vertices. This collection cannot be empty because there is no way to have a closed loop in $\partial\Delta$ without having at least one vertex in the interior of Δ . But that is impossible, by (3) above.
6. If (6) occurs, then by (3) we know there are no isolated vertices in the interior of Δ and by (4) we know there are no trees. So the only possibility is that the interior of Δ contains a single vertex of sign $-\epsilon$. But then, by Lemma 3.3, X_1 admits an exchange move of type (b, b) or $(bb)^*$ and we can use it to reduce the complexity. But that is impossible.
7. The proof of (7) is slightly more complicated, but the ideas are the same as those used already. We refer the reader to the proof of Theorem 3.1 of [4] for details, and content ourselves with two key examples which illustrate the main ideas in the proof. See Figure 40. In sketch (a)

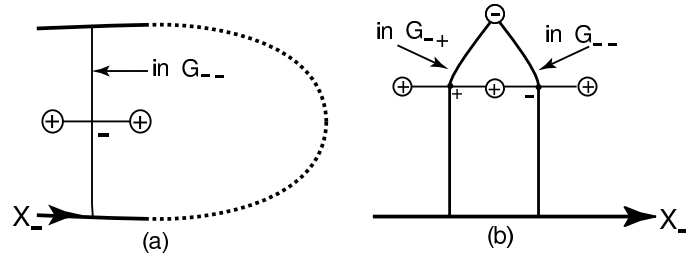


Figure 40: Examples needed for the proof of Lemma 4.5, part (7)

$l = E_1 \cup E_3$. The existence of the separating leaf shows that X_ϵ admits a destabilization, contradicting our assumption about minimum complexity. In sketch (b) $l = E_1 \cup E_2 \cup E_3$ and X_- admits an ab exchange move, again contradicting minimum complexity. In more general examples we can reduce to these cases by the use of changes in foliation and exchange moves. The key fact is that the hypothesis that we are working with good discs allows us to apply all the ideas used in the proof of Theorem 3.1 of [4]. \parallel

Proposition 4.3 *The following are consequences of Lemma 4.5 and of our assumption of minimum complexity:*

1. There are no $a_\epsilon s$ or $a_\epsilon a_\epsilon$ singularities in $P(\mathcal{TA})$.

2. Suppose that $\alpha \subset G_{\epsilon, \delta}$ is a path with $\partial\alpha \in X_\epsilon$. Let Δ be the disc on $P(\mathcal{TA})$ which is split off by α . Then $\text{int}(\Delta)$ contains a puncture end-point of a $\gamma_{-\epsilon}$ clasp arc.
3. Suppose that $\alpha \subset G_{\epsilon, \delta}$ is a loop bounding a disc Δ in $P(\mathcal{TA})$. Then $\text{int}(\Delta)$ contains at least two puncture end-points of clasp arcs, one from γ_ϵ^i and one from $\gamma_{-\epsilon}^i$. In particular, both endpoints are associated with the same clasp intersection in \mathcal{TA} .
4. If $v \in G_{\epsilon, \delta}$ is an endpoint vertex, then either $\text{link}(v)$ contains a puncture endpoint of a clasp arc or v lies in a normal neighborhood of a clasp arc.

The remainder of our results in this subsection will deal with the special case where $n_1 = 0$. This special case implies that, after a small isotopy of X_- in the complement of \mathbf{A} we may assume that \mathcal{TA} is embedded and every subdisc of $P(\mathcal{TA})$ is good.

Corollary 1 *Assume $n_1 = 0$. Suppose that $\alpha_1 \subset G_{\epsilon, \delta}$ and $\alpha_2 \subset G_{\epsilon, -\delta}$ are edgpaths having their endpoints on $X_{-\epsilon}$ (resp. near X_ϵ). Then $\alpha_1 \cap \alpha_2 = \emptyset$.*

Proof: Statement (6) of Lemma 4.5 asserts that $\alpha_1 \cup \alpha_2$ cannot cut off a good disc on $P(\mathcal{TA})$, and since we have assumed that $n_1 = 0$ this means that they cannot cut off any disc, so if $\alpha_1 \cap \alpha_2 \neq \emptyset$ then they intersect transversally at most once. This point of intersection will necessarily be a vertex p of parity ϵ .

Let $x_i \cup y_i = \partial\alpha_i$, $i = 1, 2$. First, consider the case when $x_1, x_2, y_1, y_2 \in X_{-\epsilon}$. Consider the path in $\alpha_1 \cup \alpha_2$ that starts at x_1 , travels along α_1 until p is reached, and then travels along α_2 until y_2 is reached, splits off a subdisc of \mathcal{TA} containing the points x_2 and y_1 . The subdisc necessarily contains three subdiscs whose boundaries satisfy the assumptions of statement (7) of Lemma 4.5. Namely:

- Δ_1 with $\partial\Delta_1 = l_1^1 \cup l_2^1 \cup l_3^1$ where $l_1^1 = x_1p \subset \alpha_1$, $l_2^1 = px_2 \subset \alpha_2$, $l_3^1 = x_1x_2 \subset X_{-\epsilon}$.
- Δ_2 with $\partial\Delta_2 = l_1^2 \cup l_2^2 \cup l_3^2$ where $l_1^2 = l_2^1$, $l_2^2 = py_1 \subset \alpha_1$, $l_3^2 = x_2x_1 \subset X_{-\epsilon}$.
- Δ_3 with $\partial\Delta_3 = l_1^3 \cup l_2^3 \cup l_3^3$ where $l_1^3 = l_2^2$, $l_2^3 = py_2 \subset \alpha_2$, $l_3^3 = y_2y_1 \subset X_{-\epsilon}$.

Next, assume that $x_1 \cup y_1$ and $x_2 \cup y_2$ are near X_ϵ . We can extend these two paths along a_ϵ -arcs to produce paths that has their boundary on X_ϵ . We denote these extensions by α_1^ϵ and α_2^ϵ . Let the endpoints $x_1^\epsilon \cup y_1^\epsilon = \partial\alpha_1^\epsilon$ and $x_2^\epsilon \cup y_2^\epsilon = \partial\alpha_2^\epsilon$ that are on X_ϵ be labeled such that, modulo the superscript for ‘extension’, we have the boundaries of the three subdiscs $\Delta_i, i = 1, 2, 3$ as before with the exception that $l_3^1, l_3^2, l_3^3 \subset X_\epsilon$. Now consider the subdisc Δ_2 and notice that there are two possibilities: Δ_2 contains a a_ϵ -arc that is adjacent to the vertex p ; or Δ_2 contains an b -arc that is adjacent to p .

To deal with the first possibility, let a be an a_ϵ -arc adjacent to p . Then a further splits Δ_2 into two subdiscs, Δ_2' and Δ_2'' where $l_1^2 \subset \Delta_2'$ and $l_2^2 \subset \Delta_2''$. Since (5) of Lemma 4.5 tells us there are no interior endpoints of our graphs we know that all endpoints of $G_{-\epsilon, -\delta} \cap \Delta_2' \subset \Delta_2'$ are on X_ϵ . If $G_{-\epsilon, -\delta} \cap \Delta_2' \neq \emptyset$ then we will have Δ_2' containing a subdisc that satisfies the assumptions of (7) of Lemma 4.5. But this subdisc will be good since $n_1 = 0$ so it cannot exist.

Finally, suppose we have Δ_2 containing an b -arc that is adjacent to p . Let p' be the vertex endpoint of this b -arc that is in the interior of Δ_2 . Since by (5) of 4.5 we cannot have an interior endpoint of our graphs, there must be a component of $G_{-\epsilon, \delta}$ and a component of $G_{-\epsilon, -\delta}$ that transversally intersect each other at p' . These two component will then have to have endpoints on X_ϵ . Thus, Δ_2 will contain a further good subdisc that satisfies the assumptions of (7) of 4.5—a contradiction of minimal complexity. Therefore our assumption that $\alpha_1 \cap \alpha_2 \neq \emptyset$ must be wrong. \parallel

We are ready to formulate the consequences of our standardization of the foliation of $P(\mathcal{TA})$.

Definition 11 Standardly tiled annulus): An annulus component of $P(\mathcal{TA})$ is *standardly tiled* if every component $C \subset G_{\epsilon, \delta}$ on the annulus satisfies the following conditions:

1. C is homeomorphic to either S^1 or $[0, 1]$, i.e. either a circle or a line.
2. If C is a circle then it is a core circle of the annulus component.
3. If C is a line with $\partial C = p \cap p'$ then $p \in X_\epsilon$ and p' is near $X_{-\epsilon}$. \square

An example is given in Figure 41 of a standardly tiled annulus component of $P(\mathcal{TA})$.

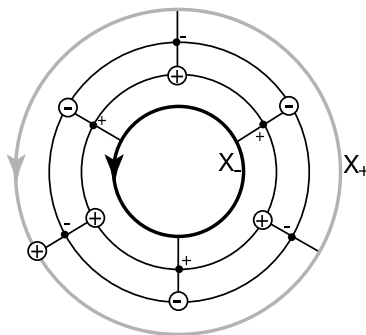


Figure 41: An example of a standardly tiled annulus component of $P(\mathcal{TA})$. There are no clasp arcs.

Corollary 2 *Let (X_+, X_-, \mathcal{TA}) be of minimal complexity with $n_1 = 0$. Then each component of $P(\mathcal{TA})$ is either an annulus which is foliated entirely with s -arcs or a standardly tiled annulus.*

Proof: The statement follows directly from Corollary 1. \parallel

Remark: We will see later (peek ahead to Section 5.2) that if there is a standardly tiled component, then we can isotopy X_- to X_+ by a sequence of handle moves. This will have the effect of settling the case when there is a component of X_- whose associated annulus contains no clasp arcs. Anticipating this fact, our argument in the material that precedes Section 5.2 will focus on the case when every clasp arc contains at least 1 singularity of the foliation.

5 Proof of the MTWS.

The machinery which we need to prove the MTWS has been set up. In this section we present our proof. While we have been able, up to now, to make the tacit assumption that we are working with knots, we now return to the general case of links. With regard to the foliation of $P(\mathcal{TA})$ we assume:

1. Every clasp arc is contained in a normal neighborhood (Proposition 4.1)
2. Every clasp arc γ_ϵ has been pushed into a sequence of leaves of the foliation, in its normal neighborhood (Proposition 4.2). The vertices in this sequence of leaves have sign $-\epsilon$.
3. The complexity $C(X_-, X_+, \mathcal{TA}) = (n_1, n_2, n_3)$ is minimal.

Theorem 1 is stated in terms of moves on block diagrams of closed braids. Our principle tool, however, is the structure which we find in braid foliations of the immersed annulus \mathcal{TA} and its preimage $P(\mathcal{TA})$. The main task that is ahead of us is to relate these two, showing that the moves which we use to push X_- across the foliated annulus \mathcal{TA} to X_+ correspond to the destabilizations, exchange moves, flypes and G-handle moves which are given in the statement of the MTWS.

In Section 5.1 we will see how we use flypes (a move on block diagrams) to reduce the entry n_1 in the complexity triple when ‘long clasp arcs’ occur. In Section 5.2 we will see how G-handle moves

(eventually defined in terms of templates) can be used to eliminate clasp arcs which are not long. After we have eliminated all clasp arcs from the foliation we will be in the situation of Corollary 2. The annulus will be embedded and standardly tiled. It will then be easy to complete the proof of parts (a) and (b) of the MTWS. A separate argument will be needed to prove parts (c) and (d).

5.1 The role of flypes

Definition 12 (Long and doubly long clasp arcs): The clasp arc $\gamma \subset \mathcal{TA}$ has two preimages in $P(\mathcal{TA})$, γ_+ and γ_- . By our conventions γ_ϵ , $\epsilon = \pm$, begins on X_ϵ and ends at an interior point of $P(\mathcal{TA})$. We say that γ is *long* if the puncture endpoint of $\gamma_+ \subset P(\mathcal{TA})$ is near X_- . Note that this does not necessarily imply that the puncture endpoint of γ_- is near X_+ . The asymmetry between the roles of γ_+ and γ_- originates in the fact that we are trying to push X_- across \mathcal{TA} to X_+ , not X_+ to X_- . We say that γ is *doubly long* if it is long and if the puncture endpoint of γ_- is near X_+ . The *length* of a long or doubly long clasp arc is the number of singular leaves which γ_+ crosses. If long clasp arcs occur, then the integer n_1 in our complexity triple is necessarily > 0 . \square

Our task in this section is to learn how to use flypes to shorten the length of long (but not necessarily doubly long) clasp arcs in the foliation of $P(\mathcal{TA})$, thereby reducing the integer n_1 in the complexity triple (n_1, n_2, n_3) . We have already seen that in the situation where there is exactly one clasp arc, we may use a microfype to push X_- across the immersed annulus \mathcal{TA} . The situation which we face now has two factors which make it significantly more complicated. The first is that we must allow for the possibility that there are $k \geq 1$ clasp arcs. The second is that if X_- has μ components, then \mathcal{TA} will be the image of μ annuli under an immersion, and we must allow for the possibility of clasp intersections between distinct annuli.

5.1.1 Constructing the thinly foliated annuli

Preparing for the shortening of long clasp arcs, we will construct a family \mathcal{S} of ‘thinly foliated annuli’ which is a subset of $P(\mathcal{TA})$. If X_- has μ components, there will be μ annuli in \mathcal{S} , each with a component of X_- as one of its boundary components and a simple closed curve in the interior of \mathcal{TA} which is transverse to the foliation as its opposite boundary component. The union of the interior boundaries will be an intermediate μ -component link which we call X'_+ . We will show how to use flypes to push X_- across \mathcal{S} to X'_+ . Since \mathcal{S} is a subset of $P(\mathcal{TA})$ which contains singularities intersected by long clasp arcs, this will shorten the long clasp arcs and reduce complexity. Our goal in this subsection is to construct \mathcal{S} . We will prove:

Lemma 5.1 *Suppose that $P(\mathcal{TA})$ contains a long clasp arc γ_+ . Then there exists a family \mathcal{S} of μ annuli, each a subannulus of $P(\mathcal{TA})$, and each with a component of X_- as one of its boundaries, such that every annulus in \mathcal{S} is either trivially foliated by s -arcs or has a foliation satisfying the following:*

- (i) *Each annulus contains at least one long clasp arc. Moreover, all of its clasp arcs are doubly long and of length 1.*
- (ii) *After an isotopy of $P(\mathcal{TA})$ which leaves X_- and the other components of $\partial\mathcal{S}$ fixed, each b -arc in \mathcal{S} may be assumed to have at least one of its endpoints on a clasp arc.*

Proof: Let γ^i be a long clasp arc. Then γ^i_+ begins on X_+ and ends near X_- . Let $N(\gamma^i_+)$ be its normal neighborhood. We focus our attention on the subrectangle $N^i_+ \subset N(\gamma^i_+)$. See the two left sketches in Figure 42. It is a subset of $N(\gamma^i_+)$, which coincides with $N(\gamma^i_+)$ when the clasp arc has length 2. It has three edges which are in $\partial N(\gamma^i_+)$. We choose an arc which is transverse to the foliation as its other ‘horizontal’ boundary. This arc will eventually be a subarc of the X'_+ boundary of \mathcal{S} and our labels anticipate this. Let $g^i_+ = \gamma^i_+ \cap N^i_+$. There are corresponding subrectangles

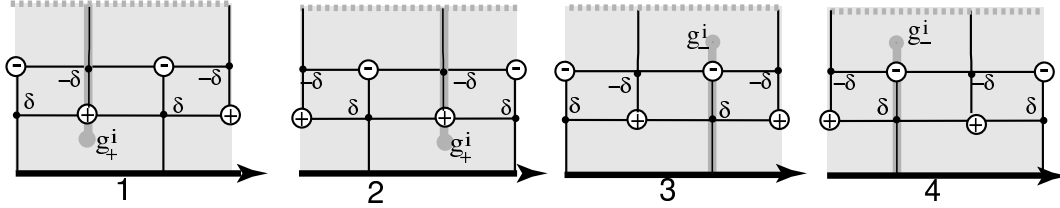


Figure 42: Normal neighborhoods of clasp arcs in \mathcal{S}

$N_-^i \subset N(\gamma_-^i)$ and we show the two possible arrangements in the two right sketches in Figure 42. As in the case of N_+^i , the rectangle N_-^i has 3 boundary edges which are in $\partial N(\gamma_-^i)$. We choose its 4th boundary edge to be an arc which is transverse to the foliation, so that the rectangle with 4 vertices and 4 singularities. As in the case of N_+^i , the top edge will eventually be used to construct the future X_+^i .

In the special case when γ_+^i has length 2 the puncture endpoint of the arc γ_-^i will be an interior point of N_-^i , but if γ^i has length ≥ 3 then $\gamma_-^i \cap N_-^i$ will separate N_-^i . However, let $\rho : P(\mathcal{TA}) \rightarrow \mathcal{TA}$ be the natural immersion. Then $\gamma_-^i \cap (\rho^{-1}(\rho(g_+^i)))$ will be a subarc of γ_-^i which begins on X_- and ends at a point in the interior of N_-^i , and we give this arc the name g_-^i . By construction, g_+^i and g_-^i have the same image in \mathcal{TA} , and determine the clasp intersection between the rectangles N_+^i and N_-^i which is induced by the clasp intersection in \mathcal{TA} corresponding to γ^i . The four cases which are illustrated in Figure 42 will be referred to as types 1,2,3,4.

Let $\mathcal{N}_{\mathcal{S}}$ be the union of all of the N_+^i and N_-^i . Note that, while $N_{\pm}^i \cap (\gamma_+^j \cup \gamma_-^j) = \emptyset$ for all $j \neq i$, there is no reason why $N_{\pm}^i \cap N_{\pm}^j$ should be empty. This leads us to the following preliminary definition of a connected collection of normal neighborhoods: Choose $N, N' \in \mathcal{N}_{\mathcal{S}}$. We say that N and N' are *connected*, and write $N \longleftrightarrow N'$, if $N \cap N' \neq \emptyset$ in $P(\mathcal{TA})$. Two examples are given in Figure 43. In the top row, N has type 1 and N' has type 2 and $N \cap N' = \partial N \cap \partial N'$. In the middle

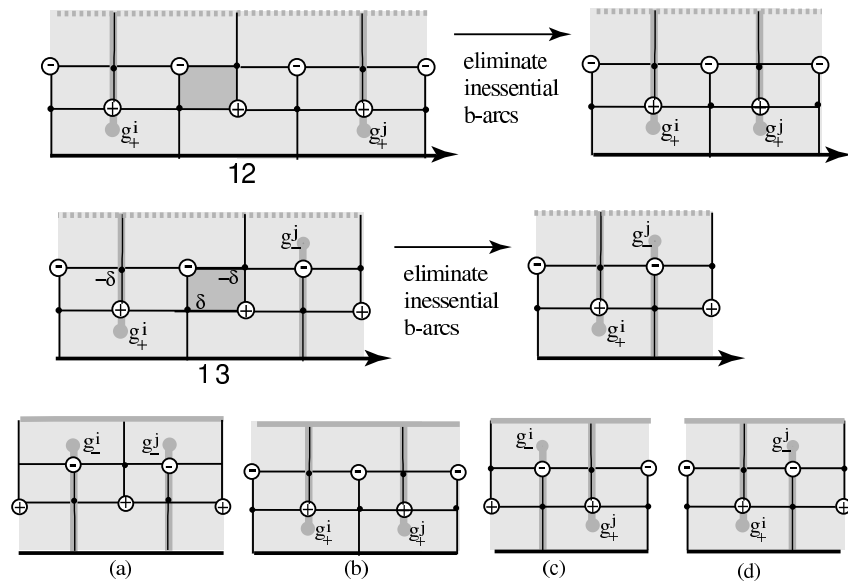


Figure 43: Adjacent pairs of foliated connected normal neighborhoods. Sketches a,b,c,d in the bottom row show all possibilities, after the elimination of inessential b -arcs.

row N has type 1, N' has type 3 and they intersect along two singular leaves and the disc between

them. Observe that this is the maximal possible intersection, because the normal neighborhood of a clasp arc never intersects another clasp arc. It follows that the possible sequences in a connected set are 12, 21, 34, 43, 14, 41, 23, 32, 13, 42. A collection of normal neighborhoods $\{N_1, \dots, N_p\} \subset \mathcal{N}_{\mathcal{S}}$ is connected if there is a connecting path between any two neighborhoods in the collection, i.e. if $N', N'' \in \{N_1, \dots, N_p\}$ then there exists a subcollection $\{N_{i_1}, \dots, N_{i_q}\} \subset \{N_1, \dots, N_p\}$ such that $N' \longleftrightarrow N_{i_1} \longleftrightarrow N_{i_2} \longleftrightarrow \dots \longleftrightarrow N_{i_q} \longleftrightarrow N''$. A connected component of $\mathcal{N}_{\mathcal{S}}$ is called a *region* and denotes by the symbol \mathcal{R} .

We now observe that each b -arc in each \mathcal{R} is in a normal neighborhood of some clasp arc. We distinguish between two types of b -arcs: those whose endpoints are vertices which do not meet a clasp arc, and those which have at least one vertex endpoint which is on a clasp arc. Let's focus on the former. Examples can be seen in the darkly shaded rectangles in Figure 43. Recall that our normal neighborhoods were created by the repeated use of finger moves, which necessarily created inessential b -arcs. So all of the b -arcs which do not intersect clasp arcs are inessential, and may be deleted by an isotopy of $P(\mathcal{TA})$ which is supported on a disc in the interior of the connected region, as in the passage from the left to the right in Figure 43. Therefore we may assume that \mathcal{R} contains no such b arcs. Notice that we have chosen our definition of complexity so that this modification does not alter the complexity. With the modification, it is easy to see that there are precisely 4 possible sequences of two modified normal neighborhoods, as illustrated in the bottom row in Figure 43, sketches (a),(b),(c),(d).

A region \mathcal{R} is either an annulus or a rectangle, as illustrated in Figure 44. If it is an annulus, then it satisfies properties (i)-(ii) of Lemma 5.1. Assume it's a rectangle. The lower horizontal boundary of \mathcal{R} is a subarc of a component of X_- , and so the connected components $\mathcal{R}_1, \dots, \mathcal{R}_q$ associated to any given component of X_- have a natural cyclic order on X_- . We would like to use this natural order to join them by bands of s -arcs to obtain annuli. However the vertical edges of the rectangles are not s -arcs. The following observation saves the day: the grey dotted horizontal boundary of each rectangle was chosen in a rather arbitrary way as an arc which is transverse to the foliation and in the interior of $P(\mathcal{TA})$, and if we now modify our choices by replacing the vertical edges of the wide rectangles by the sketches on the right in Figure 44(e)-(h) we will be in business. Sketches

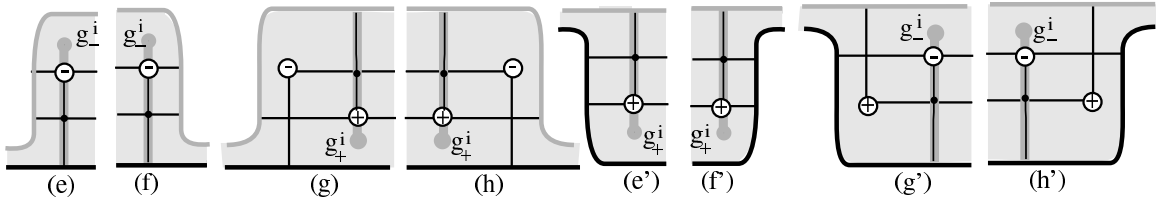


Figure 44: Possible arrangements of clasp arcs in adjacent intersecting normal neighborhoods in $P(\mathcal{TA})$, near the right and left boundaries of a connected collection of normal neighborhoods

(e) and (f) are obtained from sketch (a) of Figure 44 by modifying the grey boundary on the left and right respectively. Note that the modified grey boundary is everywhere transverse to the leaves of the foliation. On the other hand, if we attempt to do the same thing in the situation of (b), choosing the grey boundary to be close to the left (resp. right) clasp arc, a point of tangency with leaves of the foliation will be introduced, so it is necessary to include the singular leaf which is on the left (resp. right) in the modified connected region, as illustrated in (g) (resp. (h)). We leave it to the reader to check that (e) and (h) are modifications of (c), and that (f) and (g) are modifications of (d). The patterns in (e)-(h) all have the property: the rightmost singular leaf is in $G_{-\delta}$. But there is a second possibility: we are given the foliation near X_- , and we do not know much about it outside the normal neighborhoods. In fact there are 4 other possible patterns for the right and left boundaries, also restricted by the fact that X_- must be transverse to fibers of \mathbf{H} . They are illustrated in sketches (e')-(h') of Figure 44. They are obtained from (e)-(h) by interchanging the

roles of grey and black.

Let's examine the possibilities for the regions. Figure 45 shows the foliated annulus and the four possible foliated disc regions in \mathcal{S} , up to the number of pairs of components of $G_{-,\delta}$ and $G_{+,-\delta}$. In each, we give examples of how the clasp arcs might be placed. To construct \mathcal{S} from the various

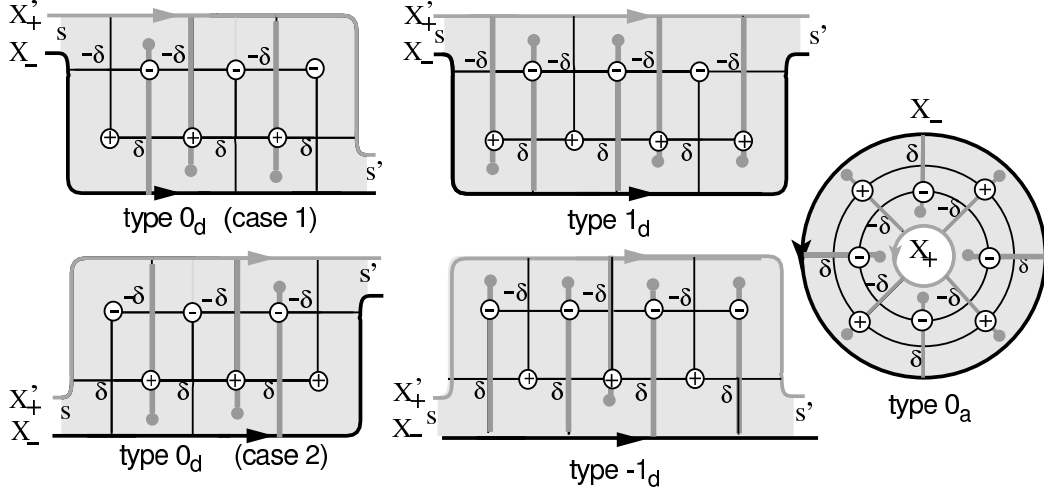


Figure 45: The non-trivially foliated regions in \mathcal{S} , with examples of the clasp arcs which intersect them

non-trivially foliated regions we first join disc regions which are consecutive as one travels along a component of X_- with bands of s -arcs which run between X_- and X'_+ . We then may also need some number of annuli which have long clasp arcs, as illustrated in Figure 44, and others which are foliated entirely by s -arcs. The latter occur whenever there is a component C such that no long clasp arc ends near C . We say that annuli which are foliated entirely by s -arcs, and also the bands which join the regions, are *trivially foliated*. In this way we obtain a family of annuli, one for each component of X_- . This completes the proof of Lemma 5.1. ||

Definition 13 (Complete collection of s -arcs): Let \mathcal{S} be an annular subset of $P(\mathcal{TA})$ which contains X_- (or a component of X_- in the case when \mathcal{X} is a link) as one of its boundary components. We consider the foliation of \mathcal{S} which is induced by the foliation on $P(\mathcal{TA})$. A (possibly empty) family of s -arcs $\mathbf{S} = \{s_1, \dots, s_i; s_i \subset \mathcal{S}\}$ is a *complete collection of s -arcs* in \mathcal{S} if (i) no two s -arcs in the collection split off a sub-band of \mathcal{S} that is foliated entirely by s -arcs, and (ii) for any other s -arc $s \subset P(\mathcal{TA})$ there exists an $s_i \in \mathbf{S}$ such that $s \cup s_i$ splits off a sub-band of \mathcal{S} that is foliated entirely by s -arcs. □

It is immediate that cutting \mathcal{S} open along a complete collection \mathbf{S} of s -arcs decomposes \mathcal{S} into a disjoint union of thinly foliated annuli and bands of s -arcs. This construction will be used in what follows.

We observe that the difference in braid index $b(X_-) - b(X'_+)$ across the union of the annuli which make up \mathcal{S} is the total number of positive vertices in \mathcal{S} minus the total number of negative vertices in \mathcal{S} . From Figure 45 we see that this difference is always either 0, 1 or -1 in a single non-trivially foliated region. Thus the motion of X_- across \mathcal{S} to X'_+ increases braid index if and only if there are more regions in \mathcal{S} of type -1 than of type $+1$. The regions of type 0 do not affect the count. We call our regions types $0_d, 1_d, -1_d, 0_a$, the subscript indicating whether the region is a disc or an annulus.

The example in Figure 46 illustrates a thinly foliated annuli which is constructed, using the methods described in the proof of Lemma 5.1 as a subset of the foliated annulus $P(\mathcal{TA})$ which was given, earlier, in Figure 30. There are 3 regions, and they have types $+1,+1,-1$. The dotted curves will be explained later. The regions are joined by 3 bands of s -arcs to construct \mathcal{S} . Therefore if we push X_- across \mathcal{S} to the light boundary (which is a curve which is in the interior of $P(\mathcal{TA})$ and transverse to the foliation) the braid index will increase by 1.

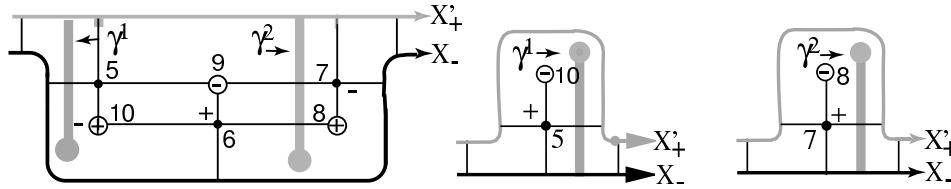


Figure 46: A thinly foliated annulus which is a subset of the foliated annulus Figure 30. The template associated to it can be seen in Figure 8(a).

5.1.2 Pushing X_- across \mathcal{S}

We now ask about the moves which are needed to push X_- across \mathcal{S} . For the rest of this section we will use bold faced type for the black boundary of \mathcal{S} and bold-faced type for all auxiliary structures and Roman type for the grey boundary, in order to stress the difference between our constructions near $\mathbf{X} = X_-$ and $\mathbf{X} = X'_+$. The non-trivially foliated regions which make up \mathcal{S} will be called the *support of the isotopy*. We shall regard the isotopy as being complete when each annulus in the modified \mathcal{S} is trivially foliated.

Proposition 5.1 *The motion of \mathbf{X} across the non-trivially foliated regions in \mathcal{S} may be realized by a sequence of flypes, followed by a braid isotopy.*

Proof: To motivate our work, observe that Figure 45 gives us, without further work, one way to isotope \mathbf{X} across the non-trivially foliated regions in \mathcal{S} , as follows: First stabilize \mathbf{X} along a neighborhood of each component of $G_{-,\delta}$ which does not meet a clasp arc. One such stabilization is possible in the example in Figure 46, and it is indicated by dotted arcs. This will place each clasp arc g_+^i in an a_+s -tile. Guided by the work we did in Section 4.3, we know that we can then use a microtype to push \mathbf{X} across each clasp arc. After that, it will be possible to do some number of destabilizations along components of $G_{+,-\delta}$. At that point the modified \mathcal{S} will be trivially foliated. The problem with this approach is that it uses stabilizations, and we want to prove the Markov Theorem *without* stabilization. As we shall see, all the stabilizations may be avoided by ‘amalgamating’ the microflypes into flypes. See Figure 47 for an example. This is the idea behind the proof of Proposition 5.1.

It will be helpful to see how the amalgamation shown in Figure 47 arises from the viewpoint of the thinly foliated annulus \mathcal{S} and the push of X_- across \mathcal{S} . See Figure 48. Our example illustrates a thinly foliated annulus which, after cutting open along a complete collection of s -arcs, has two non-trivially foliated regions of the types illustrated in the middle column of Figure 45. There are two pairs of clasp arcs, labeled (γ_+^1, γ_-^1) and (γ_+^2, γ_-^2) . Since there are only two regions in the foliation of $P(\mathcal{TA})$ there is a unique way to join them. The sequence of changes in the passage (i) \rightarrow (ii) \rightarrow (iii) \rightarrow (iv) of Figure 48 are a stabilization, two microflypes and a destabilization to push X_- across \mathcal{S} . At the end of the passage across \mathcal{S} the X_- boundary of \mathcal{S} will be separated from the X_+ boundary by nothing but s -arcs. We now show that X_+ may be obtained from X_- by a positive flype with all weights 1 and the braid σ_1^4 in the braid box. We will show it is the ‘amalgamation’ of the braid blocks associated to two microflypes, both of sign $(+, +)$. The vertex

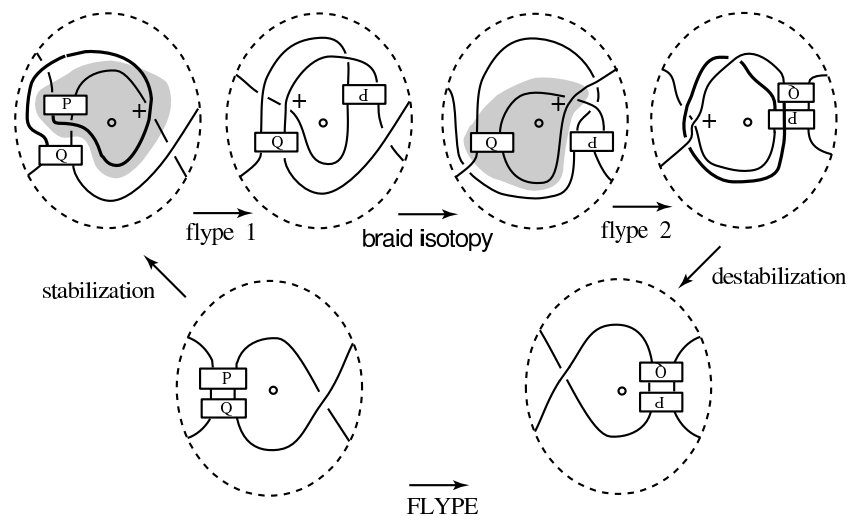


Figure 47: A stabilization, two microflypes and a destabilization which can be amalgamated into a flype.

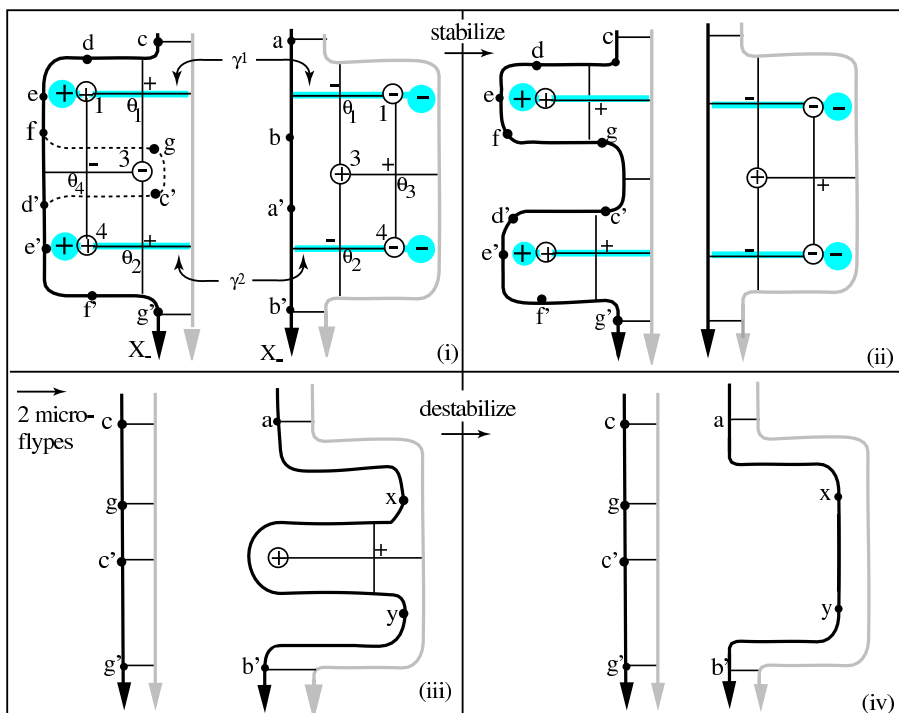


Figure 48: The isotopy of X_- across \mathcal{S} in a simple example

labels 1,2,3,4 and the singularity labels $\theta_1, \theta_2, \theta_3, \theta_4$ are consistent with the conditions of Lemma 3.1. The fact that the clasp arcs were placed in singular leaves shows that some of the vertex and singularity labels necessarily coincide on the two discs.

Our task is to construct the embedding of X_- in 3-space. From sketch (ii) of Figure 48 we notice that after the stabilization the subarc $fd' \subset X_-$ in sketch (i) will have been replaced by a new arc $fgc'd'$ which is entirely in the interior of \mathcal{S} . We show this arc as a dotted arc in sketch (i) of Figure 48. (It is also shown as a dotted arc in the left sketch of Figure 49). After the stabilization we will be able do two microfypes, as in the left sketch of Figure 49. (Remark: the sign of the singularity at polar angle θ'_3 in the right disc is negative, but the sign of the corresponding half-twist in sketch (i) of Figure 49 is positive. See Figure 19). It follows from all this that $ab \cup cdef \subset X_-$ is embedded as a final truncation of a microfype diagram, and that $a'b' \cup d'e'f'g' \subset X_-$ is embedded as an initial truncation of a second microfype diagram. In both cases the underlying microfype has sign $(+, +)$, by the rules which were given in Lemma 4.3.

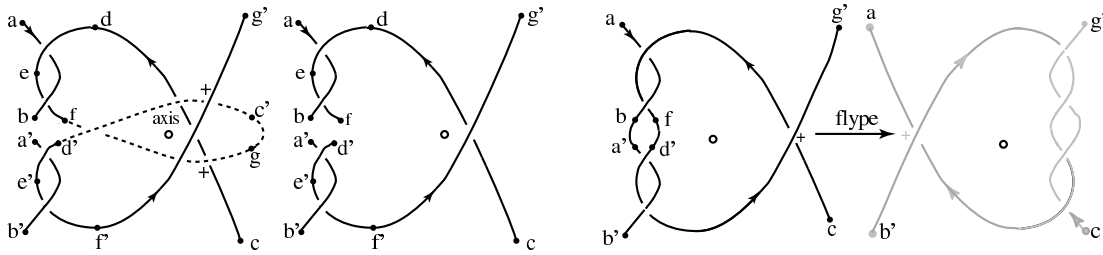


Figure 49: The 3-space embeddings of X_- and X_+ in the Example in Figure 48

Figure 49 illustrated ‘vertical’ amalgamation of microfypes. A similar example illustrates ‘horizontal’ amalgamation. See Figure 50. Sketches (i) and (ii) show the regions which make up a thinly

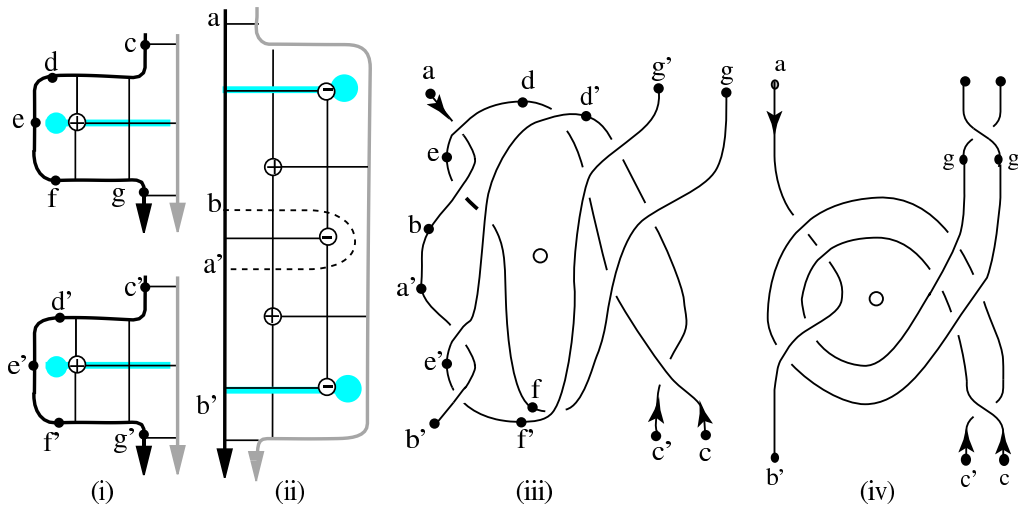


Figure 50: Amalgamating microfypes can result in flypes with weighted strands

foliated annulus. The angular data is assumed to have been chosen so that the same non-singular fiber of \mathbf{H} contains the points d and d' , also a second such fiber contains f and f' and so forth. The fact that the subarcs $cdefg$ and $c'd'e'f'g'$ bound a disc region in \mathcal{S} which has vertex sum $+1$ shows that those strands each encircle the axis once. After stabilizing X_- in sketch (ii) along the dotted

arc which begins at b and ends at a , we see that two microflypes are possible. However (exactly as in the case illustrated in Figures 48 and 49) the dotted arc is not part of X_- . It follows that the two microflypes, illustrated in sketch (iii) of Figure 50 can be amalgamated to give a flype with weighted strands, as illustrated in sketch (iv). Two such flypes (one admissible and the other inadmissible) occur in Figure 52 (see the right sketch). Note that in both examples (Figures 49 and 50) we start with two microflypes of sign $(+, +)$, and in both cases we join b to a' , however in the example of Figure 49 the amalgamation joins f to d' , but in the example of Figure 50 it does not.

With these examples in mind, we begin the proof of Proposition 5.1. Let $\rho : P(\mathcal{TA}) \rightarrow \mathcal{TA}$ be the natural projection. The left sketch in Figure 51 is an attempt to suggest how subarcs of \mathbf{X} fit together in $\rho(\mathcal{S})$, near a clasp arc. By hypothesis, both g_-^i and g_+^i have been pushed into their nearby chains of singular leaves. Since g_-^i begins on \mathbf{X} , one of the endpoints of g_-^i is a point $\mathbf{q}_-^i \in \mathbf{X}$. The fact that g^i is doubly long shows that one of the endpoints of g_+^i is near (but not on) \mathbf{X} . The singular leaf which contains it ends at a point $\mathbf{q}_+^i \in \mathbf{X}$. Since our clasp arc is doubly long, there is an analogous picture near X . Both are illustrated in Figure 51.

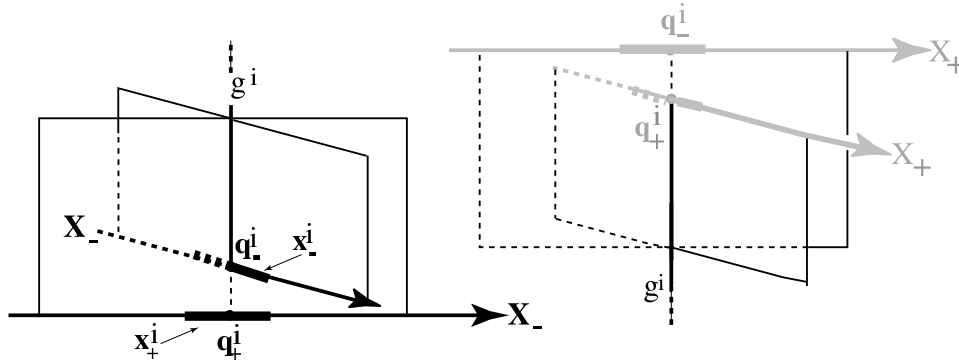


Figure 51: The four microstrands associated to a doubly long clasp arc

Notation ($\mathbf{x}_+^i, \mathbf{x}_-, \mathbf{x}_+^i, \mathbf{x}_-^i$): We fix subarcs $\partial_- N(g_-^i)$ (resp. $\partial_- N(g_+^i)$) of \mathbf{X} , where $\partial_- N(g_-^i)$ (resp. $\partial_- N(g_+^i)$) is a neighborhood of \mathbf{q}_-^i (resp. \mathbf{q}_+^i) on \mathbf{X} . The subarc $\partial_- N(g_\epsilon^i)$ is chosen so that it does not intersect the subarc associated to adjacent singular leaves on \mathbf{X} , also so that the arcs $\partial_- N(g_-^i)$ and $\partial_- N(g_+^i)$ have the same angular support $[\theta_{i_1}, \theta_{i_2}] \subset \mathbf{H}$. We call these arcs the black microstrands. There are, of course, similar thick grey microstrands $\partial_+ N(g_-^i)$ and $\partial_+ N(g_+^i)$ of X . We will need to use these arcs repeatedly in what follows and the notation is awkward. The symbols ∂_-, ∂_+ indicate whether the arc in question is a subarc of \mathbf{X} or X . But our color code shows the same thing. We accordingly adopt the simplified notation:

$$\begin{aligned} \mathbf{x}_-^i &= \partial_- N(g_-^i) \\ \mathbf{x}_+^i &= \partial_- N(g_+^i) \\ \mathbf{x}_-^i &= \partial_+ N(g_-^i) \\ \mathbf{x}_+^i &= \partial_+ N(g_+^i) \end{aligned}$$

from now on. Notice that the isotopy of \mathbf{X} across \mathcal{S} will necessarily map $\mathbf{x}_-^i \rightarrow \mathbf{x}_-^i$ (resp. $\mathbf{x}_+^i \rightarrow \mathbf{x}_+^i$) because the isotopy pushes \mathbf{X} across $N(g_-^i)$ (resp. $N(g_+^i)$) to X .

Construct disjoint solid cylinders $\mathbf{B}_-, \mathbf{B}_+$ in 3-space which have the structure of blocks, as defined in Section 1 of this paper. We call the cylinders microblocks. The microblock $\mathbf{B}_\epsilon^i, \epsilon = \pm$, is a foliated tubular neighborhood in 3-space of the arc \mathbf{x}_ϵ^i . It intersects the fibers of \mathbf{H} in the interval $[\theta_{i_1}, \theta_{i_2}]$. We also have, without further work, two grey microblocks associated to X . We summarize what we have learned:

Lemma 5.2 *Let $\gamma^i = \{\gamma_-^i, \gamma_+^i\}$ be a doubly long clasp arc pair in $P(\mathcal{TA})$ or a subsurface of $P(\mathcal{TA})$ which intersects contains in its boundary the four microstrands $\mathbf{x}_-^i, \mathbf{x}_+^i, \mathbf{x}_-^i, \mathbf{x}_+^i$. Then there are two*

microblocks associated to γ^i , namely the black and grey microblocks $\mathbf{B}_-, \mathbf{B}_+$ which contain the black microstrands $\{\mathbf{x}_-, \mathbf{x}_+\}$ and the grey microstrands $\{\mathbf{x}_-, \mathbf{x}_+\}$ respectively. Moreover when \mathbf{X} is pushed across the subsurface of $P(\mathcal{TA})$ to X , the block \mathbf{B}_- is sent to the block \mathbf{B}_+ .

We now turn our attention to the matter of amalgamating the microblocks into larger blocks, keeping in mind that we amalgamate black microblocks only if the corresponding grey microblocks can also be amalgamated.

Definition 14 (Amalgamating block): Let $B \subset S^3 - \mathbf{A}$ be a 3-ball having the structure of $\Delta \times [0, 1]$, where Δ is a disc, such that the following conditions are satisfied:

1. $B \cap H_\theta$ is either empty or is equal to $\Delta \times \{\phi\}$ for some $\phi \in [0, 2\pi]$. Moreover, there exist some $H_\theta \in \mathbf{H}$ for which the intersection with B is empty.
2. $\partial B \cap \mathbf{X} \subset (\Delta \times \{0\}) \cup (\Delta \times \{1\})$. Moreover the discs $\Delta \times \{0\}$ and $\Delta \times \{1\} \subset \partial B$ are contained in non-singular disc fibers of \mathbf{H} . (Remark: to understand this condition, recall that we make a distinction between a braid block and a braiding assignment to the block. The braiding assignment must of course agree with the intersection of \mathbf{X} with the top and bottom of the braid block, and that is why we need to record this data).
3. Each circle of $\partial \Delta \times \{s\} \subset \partial B$, for $0 \leq s \leq 1$ transversally intersects $\rho(\mathcal{S}) \subset \mathcal{TA}$.
4. $B \cap X = \emptyset$.
5. $B \cap \rho(\mathcal{S})$ does not contain any singular points of the foliation.

If such a 3-ball \mathbf{B} and blocks $\{\mathbf{B}_-, \dots, \mathbf{B}_+\}$ associated with \mathbf{X} exist, then we say that $\{\mathbf{B}_-, \dots, \mathbf{B}_+\}$ can be amalgamated into the block \mathbf{B} and that \mathbf{B} is an amalgamating block. \square

We think of the blocks associated to \mathbf{X} as being colored black. There is an analogous definition in which the roles of the black boundary \mathbf{X} and the grey boundary X are interchanged, and the color black is replaced by grey.

We want to build the embedding of that part of \mathbf{X} which changes when we push \mathbf{X} across \mathcal{S} . Our starting point is the collection of black microblocks and their associated microstrands $\mathbf{x}_-, \mathbf{x}_+$, which we know must be mapped to the corresponding grey microblocks and their associated microstrands.

We next define the concept of a connected family of subarcs of \mathbf{X} . Let $\{\mathbf{x}_-, \mathbf{x}_+, \dots, \mathbf{x}_-, \mathbf{x}_+\}$ be the collection of black microstrands. Choose $\mathbf{x}_\epsilon^i, \mathbf{x}_\delta^j \in \{\mathbf{x}_-, \mathbf{x}_+, \dots, \mathbf{x}_-, \mathbf{x}_+\}$. We say that $\mathbf{x}_\epsilon^i, \mathbf{x}_\delta^j$ are connected, and write $\mathbf{x}_\epsilon^i \longleftrightarrow \mathbf{x}_\delta^j$, if either $i = j$ and $\epsilon = -\delta$ or if \mathbf{x}_ϵ^i and \mathbf{x}_δ^j belong to the boundary of the same non-trivially foliated region in \mathcal{S} . A collection of subarcs of $\{\mathbf{x}_-, \mathbf{x}_+, \dots, \mathbf{x}_-, \mathbf{x}_+\}$ is connected if for any $\mathbf{x}_\epsilon^i, \mathbf{x}_\delta^j$ in the collection there exists a subcollection $\{\mathbf{x}_{i_1}, \dots, \mathbf{x}_{i_q}\} \subset \{\mathbf{x}_1, \dots, \mathbf{x}_p\}$ such that

$$\mathbf{x}_\epsilon^i \longleftrightarrow \mathbf{x}_{i_1} \longleftrightarrow \mathbf{x}_{i_2} \longleftrightarrow \dots \longleftrightarrow \mathbf{x}_{i_q} \longleftrightarrow \mathbf{x}_\delta^j.$$

A connected collection $\{\mathbf{x}_1, \dots, \mathbf{x}_{2p}\}$ is maximal if every connecting path between two neighborhoods in the collection is also in the collection. A maximal connected collection $\{\mathbf{x}_1, \dots, \mathbf{x}_{2p}\}$ has uniform length if there exists an interval $[\theta_1, \theta_2] \subset [0, 2\pi]$ such that the image of each component of $(\mathbf{X} \cap (\cup_{1 \leq i \leq 2p} \mathbf{x}_i))$ under the projection map $\pi : H_\theta \rightarrow \theta$ is $[\theta_1, \theta_2]$. A maximal connected collection $\{\mathbf{x}_1, \dots, \mathbf{x}_{2p}\}$ of uniform length is an admissible collection if:

1. Every component of $(\mathbf{X} \cap (\cup_{1 \leq i \leq 2p} \mathbf{x}_i))$ is a component of $(\mathbf{X} \cap (\cup_{\theta \in [\theta_1, \theta_2]} H_\theta))$.
2. For any $\mathbf{x}_\epsilon^i, \mathbf{x}_\delta^j \subset \{\mathbf{x}_1, \dots, \mathbf{x}_{2p}\}$ for which there is a path of arcs $\mathbf{x}_\epsilon^i \longleftrightarrow \mathbf{x}_{j_1} \longleftrightarrow \mathbf{x}_{j_2} \longleftrightarrow \dots \longleftrightarrow \mathbf{x}_{j_q} \longleftrightarrow \mathbf{x}_\delta^j$ where $\mathbf{X} \cap (\cup_{j_1 \leq j \leq j_q} \mathbf{x}_j) \subset (\cup_{\theta \in [\theta_1, \theta_2]} H_\theta)$ we have $\{\mathbf{x}_{j_1}, \dots, \mathbf{x}_{j_q}\} \subset \{\mathbf{x}_1, \dots, \mathbf{x}_{2p}\}$.

In the above definition we have focussed on the black boundary of \mathcal{S} . The same definition applies to the grey boundary, although in general its defining interval $[\theta'_1, \theta'_2]$ is different from $[\theta_1, \theta_2]$. If our black collection $\{\mathbf{x}_1, \dots, \mathbf{x}_{2p}\}$ is admissible and if there is a corresponding grey collection which is also admissible, and if there is a 1-1 correspondence between pairs $(\mathbf{x}_+^i, \mathbf{x}_-^i) \subset \{\mathbf{x}_1, \dots, \mathbf{x}_{2p}\}$ and pairs $(x_+^i, x_-^i) \subset \{x_1, \dots, x_{2p}\}$ given by the clasp arcs g^1, \dots, γ^p , we say that $\{\mathbf{x}_1, \dots, \mathbf{x}_{2p}\}$ is (bg)-admissible (to be read ‘black and grey admissible’).

We wish to organize the microstrands in a (bg)-admissible collection into strata. Let $\{\mathbf{x}_1, \dots, \mathbf{x}_{2p}\}$ be a (bg)-admissible collection. For every \mathbf{x}_-^i in this collection we know that \mathbf{x}_+^i is also in the collection. We say that \mathbf{x}_-^i and \mathbf{x}_+^i are at the same level because they are supported in the same θ -interval. If $\mathbf{x}_\epsilon^i, \mathbf{x}_\delta^j$ are in the collection we say that \mathbf{x}_ϵ^i precedes \mathbf{x}_δ^j if \mathbf{x}_ϵ^i and \mathbf{x}_δ^j belong to the same non-trivially foliated region in \mathcal{S} and \mathbf{x}_ϵ^i precedes \mathbf{x}_δ^j in the given orientation on the black boundary of the region. Now recall that $\{\mathbf{x}_1, \dots, \mathbf{x}_{2p}\}$ is (bg)-admissible, so that there are matching definitions for the grey microstrands. We say that \mathbf{x}_ϵ^i is (bg)-before \mathbf{x}_δ^j if \mathbf{x}_ϵ^i precedes \mathbf{x}_δ^j and \mathbf{x}_ϵ^i precedes \mathbf{x}_δ^j . We note that it can happen that \mathbf{x}_ϵ^i precedes \mathbf{x}_δ^j , but that \mathbf{x}_ϵ^i does not precede \mathbf{x}_δ^j .

A path of microstrands $\mathbf{x}_1 \longleftrightarrow \mathbf{x}_2 \longleftrightarrow \dots \longleftrightarrow \mathbf{x}_p$, is (bg)-descending, with ends \mathbf{x}_1 and \mathbf{x}_p if:

- \mathbf{x}_1 and \mathbf{x}_2 are (bg)-level,
- \mathbf{x}_2 is (bg)-before \mathbf{x}_3 ,
- \mathbf{x}_3 and \mathbf{x}_4 are (bg)-level,
- \mathbf{x}_4 is (bg)-before \mathbf{x}_5, \dots ,
- \mathbf{x}_{2p-1} and \mathbf{x}_{2p} are (bg)-level.

A path of microstrands is (bg)-level, with ends $\mathbf{x}_1, \mathbf{x}_{2p}$, if $\mathbf{x}_1 \neq \mathbf{x}_{2p}$ (we do not rule out $\mathbf{x}_1 = \mathbf{x}_{2p}$) and if:

- \mathbf{x}_1 and \mathbf{x}_2 are (bg)-level,
- \mathbf{x}_2 is (bg)-before \mathbf{x}_3 (respectively \mathbf{x}_3 is (bg)-before \mathbf{x}_2),
- \mathbf{x}_3 and \mathbf{x}_4 are (bg)-level.
- \mathbf{x}_5 is (bg)-before \mathbf{x}_4 (respectively \mathbf{x}_4 is (bg)-before \mathbf{x}_5),
- \dots, \mathbf{x}_{2p-1} and \mathbf{x}_{2p} are (bg)-level.

Let $\vec{\mathbf{x}}$ be a (bg)-admissible collection between disc fibers H_{t_1}, H_{t_2} . We say a subcollection $\{\mathbf{x}_{i_1}, \dots, \mathbf{x}_{i_r}\} \subset \vec{\mathbf{x}}$ is a (bg)-top of the collection and $\{\mathbf{x}_{j_1}, \dots, \mathbf{x}_{j_r}\}$ is a (bg)-bottom of the collection if:

- $\{\mathbf{x}_{i_1}, \dots, \mathbf{x}_{i_r}\} \cap \{\mathbf{x}_{j_1}, \dots, \mathbf{x}_{j_r}\} = \emptyset$
- Both $\{\mathbf{x}_{i_1}, \dots, \mathbf{x}_{i_r}\}$ and $\{\mathbf{x}_{j_1}, \dots, \mathbf{x}_{j_r}\}$ are (bg)-level.
- For each $\mathbf{y} \in \{\mathbf{x}_{i_1}, \dots, \mathbf{x}_{i_r}\}$ there exist a $\mathbf{z} \in \{\mathbf{x}_{j_1}, \dots, \mathbf{x}_{j_r}\}$ and a subcollection $\{\mathbf{x}_{k_1}, \dots, \mathbf{x}_{k_s}\} \subset \vec{\mathbf{x}}$ such that $\mathbf{y} \longleftrightarrow \mathbf{x}_{k_1} \longleftrightarrow \dots \longleftrightarrow \mathbf{x}_{k_s} \longleftrightarrow \mathbf{z}$ is (bg)-descending.
- Similarly, for each $\mathbf{x}' \in \{\mathbf{x}_{j_1}, \dots, \mathbf{x}_{j_r}\}$ there exist a $\mathbf{x}'' \in \{\mathbf{x}_{i_1}, \dots, \mathbf{x}_{i_r}\}$ and a subcollection $\{\mathbf{x}_{k_1}, \dots, \mathbf{x}_{k_s}\} \subset \{\mathbf{x}_1, \dots, \mathbf{x}_p\}$ such that $\mathbf{x}' \longleftrightarrow \mathbf{x}_{k_1} \longleftrightarrow \dots \longleftrightarrow \mathbf{x}_{k_s} \longleftrightarrow \mathbf{x}''$ is (bg)-descending.

Lemma 5.3 *Let $\{\mathbf{x}_1, \dots, \mathbf{x}_{2p}\}$ be a (bg)-admissible collection of microstrands in \mathbf{X} which has a (bg)-top and (bg)-bottom. Then there exists a black block \mathbf{B} that is an amalgamation of all of black microblocks associated to the collection $\{\mathbf{x}_1, \dots, \mathbf{x}_{2p}\}$ and a similar grey block \mathbf{B} that is an amalgamation of the corresponding microblocks associated to $\{x_1, \dots, x_{2p}\}$ and an isotopy of \mathbf{X} across \mathcal{S} that sends \mathbf{B} to \mathbf{B} .*

Proof: We stratify our admissible collection into sequences of level paths and descending paths with respect to \mathbf{X} . The connecting strands between the microstrands in each descending path are the connecting subarcs of \mathbf{X} . As was observed earlier, after Definition 14, the blocks associated to two level paths can always be amalgamated. The blocks that are associated to descending paths can also be amalgamated. The net result of all this amalgamation is a black block \mathbf{B} . There is a corresponding grey block B , because our collection is (bg)-admissible and has a (bg)-top and a (bg)-bottom. We map \mathbf{B} to B by mapping each pair of microblocks for \mathbf{B} to the corresponding pairs of microblocks for B . In this way we obtain blocks and braiding assignments for the blocks, and the braiding assignment for \mathbf{B} goes to the corresponding braiding assignment for B when we map \mathbf{B} to B . ||

Remark: The blocks \mathbf{B} and B will include a subset (possibly proper) of the collection of all the black and grey microstrands associated to all of the doubly long clasp arcs in \mathcal{S} .

Remark: The reader should now be in a position to use Figure 30 to verify precisely how we found the template in Figure 9. In this example the push of X_- across \mathcal{S} is realized by a flype (which increases braid index by 1, followed by two exchange moves, which are in turn followed by a second flype which decreases the braid index by 1. The total change in the passage from the bottom left sketch in Figure 9 to the bottom right sketch is zero.

Completion of the proof of Proposition 5.1: The proof divides into two cases.

Case 1: Assume that all of the black microstrands associated to the black boundary of \mathcal{S} can be amalgamated into a black block \mathbf{B} , which maps to a grey block B . The remaining issue is to prove that the map which takes \mathbf{B} to B in Lemma 5.3 is realized by a flype, where we allow the flype to have weighted strands.

In the special case when \mathcal{S} is the annulus of Figure 13, the blocks \mathbf{B} and B each contain exactly one full twist and we have already shown that the motion taking \mathbf{B} to B is a microflype. (See the example near the end of Section 2, and the detailed discussion in Section 4.3.)

For the general case, let $\mathbf{A}(\mathbf{B}) = \{H_\theta \in \mathbf{H} \mid \mathbf{B} \cap H_\theta \neq \emptyset\}$, and let $\mathbf{A}'(\mathbf{B})$ be the complement of $\mathbf{A}(\mathbf{B})$ in the interval $[0, 2\pi]$. The subarcs of X_- that enter and leave the block \mathbf{B} are precisely those in $\mathbf{X} \cap \mathbf{A}'(\mathbf{B})$. We need to show that their embeddings correspond to the embeddings which are illustrated in Figure 8(a), and to show that the motion taking $\mathbf{B} \cup (\mathbf{X} \cap \mathbf{A}'(\mathbf{B}))$ to $B \cup (X \cap A'(B))$ is a flype with weighted strands, as depicted in the passage from the left sketch to the right sketch in Figure 8.

There are two kinds of amalgamations of strands, illustrated by the examples in Figures 49 and 50. We refer to the first as ‘vertical amalgamation’ and the second as ‘horizontal amalgamation’. Horizontal amalgamation changes the weights on some of the strands, but vertical amalgamation leaves the weights invariant but changes the braid inside the block.

The thinly foliated annuli which gave us the blocks \mathbf{B} and B are a union of disc regions of type 0_d , -1_d and 1_d . Our first observation is that if we have a collection of thinly foliated annuli of type 0_d , -1_d , or 1_d associated with blocks \mathbf{B} and B , then all the parity assignments to the singularities will be coherent. To understand this, first see Definition 6 and Lemma 4.3. This lemma tells us that the signs of all of the singularities near X_- , in all thinly foliated discs associated with block \mathbf{B} , will have the same parity; similarly all the signs of all the singularities near X_+ will have the same parity, in all the thinly foliated discs associated with block B . Finally, the parities of the singularities near X_- are opposite to those near X_+ . Thus the associated microflypes all have the same sign. This will be a key point when we amalgamate the microblocks and want to be sure that the strands fit together nicely. The example in Figure 50 makes the issue clear.

To continue, let’s go back to Figure 8, and study the weights on the strands in the passage from left to right in sketch (a). Observe that there are groups of arcs with w strands and also with k

strands (respectively w' and k' strands). In the passage from the initial braid diagram to the final braid diagram they increase (resp. decrease) in angular length. We now go to Figure 45. Recall that \mathcal{S} is a union of regions of type $1_d, -1_d$ and 0_d , so that $\mathbf{X} \cap \mathbf{H}(\mathbf{B})$ is a subset of the black boundaries of these regions. Notice that $\mathbf{A}(\mathbf{B})$ and $\mathbf{A}(\mathbf{B})$ can be assumed to be arbitrarily small by rescaling in $[0, 2\pi]$. Notice also that we can ignore the parts of $\mathbf{X} \cap \mathcal{S}$ and $X \cap \mathcal{S}$ which are in the bands of s -arcs, because \mathbf{X} and X are essentially identical in those bands. Thus our concern is essentially with the motion of \mathbf{X} and X across the disc regions in \mathcal{S} .

We observe that:

- If \mathcal{S} contains a region of type 1_d , then the strands of $\mathbf{X} = X_-$ which enter $\mathbf{H}(\mathbf{B})$ in that region will have angular length which exceeds the angular length of the strands of $X = X_+$ which leave $\mathbf{H}(\mathbf{B})$. Similarly, the strands of $\mathbf{X} = X_-$ which exit $\mathbf{A}(\mathbf{B})$ in that region will have angular length which exceeds the angular length of the strands of $X = X_+$ which leave $\mathbf{A}(\mathbf{B})$. From this it follows that if there is a type 1_d region, then its boundary arcs could contribute 1 to w' and 1 to k' . The contribution to $w' - k = k' - w$ is 1.

For similar reasons,

- A type -1_d region could account for a contribution of 1 to w and 1 to k . The contribution to $w' - k = k' - w$ is -1.
- A type 0_d (top left sketch) could account for a contribution of 1 to w and 1 to k' . The contribution to $w' - k = k' - w$ is 0.
- A type 0_d region (bottom left sketch) could account for a contribution of 1 to w' and 1 to k . The contribution to $w' - k = k' - w$ is 0.

From all this we conclude that disc regions of type 0_d induce vertical amalgamations of flypes, whereas disc regions of type $\pm 1_d$ induce horizontal amalgamation of microflypes. Inductively, one sees that the motion that takes the amalgamated black block to the amalgamated grey block is always realized by a flype, because the underlying motions were determined by microflypes.

Case 2: In the more general case, there are several (bg)-admissible collections of black microstrands, whose union is all of the black microstrands associated to the black boundary of \mathcal{S} . This could happen in two ways:

Case 2.1: Each (bg)-admissible collection of microstrands either has empty intersection with a non-trivially foliated region in $\mathcal{S} \setminus \mathbf{S}$ or, if it has non-empty intersection then it includes all the black microstrands associated to that region. In this situation several independent flypes (one for each (bg)-admissible collection) are needed to push \mathbf{X} across \mathcal{S} . An example which illustrates this is given in Figure 52.

Case (2.2): There is a (bg)-admissible collection of microstrands which has non-empty intersection with some non-trivially foliated region \mathcal{R} of $\mathcal{S} \setminus \mathbf{S}$ but does NOT include all of the black microstrands associated to \mathcal{R} . If so we would like to subdivide \mathcal{R} into subregions $\mathcal{R}_1, \mathcal{R}_2$ and then possibly subdivide again and again until we have k subregions $\mathcal{R}_1, \dots, \mathcal{R}_k$ such that \mathbf{X} can be pushed across $\mathcal{R}_1 \cup \dots \cup \mathcal{R}_k$ by a sequence of k independent flypes. If this is possible, then we will have reduced (2.2) to (2.1). We consider one such subdivision. There are 4 possibilities, according as the required subdivision point is between the two clasp arcs in the position of (a),(b),(c) or (d) of Figure 43. The 4 cases are illustrated in Figure 53: In the situation of Figure 53(a), the subdivision is very easy. Suppose that the microstrands \mathbf{x}_-^i and \mathbf{x}_-^j associated to the clasp arcs g_-^i, g_-^j belong to a set which is b-admissible but not (bg)-admissible. We then subdivide the associated non-trivially foliated region of \mathcal{S} by running the grey boundary around a neighborhood of the component of

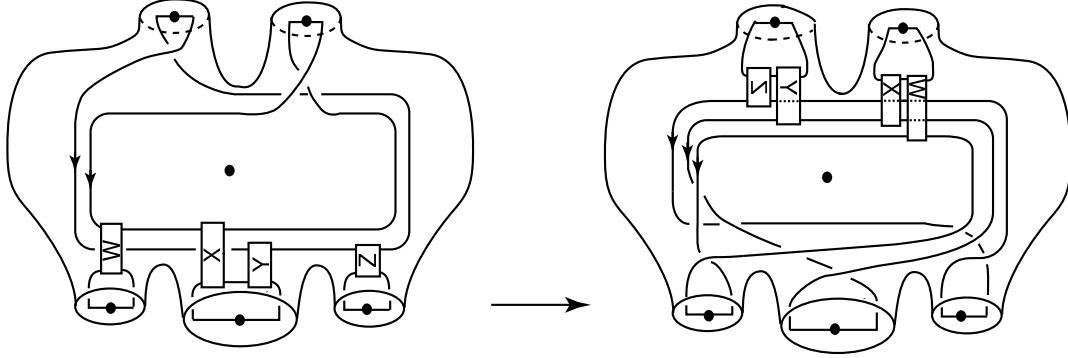


Figure 52: An example of two independent flypes

$G_{+,-\delta}$ which is in between the two microstrands \mathbf{x}^i and \mathbf{x}^j to cut the region into 2 non-trivially foliated regions. The same sort of subdivision is needed in cases (b), (c), (d), however in those cases the obvious subdivision always leads to points of non-transversality of the new grey boundary with leaves of the foliation. To take care of this we need to add inessential b -arcs before we can subdivide

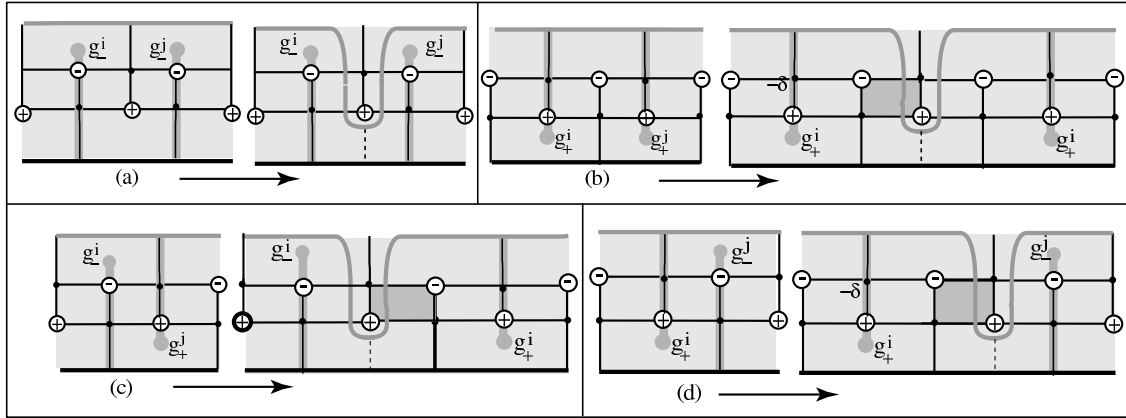


Figure 53: Subdividing non-trivially foliated regions in \mathcal{S}

the associated region in \mathcal{S} into two regions. See Figure 53(b), (c), (d). The addition of inessential b -arcs is always realized by an isotopy which is supported in the interior of $P(\mathcal{TA})$, so that it does not affect the black and grey boundary curves. The changes in the grey boundary do affect the type of the region. In particular each of the changes in the grey boundary which we show in Figure 53 moves a positive vertex out of \mathcal{S} , a motion which is later compensated for by a destabilization of the new black boundary. In this way we construct, for each (bg) -admissible collection, a flype which takes the associated black block to its grey companion. In the most extreme case of subdivision our flypes will be microflypes.

The proof of Proposition 5.1 is complete. \parallel

Remark 1: Note that the process of subdivision which we just described can change a region of, for example, type -1 to two regions of type 0. However, the total sum of the signs of the vertices (after all the destabilizations have been completed) is unchanged.

Remark 2: Proposition 5.1 is the first example, in our proof, where we may have encountered a candidate for a template in $\mathcal{T}(m)$. If the flypes in the sequence in Proposition 5.1 are all admissible,

we do not need any new templates. However, it may happen that one (or more) of them is inadmissible, but that others are braid-index reducing and so the entire sequence is non-increasing on braid index. If so, the sequence of flypes may give us a template in $\mathcal{T}(m)$. The actual construction will occur when we get to the proof of part (d) of the MTWS, in Section 5.3.

5.2 The role of exchange moves and handle moves

We assume in this section that there are no long clasp arcs. With this assumption we investigate discs that are not good. In Section 1 of this paper we gave a preliminary definition of a block-strand tree and of a G-handle move over a block-strand tree. These concepts were defined in terms of block diagrams of a closed braid, and we needed them in order to be able to state the MTWS. Our goal in this section is show how G-handle moves arise naturally when we assume that there are no long clasp arcs, but that there are discs that are not good, and we need to push X_- across those discs.

Example 1: As usual, it will be helpful to begin with an example. See Figure 54, which illustrates four discs on $P(\mathcal{TA})$. None of our discs is good (because each contains the puncture endpoint of clasp arcs). On the other hand, each is an embedded subset of $P(\mathcal{TA})$ (because no one disc contains a clasp arc pair). None of the clasp arcs is long (because all of the puncture endpoints are on b -arcs).

While we have gone to some pains to insure that all clasp arcs are in normal neighborhoods, in this example of a G-handle move we choose to ignore the normal neighborhoods for reasons of space, as we need to focus on the essential features of a G-handle move, and normal neighborhoods would simply enlarge the pictures to the point where they would obscure the features that are of interest. (Remark: normal neighborhoods were created by adding many many inessential b -arcs; going the other way, they can always be deleted by an isotopy of the surface).

Ignoring the clasp arcs momentarily, we see that each disc is exactly like the shaded disc in the upper left sketch in Figure 22, i.e. it contains a positive vertex of valence 2 and type ab , and singularities of opposite sign. Each of our 4 regions contains in its boundary a subarc of X_- and a subarc of X_+ , colored dark and light respectively. These arcs are labeled $1_{\pm}, 2_{\pm}, 3_{\pm}$ and 4_{\pm} . If the clasp arcs were not there we could use four ab -exchange moves to push the four subarcs of

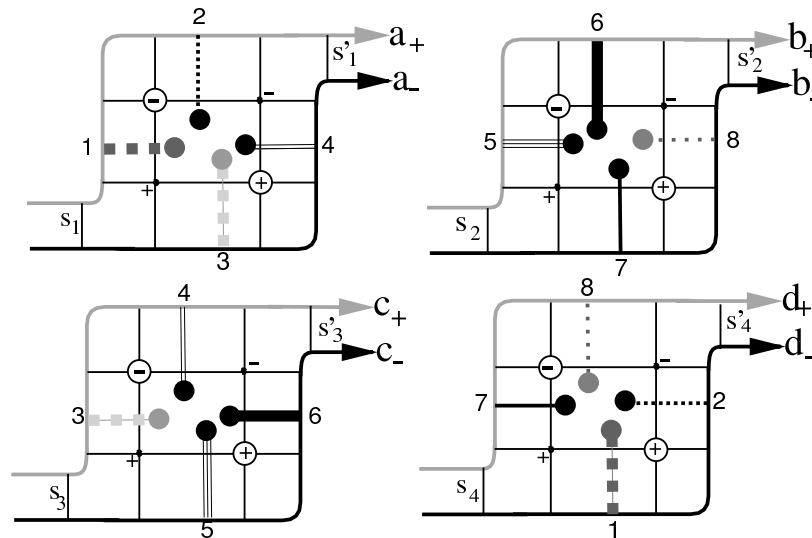


Figure 54: Foliated subsurfaces of $P(\mathcal{TA})$ which are the support of the G-handle move of Figure 7.

X_- across the disc to X_+ . Label the discs \mathcal{R}_1 (top left), \mathcal{R}_2 (top right), \mathcal{R}_3 (bottom right) and \mathcal{R}_4 (bottom left). Since \mathcal{R}_1 intersects \mathcal{R}_3 along clasp arcs a and b, and \mathcal{R}_4 along clasp arcs c and d, we cannot complete the move on strand 1 until we begin the moves on strands 3 and 4. But then, the motions of strands 3 and 4 across discs \mathcal{R}_3 and \mathcal{R}_4 cannot be completed because those discs have clasp intersections with \mathcal{R}_2 , and in fact no one of the motions can be completed until all of the others are completed too. That is, we have a G-handle move. This G-handle move was discussed in Section 1 to this paper, and was depicted in Figure 7. More general G-handle moves will be based upon more general ‘handle regions’ in the foliation. We discuss these next.

Example 2: In Figure 55 a subarc of X_- can be pushed across the shaded regions in sketch (a) by two exchange moves: the first across the darkly shaded disc (containing the vertices v and w and the singularities s and r). After that a second ab -exchange move is possible across the lighter shaded disc, which contains the vertices v', w' and the singularities s', r' . We investigate the associated block-strand diagram. Later we will investigate the general situation when this disc is not a good disc. The support of the first exchange move is a ‘pouch’ \mathcal{P} which is pierced twice by the axis, at

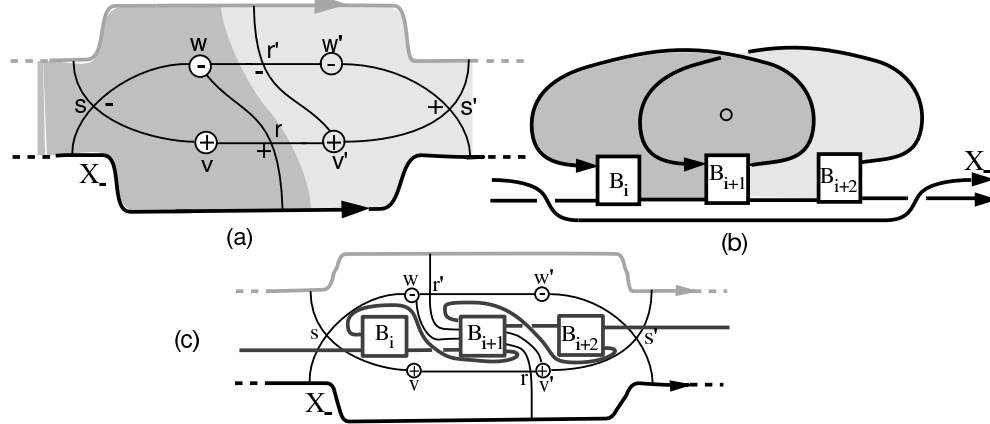


Figure 55: (a) The foliation on $P(\mathcal{TA})$. (b) The block-strand tree. (c) The two viewpoints are put together.

v and w . Since the foliation of \mathcal{P} contains only essential b -arcs, the closed braid must wrap around the braid axis (perhaps with many strands traveling along together, say t strands in all) in between the two pierce-points v and w . The first exchange move is a push of the subarc $\alpha \subset C$ across C , crossing the axis twice as it does so, at v and w , to $\alpha' = (\partial C \setminus \alpha)$. In the situation in Figure 55(a) we also have a second exchange move, across a second pouch C' , with $\alpha' = \partial C \cap \partial C'$. There will also be t' braid strands wrapping about the axis in between v' and w' , and perhaps a braid in between the weighted strands t and t' . Keeping the entire picture in mind we turn to Figure 55(b). It shows a picture of a block-strand tree which is part of a closed braid diagram. There are 3 blocks, labeled B_i, B_{i+1}, B_{i+2} and two weighted strands, labeled $t(i, i+1)$ and $t(i+1, i+2)$, traveling around the braid axis. The subarc of X_- is *not* part of the root and will be discussed later.

In Figure 55(c) we put together the information in Figure 55(a) and (b). The region \mathcal{R} of (a) is to be thought of as a very flexible disc with two pouches. We are looking through the pouches to the block and strand tree which is visible inside them. The braid axis \mathbf{A} pierces the pouches in axis pieces vw and $v'w'$. The darker pouch (we called it C) is the support of the first ab -exchange move in sketch (a). It covers the darker Δ -disc. The lighter shaded pouch C' covers the lighter Δ disc. The motion of $\alpha \subset \partial \mathcal{R}$ can now be seen to be a handle move over the two pouches to α' . The handle move is over the braid blocks B_i, B_{i+1}, B_{i+2} and the weighted strands, which are now labeled $t(i, i+1)$ and $t(i+1, i+2)$.

Definition 15 (Block-strand tree): Our interest now is in the subset of a block-strand diagram which is associated to foliated regions like the ones described in Examples 2 and 3. See Figure 6, assuming, initially, that the block B' and everything that is attached to it has been deleted. A collection of braid blocks $\{B_1, \dots, B_l\}$ and weighted strands $\{s(1, 2), \dots, s(i, i+1), \dots\}$, $1 \leq i \leq l$, and additional weighted strands $\{t^1(1, 2), \dots, t^{k_1}(1, 2), t^1(2, 3), \dots, t^{k_2}(2, 3), \dots, t^1(i, i+1), \dots, t^{k_i}(i, i+1), \dots\}$ is a *root* if the following conditions are satisfied:

- $s(i, i+1)$, $1 \leq i \leq l$ has endpoints at the bottom of B_i and at the top of B_{i+1} .
- $t^j(i, i+1)$, $1 \leq j \leq k_i$ has endpoints at the top of B_i and at the bottom of B_{i+1} .
- There exist embedded discs $\Delta(i, i+1, j) \subset S^3$ satisfying the following further conditions:
 - These Δ -discs have disjoint interiors. Also, for each $t^j(i, i+1)$, $1 \leq j \leq k_i$ there is one associated disc.
 - \mathbf{A} intersects each Δ -disc transversally in a single point.
 - $\partial\Delta(i, i+1, j) \subset t^j(i, i+1) \cup B_i \cup s(i, i+1) \cup B_{i+1}$. Also $\Delta(i, i+1, j) \cap s(i, i+1) = s(i, i+1)$ and $\Delta(i, i+1, j) \cap t^j(i, i+1) = t^j(i, i+1)$.
 - If $\Delta(i, i+1, j)$ and $\Delta(i, i+1, j')$ are distinct Δ -discs which are intersected in succession by some meridian loop of $s(i, i+1)$ then there exist $\Delta(i-1, i, m)$ and $\Delta(i+1, i+2, q)$ such that the unoriented \mathbf{A} intersects first $\Delta(i, i+1, j)$, then $\Delta(i-1, i, m)$ and $\Delta(i+1, i+2, q)$ (in either order); then $\Delta(i, i+1, j')$; then all other Δ -discs.
 - For each $\Delta(i, i+1, j)$ there exist a $\Delta(x, y, z)$ with either $(x, y, z) = (i-1, i, m)$ or $(x, y, z) = (i+1, i+2, q)$. Moreover, the unoriented \mathbf{A} intersects in succession $\Delta(i, i+1, j)$, $\Delta(x, y, z)$; then all remaining Δ -discs.

Given a fibration-axis pair (\mathbf{H}, \mathbf{A}) a *radial sphere* is a 2-sphere that is transversally intersected by \mathbf{A} twice and is transverse to all of the disc fibers of \mathbf{H} . An *axis piece* α in a radial sphere S is a closed arc whose interior is transverse to the disc fibers of \mathbf{H} and which has empty intersection with at least one disc fiber. Axis pieces $\alpha, \beta \subset S$, are *loop equivalent* if $\partial\alpha = \partial\beta = \alpha \cap \beta$ and if $\alpha \cup \beta$ bounds a 2-disc $\delta \subset S$ such that $\delta \cap \mathbf{A} = \emptyset$.

A *branch* is a block-strand pair, $(B, t) \subset \mathcal{B}$, along with a 2-disc Δ such that:

- Δ is transversally intersected by \mathbf{A} at one point.
- $\partial\Delta = t \cup a$ where $a \subset \partial B$. Specifically, a is an arc made up of three segments, $a = a_T \cup a_S \cup a_B$ where: a_T is on the top of B ; a_S is on the side of B ; and a_B is on the bottom of B .
- $\text{int}(\Delta) \cap \mathcal{B} = \emptyset$

The braid box B' and the weighted strand which emerges from it and loops around the axis is an example, where now we assume that the braid boxes B'_1 and B'_2 and the strands that emerge from them and loop around the two axis pieces are not there.

Iterating the construction of attaching a branch to a root, we obtain a *block-strand tree*. \square

Our next goal is to identify the roots and branches and the tree in the foliation of $P(\mathcal{TA})$. Let $\mathbf{S} \subset P(\mathcal{TA})$ be a complete collection of s -arcs. For present purposes a region $\mathcal{R} \subset P(\mathcal{TA}) - \mathbf{S}$ is either a rectangular shaped subdisc or a subannular region of $P(\mathcal{TA})$. Thus, as before, if \mathcal{R} is a subdisc then $\partial\mathcal{R} = s \cup Y_+ \cup s' \cup Y_-$, where: s and s' are subarcs of leaves in the foliation of $P(\mathcal{TA})$; and Y_+ and Y_- are oriented arcs transverse to the foliation in the positive direction. If \mathcal{R} is a subannulus then $\partial\mathcal{R} = Y_+ \cap Y_-$ where Y_\pm are oriented curves transverse to the foliation in the positive direction. Inside these regions we will have the induced foliation. While our regions may be intersected by clasp arcs, we are not concerned with them at this time.

Definition 16 (Root foliation): Let $\mathcal{R} \subset P(\mathcal{TA}) - \mathbf{S}$ be as above. Let C be a component of $\mathcal{R} \cap G_{\epsilon, \delta}$. We say that \mathcal{R} has a *root foliation* if:

1. C is homeomorphic to either S^1 or $[0, 1]$.
2. If C is homeomorphic to S^1 then \mathcal{R} is an annulus and C is homotopically equivalent to a core circle of \mathcal{R} .
3. If C is homeomorphic to $[0, 1]$ then C has an endpoint on Y_{\pm} and an endpoint near Y_{\mp} . \square

Examples of regions \mathcal{R} which support root foliations are in Figure 55(a). The reader is encouraged to go back to Definition 11 and to compare it to Definition 16. The main point is that we are building up to the notion of a G-handle move that is not based on a circular block-strand tree.

Proposition 5.2 *Let $\mathcal{R} \subset P(\mathcal{TA}) - \mathbf{S}$ be a component which is embedded, where \mathbf{S} might be empty.*

1. *Assume that all b -arcs are essential. Assume that \mathcal{R} has a root foliation. Then the isotopy which corresponds to pushing a component of X_- across \mathcal{R} is a handle move over a root.*
2. *If \mathbf{S} is empty on some component of \mathcal{R} , then in the situation of (1) above \mathcal{R} will be an annulus (see Figure 41 that is standardly tiled, and again pushing X_- across that component $\mathcal{R} \subset pa$ will be a handle move.*

Proof: The isotopy of the braid across a region which has a root foliation can be realized by a sequence of ab -exchanges. To see this, notice that a pouch \mathcal{P}_i is associated to each such region, and since the regions are crossed in a definite order the pouches can be joined in the same order. The assumption that each b -arc is essential implies that \mathcal{P}_i cannot be removed by isotopy, and so has associated to it a new braid block or blocks. The unions of all of the \mathcal{P}'_i 's gives a disc region \mathcal{P} with a subarc of X_- in its boundary. The union of all of the blocks is a root. The isotopy of the subarc of X_- across \mathcal{P} is a handle move across this root. The case of a circular loop of pouches is no different...just imagine that, for example, the dark and light pouches in Figure 55(a) were part of a circular chain of pouches (this is exactly the situation we depicted in Figure 41 then we could push across the entire annulus by a sequence of exchange moves.) \parallel

Example 3: In Figure 6 we saw how a root in a block-strand diagram could be expanded to a block-strand tree. We now wish to identify the analogous concept in the foliation. As before, it will be helpful to see examples before we give the general definition. We first illustrate how the very simple pouch in Figure 54(b) might itself develop a pouch...to do it, just put your fist inside the pouch and push out a bubble which intersects the braid axis twice! Figure 56(a) shows the new foliation of the region \mathcal{R} of Figure 56(a). In the new foliation the arc α cannot be pushed across \mathcal{R} by an ab exchanges, but bb -exchange moves come to the rescue. The new vertex x has valence 2 and type (b, b) . Lemma 3.3, part (2), applies. We can do a bb exchange, and then remove the resulting inessential b -arcs. The resulting change in foliation takes us back to the situation of Figure 54(a). Now an ab exchange is possible, pushing α to α' as we did before. As for the corresponding braid picture, the presence of the new vertices x, y means that the block B' of sketch Figure 54(d) has grown new branches, and the handle move over the resulting tree is now a bb exchange followed by an ab exchange.

Example 4: Our next example, in Figure 56(b), shows the changes in foliation when we grow new branches in two different ways in the foliation of the region \mathcal{R} of Figure 55(a). The changes are supported inside the region $wsvv'r'w$. The branch associated to the new vertices x and y (resp. x' and y') is attached to the strand joining blocks B_{i+1} and B_{i+2} (resp. blocks B_i and B_{i+1}). The root diagram of Figure 55(b) has changed to a block-strand tree. In the foliation, the growth has all been

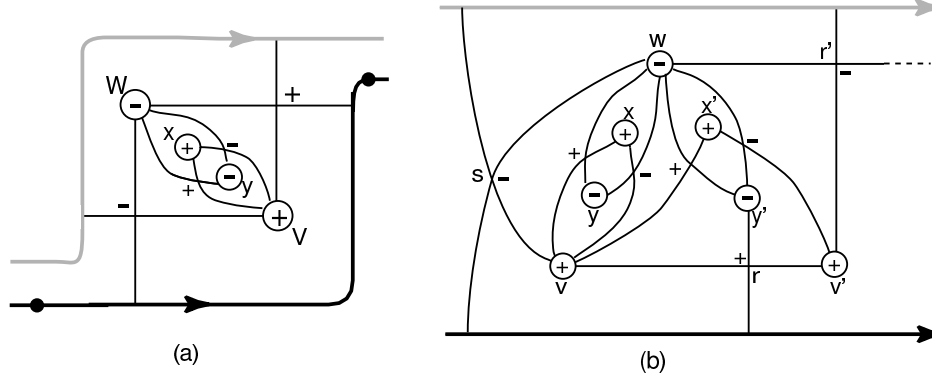


Figure 56: Expanding root foliations to tree foliations

‘inward’. This time two bb exchanges and two ab exchanges are needed to realize the handle move over the block-strand tree. The reason handle moves can be hard to visualize is because the part of the surface that undergoes the change in foliation is always far away from the block-strand tree in the closed braid. Putting this in another way, the foliated surface points out the way to organize very big handle moves, some of which can be quite difficult to see in the closed braid diagram, but the net result is to simplify a closed braid representative of a knot.

Definition 17 (Tree foliation): A region \mathcal{R} has a *tree foliation* if, after a sequence of bb -exchanges the foliation is reduced to a root foliation. \square

The next proposition shows how a tree foliation imposes a block decomposition on our two braids:

Proposition 5.3 *Let $\mathcal{R} \subset P(\mathcal{TA}) - \mathbf{S}$ be a component whose image is embedded. Assume that all b -arcs are essential. Assume that \mathcal{R} has a tree foliation. Then the isotopy which corresponds to pushing X_- across \mathcal{R} is a handle move over a block-strand tree.*

Proof: The isotopy of the braid through the sequence of bb -exchanges corresponds to collapsing a tree to its root. After that, an isotopy of X_- across the new \mathcal{R} corresponds to a handle move over this root. \parallel

Remark 5.1 Two remarks are in order. They relate to Propositions 5.2 and 5.3.

1. In both propositions the basic assumption is that the region \mathcal{R} is embedded. Of course this will be the case if no clasp arcs intersect \mathcal{R} . But it will also be the case if all that we assume is that (a) there are no long clasp arcs which intersect \mathcal{R} , and (b) each clasp arc which intersects \mathcal{R} has an endpoint on X_- . For, if so the image of \mathcal{R} in \mathcal{TA} must be embedded.
2. After a handle move across \mathcal{R} trivial loops (end tiles on the tabs) may be revealed. Later, when we get to the final steps in the proof, we will remove them by destabilization.

We are finally ready to consider the most general case, when we have several related regions $\mathcal{R}_1, \dots, \mathcal{R}_k$ which are intersected by paired clasp arcs. Thus the handle move across one \mathcal{R}_i will have to be interrupted midway to do part of the handle move along an associated \mathcal{R}_j .

Definition 18 (G-handle foliation): Let $\{\mathcal{R}_1, \dots, \mathcal{R}_k\} \subset P(\mathcal{TA})$ be a collections of regions such that each $\text{int}(\mathcal{R}_i)$, $1 \leq i \leq k$, is embedded in $S^3 - (X_- \cup X_+)$ and each \mathcal{R}_i has a tree foliation.

Assume each \mathcal{R}_i has at least one clasp arc with an endpoint on X_- and at least one clasp arc with an endpoint on X_+ , and with the puncture endpoints on b arcs in \mathcal{R}_i , so that in particular no clasp arcs is long. Moreover, assume that the image of $\{\mathcal{R}_1, \dots, \mathcal{R}_k\}$ in \mathcal{TA} is connected. Then the collection of regions is said to have a *G-handle foliation*. \square

Proposition 5.4 *Let $\{\mathcal{R}_1, \dots, \mathcal{R}_k\} \subset P(\mathcal{TA})$ be a collections of regions which, taken together, have a G-handle foliation. Then an isotopy of X_- to X_+ across the regions $\{\mathcal{R}_1, \dots, \mathcal{R}_k\}$ is realized by a G-handle move.*

Proof: Since each region \mathcal{R}_i is embedded, the isotopy of any one arc $\mathcal{R}_i \cap X_-$ across \mathcal{R}_i to $\mathcal{R}_i \cap X_+$ corresponds to a handle move. Moreover, since each region contains clasp arcs having endpoints on both X_- and X_+ and since their image in \mathcal{TA} is connected, we have an interdependence of the isotopies across all the regions. Thus, an isotopy across the collection $\{\mathcal{R}_1, \dots, \mathcal{R}_k\}$ is a G-handle move. \parallel

The moves that are used in the passage from $X_- \rightarrow X_+$ in the MTWS are: destabilization, exchange moves, G-handle moves and flypes. A single block-strand diagram suffices to describe the destabilization move and the exchange move. We now ask whether (for fixed braid index $n = b(X_-)$) the G-handle moves needed to consider all possible G-handle moves on a braid of braid index n can be described by finitely many before-after block diagram pairs? The answer to that question is not difficult:

Lemma 5.4 *G-handle moves have the following properties:*

1. *They preserve braid index.*
2. *For each fixed braid index m they are described by a finite set $\mathcal{E}(m)$ of templates.*

Proof:

1. A G-handle move is a sequence of inter-related handle moves over block-strand trees, and a handle move can always be replaced by a sequence of exchange moves. Since exchange moves preserve braid index, it follows that G-handle moves do too.
2. We consider the unfolded version of a block-strand tree. Each outermost root with n_i strands contributes n_i to the braid index. Working our way systematically toward the root, each bud involves a new block with n_j strands. Thus if a block-strand tree contains k roots with buds, the braid index will be at least k . This implies that for a given braid index there is a bound on the number of possible block-strand trees, which implies that there is a bound on the number of handle moves in the sequence. But then, only finitely many distinct G-handle moves can occur. \parallel

5.3 The proof of parts (a), (b) and (c) of the MTWS

We are given two closed braids X_- and X_+ which represent the same oriented link type \mathcal{X} . By hypothesis the braid index of X_+ is minimal for all closed braid representatives of \mathcal{X} . Using the construction which was given in Section 2 we may assume that X_1 and X_2 cobound an immersed annulus \mathcal{TA} . This annulus has the properties which are given in Proposition 2.1. By the work which was done in Section 4 we may further assume that \mathcal{TA} supports a braid foliation, and that every clasp arc pair lies in a union of singular leaves and in a normal neighborhood. Our complexity function is $C(\mathcal{TA}) = (n_1, n_2, n_3)$. Here n_1 is the number of singular points contained in the clasp arcs and n_2 (resp. n_3) is the number of vertices (resp. singularities) in the foliation of \mathcal{TA} .

5.3.1 Proof of part (a):

If the foliation has a vertex v of valence 2, and if $\text{link}(v)$ a good disc, then either X_- or X_+ will admit an exchange move. By Lemma 4.5, after some number of exchange moves we may assume that properties (1)-(6) of that lemma hold. Notice that exchange moves (on either X_- or X_+) reduce the complexity and preserve braid index. The exchange moves in question are, in fact, the sequence of exchange moves in the statement of part (a) of the MTWS. These exchange moves address the complication which was exhibited in Figure 5, namely that exchange moves (on both X_- and X_+) can result in arbitrarily many distinct conjugacy classes of closed braids which represent the same knot or link type. However, if we minimize the n_2 and n_3 in the complexity triple, using Lemma 4.5, that issue no longer exists.

5.3.2 Proof of part (b):

After this point in the proof we will be dealing exclusively with X'_- and X'_+ . However, to simplify notation we assume that the step was vacuous and revert to the symbols X_- and X_+ . From this point on all the changes that we make will be changes in X_- . Note that Lemma 4.5 only applies to the complement of the normal neighborhoods of the clasp arcs, but now we begin to study the entirety of \mathcal{TA} . The proof breaks down into three cases.

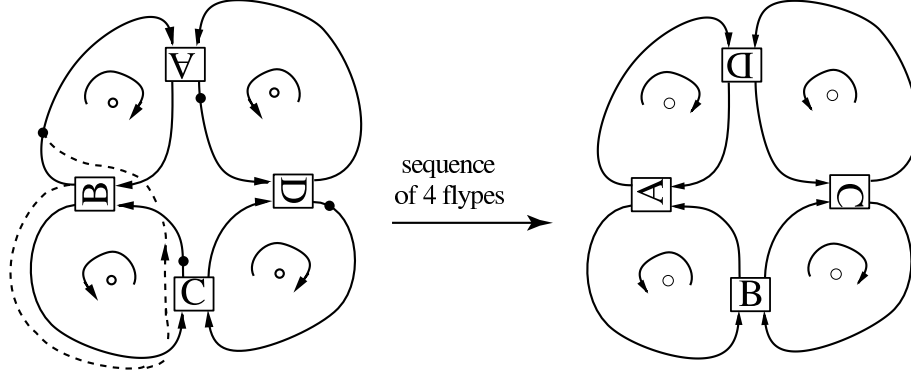
Case 1: $n_1 = 0$. If there are clasp arcs, then by Proposition 4.2 we may assume that they have pushed into leaves of the foliation. Since the clasp arcs contain no singularities of the foliation, we may assume that they are contained entirely in a -arcs or s -arcs. But then they may be removed by braid isotopies which shorten the a -arcs or s -arcs, reducing to the case when there are no clasp arcs. So we may assume that there are no clasp arcs.

Going back to the construction in §2, we note that clasp arcs arose in our constructions in a very particular way. The construction began with the choice of a Seifert surface \mathbf{F}_+ for the link which we called X_+ and a preferred longitude $X'_+ \subset \mathbf{F}_+$ for X_+ . The links X_+ and X'_+ are in general geometrically linked. We pushed X'_+ across a family of disjoint discs D_1, \dots, D_k to construct a link X''_+ which is isotopic to X'_+ and geometrically unlinked from X_+ . The clasp arcs arose precisely because of the geometrical linking between X_+ and X'_+ . So if there are no clasp arcs, then X_+ and X'_+ must have been geometrically unlinked. But then \mathcal{X} can only be the μ component unlink for some $\mu \geq 1$.

Each component of the unlink bounds an embedded disc. By the main result in [11] we may push X_- to X_+ so that (up to braid isotopy) we use only exchange moves and destabilizations. Each exchange move and each destabilization reduces the entries n_2 and n_3 in $C(\mathcal{TA})$. This is essentially the argument that is given in [4] to prove the MTWS in the special case of the unlink. See Theorem 4.3 of [4].

Case 2. $n_1 > 0$ and the foliation of $P(\mathcal{TA})$ contains clasp arcs, but no long clasp arcs:

At this point we need to consider a case which we have systematically ignored up to now. It may happen that there is a component of $P(\mathcal{TA})$ which contains a thinly foliated annulus \mathcal{S} of type 0_a , as in Figure 45. Of course the restriction of the foliation to this annulus has long clasp arcs, so we know that the motion across \mathcal{S} is realized by a sequence of flypes. See Figure 57 for the sequence of flypes which re needed in the case of the annulus of type 0_a in Figure 45. There are 4 pairs of clasp arcs, and we need four flypes to push X_- across the annulus. To see why the motions are flypes, go back to Figure 4, where it is shown how a Markov tower which consists of a stabilization, slide, flip and then a destabilization can be replaced by a flype. In the case which is illustrated here, a positive stabilization along the short arc which is between each braid box and the black dot which follows it, as illustrated by the dotted arc at one of them. Then slide and flip the block. Then destabilize. The stabilize-slide-flip-destabilize sequence can be replaced by a flype. We remark that this particular sequence of flypes is admissible, because the braid index change across the annulus is zero.

Figure 57: Pushing X_- across the type 0_a annulus of Figure 45.

We pass to the case when there are no type 0_a annuli in $P(\mathcal{TA})$. Then s -arcs must occur. Let \mathbf{S} be a complete collection of s -arcs in the foliated annulus $P(\mathcal{TA})$. Call a component $\mathcal{R} \subset P(\mathcal{TA}) \setminus \mathbf{S}$ a *handle region* if it contains no clasp arcs or if it contains one or more short clasp arcs, each having an endpoint on $\partial\mathcal{R} \cap X$. Notice that a handle region is always embedded under the natural map which takes $P(\mathcal{TA})$ to \mathcal{TA} . For, if it contains the puncture endpoint of a clasp arc γ_- it cannot contain its mate γ_+ , because γ_+ begins on X_+ , but by definition all short clasp arcs in a handle region begin on X_- . It may also happen that there is a family of handle regions which are intersected by short clasp arcs of *both* type γ_- and type γ_+ . If so, define an equivalence relation on the components of $P(\mathcal{TA}) \setminus \mathbf{S}$, as follows: $\mathcal{R}_p \sim \mathcal{R}_q$ if there exists $\gamma_+ \subset \mathcal{R}_p$ which is paired with $\gamma_- \subset \mathcal{R}_q$. Moving X across an equivalence class of regions $\{\mathcal{R}_1, \dots, \mathcal{R}_m\}$ is a G-handle move. By Propositions 5.2, 5.3 and 5.4 the isotopy of $X_- \cap \partial\mathcal{R}$ across \mathcal{R} is realized by a handle move or a G-handle move.

So we start by eliminating all handle regions. As we do so, subarcs of the original link X_- will be replaced by new subarcs, also new handle regions may be created and new regions which have empty intersection with the clasp arcs may occur. In the latter case we need to apply the methods of Case 1. As in [4] the isotopy across any region which is either a disc or an annulus and which has empty intersection with the clasp arcs can be realized by changes of fibration, destabilization and exchange moves.

It may happen that after all these changes a clasp arc which was short becomes long. If so, we pass to Case 3, returning to Case 2 after eliminating all long clasp arcs. Notice that handle moves and G-handle moves reduce complexity.

Case 3. $n_1 > 0$. **The foliation of \mathcal{TA} contains clasp arcs, and some of them are long:** By the construction which was given in Lemma 5.1, we find a family \mathcal{S} of subannuli of $P(\mathcal{TA})$ which support a thin foliation. Some of these components may be trivially foliated, but because there is at least one long clasp arc they are not all trivially foliated.

By Proposition 5.1 we may use a sequence of flypes to push X_- across \mathcal{S} . The new X_- may or may not have long clasp arcs. If it does, we repeat the construction as often as needed until there are no more long clasp arcs. Notice that the flypes which we use will in general have weighted strands, so we cannot assume that they preserve the braid index, but they always reduce the complexity 3-tuple $C(\mathcal{TA}) = (n_1, n_2, n_3)$ because they reduce the number n_1 of singular leaves which the long clasp arc crosses. Now, after some number of such moves we may find ourselves in the situation where there are no more long clasp arcs, but that we are in the situation of case 2. We then use handle moves and G-handle moves to further reduce the complexity. As noted in the proof for case 2, it can happen that new long clasp arcs are created during these modifications, in which case we repeat the construction of the thinly foliated annuli and use flypes to push across them. Continuing

in this way, we eventually push X_- to X_+ . Each step is either a destabilization, an exchange move, a G-handle move or a sequence of flypes with weighted strands. Now observe that destabilizations reduce n_3 , exchange moves reduce n_2 and n_3 , and the most general G-handle moves and flypes reduce n_1, n_2 and n_3 . Thus parts (a) and (b) of Theorem 1 are true. \parallel

5.3.3 Proof of part (c)

The only problem with the sequence of moves which we produced in the course of the proof of parts (a) and (b) of the MTWS is that, when there are long clasp arcs, the sequence of flypes which we need to use to push across $P(\mathcal{TA})$ may include inadmissible flypes. Of course, we know that if we have a complexity-reducing sequence $X'_- = X^1 \rightarrow X^2 \rightarrow \dots \rightarrow X^r = X'_+$, like the one given in part (b) of the MTWS, then if X^p is the first inadmissible flype it is trivial to say that the move $X^p \rightarrow X^r$ is both complexity-reducing and braid index reducing. Thus part (c) of the MTWS follows immediately from parts (a) and (b).

5.4 The proof of part (d) of the MTWS.

There has been very little hint in our work up to now which suggests the finiteness statement of part (d) of the theorem. Our main task in this section is to prove it.

5.4.1 Construction of the templates

The reader is referred to Section 1 for the definition of a template. We are interested now in the templates whose initial block-strand diagrams support X_- and whose final block-strand diagram supports X_+ . This is a different focus than the one we have had up to this point, because our work has concentrated on the support of the isotopies that realize flypes, exchange moves, handle moves and G-handle moves, but now we consider the entire isotopy from X_- to X_+ . Choose any fixed integer $m \geq 2$. We will be working with the pairs of closed braids $\mathbf{X}_{m,n}$ which represent all link types of braid index n . The templates $\mathcal{T}(m,n)$ which we will construct have two kinds of blocks: blocks that move during the isotopy from X_- to X_+ and blocks that are fixed throughout the isotopy. The former will be familiar to the reader. The latter are new, even though we saw many examples in the Introduction to this paper, when we defined templates. We will also need to study the possibilities for the strands that join the fixed and moving blocks:

Blocks that move: The reader is referred to Section 5.1 for the definitions of long and doubly long clasp arcs. Every block in a block-strand diagram pair that changes position during the isotopy from X_- to X_+ arises when there are doubly long clasp arcs in $P(\mathcal{TA})$. For an example, see the block R in the template of Figure 3. The associated foliated annulus is given in Figure 13. It contains exactly one long clasp arc. A second example is given in the template which was illustrated in the boxed subset of Figure 9. The associated foliated annulus $P(\mathcal{TA})$ was shown in Figure 30. It has no doubly long clasp arcs. The associated template contains no blocks that move during the isotopy from X_- to X_+ . There will also be a third ingredient that could, in principle, upset the finiteness, and that is the question of whether there are finitely many ways to join the blocks:

Blocks that are fixed: A template will in general also include blocks are outside the support of the isotopy of X_- across \mathcal{TA} to X_+ . We have not considered these in any systematic way, up to this point, however they could be seen in examples. One example is the blocks P and Q in Figure 3. Another is the blocks W, X, Y, Z in the boxed pair of block-strand diagrams in Figure 30. To understand how fixed blocks arise, we consider the H_t -sequence associated to the foliation of \mathcal{TA} and $P(\mathcal{TA})$ in the fibration \mathbf{H} . Let $\{t_0, t_1, \dots, t_\zeta\} \subset [0, 2\pi)$ be a cyclic listing of all the angles at which the corresponding $H_{t_i} \in \mathbf{H}$ contains a singularity, ordered according to their natural cyclic

order in **H**. Let $P(\mathcal{TA})_{\text{tiled}} \subset P(\mathcal{TA})$ be that portion of \mathcal{TA} that is not foliated by s -arcs. If we focus in on the components of $\cup_{t_i \leq t \leq t_{i+1}} (H_t - (H_t \cap \mathcal{TA}_{\text{tiled}}))$, we see that each component has a $\{\text{disc}\} \times [0, 1]$ structure. Let $C \subset \cup_{t_i \leq t \leq t_{i+1}} (H_t - (H_t \cap \mathcal{TA}_{\text{tiled}}))$ be such a connected component having structure $\Delta \times [t_i, t_{i+1}]$. Now C may contain a number of s -arc bands, which inside C braid together. We can amalgamate this braiding of s -arc bands into a single block $B(C)$. Thus away from $B(C)$ the s -arc bands are the trivial braid.

Next, let $C' \subset \cup_{t_{i+1} \leq t \leq t_{i+2}} (H_t - (H_t \cap \mathcal{TA}_{\text{tiled}}))$ be a connected component such that $C \cap H_{i+1} = C' \cap H_{i+1}$. In particular, $C \cap H_{i+1}$ does not contain a singularity or clasp arc. Let $B(C')$ be the block containing the braiding of s -arc bands in C' . Then we can amalgamate block $B(C)$ and $B(C')$.

Examples of fixed blocks are given in both Figures 13 and 30. In the former the fixed blocks are P and Q . In the latter they are W, X, Y, Z .

The issue of whether there might be an unbounded number of fixed blocks is essentially the issue of whether, in the foliated annulus $P(\mathcal{TA})$, there is a bound on the number of bands of s -arcs which join up the disc regions in the foliated annulus $P(\mathcal{TA})$.

The strands that join the blocks: We have already seen that the moving blocks are associated to the intersection of \mathcal{TA} with the union \mathcal{N} of all normal neighborhoods of doubly long clasp arcs. We have also seen that the fixed blocks are associated to regions where the tiling of \mathcal{TA} is by bands of s -arcs. We shall see that the strands that join the blocks are associated to the part of \mathcal{TA} which is in the complement of \mathcal{N} and the bands of s -arcs, and is ‘near’ the boundary, in a sense that will be made precise in Section 5.4.3 below.

The bounded nature of both types of blocks, and of the strands that join them, will be established when we prove the following lemma:

Lemma 5.5 (The Finiteness Lemma): *Let X_-, X_+ be closed braid representatives of \mathcal{X} . Assume that $b(X_-) = m$ and $b(X_+) = n$ are fixed and that n is minimal for all closed braid representatives of \mathcal{X} . Assume that the complexity $C(X_-, X_+, \mathcal{TA})$ is minimal. Assume that $P(\mathcal{TA})$ has $0 \leq c \leq \infty$ doubly long clasp arcs. Then the following bounds exist:*

- (i) *The number of moving blocks in the passage from $X_- \rightarrow X_+$ has an upper bound which depends on the sum $m + n$.*
- (ii) *The number of fixed blocks formed by the amalgamation of blocks containing braidings of s -arc bands is also bounded, and the bound again depends on $m + n$.*
- (iii) *There is a bound, which again depends on $m + n$ on the number of distinct ways that the blocks formed in (1) and (2) above can be joined up to form block-strand diagrams.*

Proof: The proof will be given in Section 5.4.4 below.

5.4.2 Finiteness in the foliation of \mathcal{TA}

In this section we consider the following question: when we fix the braid indices of X_- and X_+ and assume that the complexity of the triple (X_-, X_+, \mathcal{TA}) is minimal, which aspects of the foliation are finite and which can grow without bound? We begin with an analysis of the constraints placed on the foliation by the fact that \mathcal{TA} is a union of annuli.

On each annular component of $P(\mathcal{TA})$ the foliation determines a cellular decomposition which goes over to a cellular decomposition of S^2 on shrinking the 2 boundary components to points. Letting V, E and F be the number of vertices, edges and tiles, the fact that $\chi(S^2) = 2$ shows that on each component of the foliated surface \mathcal{TA} we have $V + 2 - E + F = 2$. Each tile has four edges and each edge is an edge of exactly 2 tiles, so that $E = 2F$. Let $E(a), E(b)$, and $E(s)$ be the number of a -, b -, and s - edges, where we count both a_+ and a_- edges as being type a . Then:

$$(2) \quad 2V = E(a) + E(b) + E(s)$$

Let W be a vertex in the foliation of $P(\mathcal{TA})$. The *valence* v of W is the number of singular leaves which have an endpoint on W . The *type symbol* of w is a cyclically ordered sequence (t_1, t_2, \dots, t_v) where each t_i is either a or b , recording the edge types encountered as one travels around W on $P(\mathcal{TA})$ in the direction of increasing θ . Here we do not distinguish between edges of type a_+ and type a_- . We say that W has *type* $(\alpha, v - \alpha)$ if the type symbol for W includes α edges of type a and $v - \alpha$ edges of type b . See Figure 58 for examples of vertices of type $(1,1)$, $(1,2)$, and $(1,3)$. Let

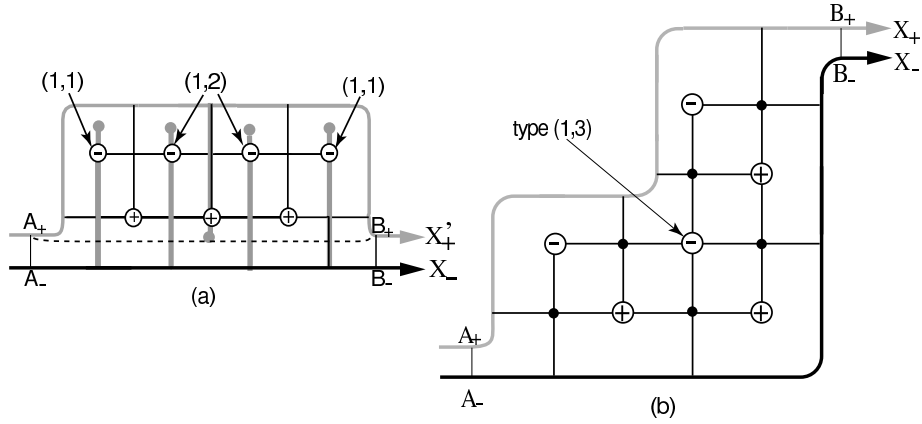


Figure 58: Vertices of type $(1, \beta)$

$V(\alpha, v - \alpha)$ be the number of vertices of valence v and type $(\alpha, v - \alpha)$ in the foliation of $P(\mathcal{TA})$. Since:

$$(3) \quad V = \sum_{v=1}^{\infty} \sum_{\alpha=0}^v V(\alpha, v - \alpha)$$

$$(4) \quad E(a) = \sum_{v=1}^{\infty} \sum_{\alpha=0}^v \alpha V(\alpha, v - \alpha)$$

$$(5) \quad 2E(b) = \sum_{v=1}^{\infty} \sum_{\alpha=0}^v (v - \alpha) V(\alpha, v - \alpha)$$

we may combine equations (2) through (5) to obtain:

$$(6) \quad \sum_{v=1}^{\infty} \sum_{\alpha=0}^v (4 - v - \alpha) V(\alpha, v - \alpha) = 2E(s)$$

Rearranging terms, we have proved that the following relationship holds:

$$(7) \quad V(1, 1) + 2V(1, 0) + 2V(0, 2) + V(0, 3) = 2E(s) + V(2, 1) + 2V(3, 0) + \sum_{v=4}^{\infty} \sum_{\alpha=0}^v (v + \alpha - 4) V(\alpha, v - \alpha),$$

with every term on both the LHS and the RHS non-negative. Notice that every vertex type appears and is counted, with the following 3 exceptions: vertices of type $(1,2)$, $(2,0)$ and $(0,4)$ do not appear in this equation because in all three cases the coefficient $(v + \alpha - 4) = 0$.

Our goal now is to learn which of the terms in Equation 7 are bounded, and which terms can grow without bound, for fixed braid indices $b(X_-) = m$ and $b(X_+) = n$. Let $\mathbf{X}_{(m,n)}$ be the set of all triples (X_-, X_+, \mathcal{TA}) of minimal complexity with $(b(X_-), b(X_+)) = (m, n)$. Choosing $(X_-, X_+, \mathcal{TA}) \in \mathbf{X}_{(m,n)}$, our goal is to understand the range of values that can be assumed by some of the terms $V(\alpha, v - \alpha)$ in Equation 7, and to understand which terms can grow without bound. Let $\mathcal{N} \subset P(\mathcal{TA})$ be the union of all normal neighborhoods of the clasp arcs. Let $P'(\mathcal{TA}) = P(\mathcal{TA}) \setminus \mathcal{N}$. Let $V'(\alpha, v - \alpha)$ be the number of vertices of type $(\alpha, v - \alpha)$ in $P'(\mathcal{TA})$.

Lemma 5.6 *Choose $(X_-, X_+, \mathcal{TA}) \in \mathbf{X}_{m,n}$. Then the following inter-related inequalities hold for the individual terms in Equation 7:*

- (1) $V(1, 0) \leq m + n$.
- (2) $V(\alpha, v - \alpha) \leq m + n$ if $\alpha \geq 2$.
- (3) *If a vertex W contributes to $V(0, 2)$ or $V(0, 3)$ then $\text{link}(W) \cap \mathcal{N} \neq \emptyset$. (Remark: there is no restriction on $V(0, 2)$ and $V(0, 3)$; they can be arbitrarily large.)*
- (4) $V'(0, 4)$ and $V'(1, 2)$ are bounded, but $V(0, 4)$ and $V(1, 2)$ can be arbitrarily large.
- (5) $E(s)$ is bounded.
- (6) $V(1, 1) \leq 2(m + n) + E(s) + \sum_{\beta=3}^{\infty} V(1, \beta)$.
- (7) $V(1, v - 1), v \geq 4$ and $V(0, v), v \geq 5$ are bounded. In particular, an increase in $V(0, 2)$ and/or $V(0, 3)$ must be balanced in Equation 7 by an increase in β in $V(0, \beta)$ or $V(1, \beta)$.

Proof: We consider the various inequalities in order:

Proof of (1) and (2). Notice that if a vertex W has type $(1, 0)$, there is an arc in the associated singular leaf that has its endpoints on the boundary of $P(\mathcal{TA})$ and splits off a disc containing W . (See Figure 18.) If we surger $P(\mathcal{TA})$ along this arc we obtain an annulus whose boundary is a braid of braid index 1 less than that of $X_- \sqcup X_+$. Similarly, a vertex W of type $(\alpha, v - \alpha)$, $\alpha \geq 2$ has an $a_\epsilon a_\epsilon$ -singular leaf adjacent to W . This singular leaf will contain an arc that has its endpoints on the boundary of $P(\mathcal{TA})$ and this arc splits off a disc whose boundary is transverse to the fibration \mathbf{H} . Thus, the boundary of this split-off disc contributes to the braid index count. Thus $V(1, 0)$ and $V(\alpha, v - \alpha)$, with $\alpha \geq 2$, cannot be greater than the braid index of $X_- \sqcup X_+$, i.e. $m + n$.

Proof of (3): By the remarks which precede the proofs of statements (4)-(7) of Lemma 4.5 of this paper, if a vertex W has type $(0, 2)$ or $(0, 3)$, and if its link is a good disc, then that vertex can be removed by changes of foliation followed by exchange moves. This reduces complexity, however, we are assuming minimum complexity. Therefore no such W , unless $\text{link}(W)$ is not good, i.e it intersects \mathcal{N} .

Proof of (4): The terms $V(0, 4)$ and $V(1, 2)$ are not present in Equation 7 because their coefficients in the double sum on the RHS are zero, so Equation 7 places no restriction on their growth. On the other hand, suppose that $V'(1, 2)$ is allowed to grow. Note that if W contributes to $V'(1, 2)$, then it is near X_- or X_+ . An example was given in Figure 55(a). In this situation we showed in Figure 55(b) that the corresponding embedding is a block-strand tree. Each new block in the tree contributes at least 1 to the braid index. This forces the braid index of $X_- \sqcup X_+$ to grow, contradicting our assumption that it is fixed at $m + n$. A similar argument applies to $V'(0, 4)$.

Proof of (5): Suppose that we have an unbounded number of s -arcs that contribute to $E(s)$. Then there will be an unbounded number of singularities of type $a_\epsilon s$ and/or sb . Notice that there is a direct

correspondence between the number of $a_\epsilon s$ -singularities and the number of vertices contributing to $V(1, 0)$ and $V(\alpha, v - \alpha)$ for $\alpha \geq 2$. But by statements (1) and (2) we know that $V(1, 0)$ and $V(\alpha, v - \alpha)$, $\alpha \geq 2$ are bounded. Thus, the only way that $E(s)$ can grow is if there is a growth in the number singularities of type sb .

Fixing \mathcal{TA} , let \mathbf{S} to be a complete collection of s -arcs in the foliation. Since we are assuming that $E(s)$ can be arbitrarily large we know that the cardinality $|\mathbf{S}|$ of \mathbf{S} is unbounded. This means that the number of components of $\mathcal{TA} - \mathbf{S}$ is unbounded. Thus, for large enough $E(s)$ there will be a component $\mathcal{C} \subset \mathcal{TA} - \mathbf{S}$ which has angular length strictly less than 2π . This means that all of the growth in the components of \mathcal{TA} split along \mathbf{S} comes from components \mathcal{C} with angular length $X_- \cap \mathcal{C}$ and $X_+ \cap \mathcal{C}$ strictly less than 2π . In particular, for such a component the set of fibers H_t for which $H_t \cap (X_- \cap \mathcal{C}) \neq \emptyset$ coincides with the set of fibers for which $H_t \cap (X_+ \cap \mathcal{C}) \neq \emptyset$, since $X_- \cap \mathcal{C}$ and $X_+ \cap \mathcal{C}$ have their endpoints on the same two bs -singularities. (This means that in the preimage $P(\mathcal{TA} - \mathbf{S})$ every component of the preimage of \mathcal{C} will itself have embedded image.) We are thus seeing a growth in the components of $\mathcal{TA} - \mathbf{S}$ that are characterized by the condition:

- There exists an $H_t \in \mathbf{H}$ with $H_t \cap (X_+ \cap \mathcal{C}) = \emptyset$ and $H_t \cap (X_- \cap \mathcal{C}) = \emptyset$.

We conclude that the following holds: Let $\{\mathcal{C}_1, \dots, \mathcal{C}_i\} \subset \mathcal{TA} - \mathbf{S}$ be the set of components for which there exists an $H_t \in \mathbf{H}$ such that $H_t \cap (X_\pm \cap \mathcal{C}_j) = \emptyset$ for all $1 \leq j \leq i$. If $E(s)$ grows then the index i must also grow.

Next notice that $H_t \cap (\cup_{1 \leq j \leq i} \mathcal{C}_j) \subset H_t$ will have i outermost b -arcs. If i grows then the number of inessential b -arcs must grow. In fact if we understand the isotopy of X_- across any one of our \mathcal{C}' s to be a G -handle move, we see that that an increase in i forces the existence of a \mathcal{C} that has all of its b -arcs inessential. But, an isotopy across a \mathcal{C} that has only inessential b -arcs can be achieved by collapsing the inessential b -arcs, i.e. by braid isotopy. This completes the proof of assertion (5).

Proof of (6): Recall that the thinly foliated annuli associated to X_- are a union of $E(s)$ disc regions of type $0_d, 1_d$ and -1_d , joined up by bands of s -arcs. Choose s -arcs with endpoints A_+, A_- and B_+, B_- as in Figure 58(a) and consider the disc region which they cut off. We examine first the situation when the region has type -1_d . Consider the dotted path joining A_+ to B_+ . It is constructed to be everywhere transverse to the foliation. It splits off a subdisc of the tiling that contains one more negative than positive vertex. Since A_- lies in the same leaf of the foliation as A_+ , and similarly for B_- and B_+ , it follows that the path in X_- between A_- and B_- has to have angular length at least 2π , because there is a change of 1 in braid index across the split-off disc. Looking at this fact another way, as we traverse X_+ from the point A_+ to B_+ we pass over the endpoints of a_+ -arcs that are adjacent to vertices of type $(1, 1), (1, 2), (1, 2), \dots, (1, 2), (1, 1)$. This implies that there are at most $b(X_+)$ subpaths in X_+ that meet first a vertex of type $(1, 1)$, then a series of vertices of type $(1, 2)$, and finally another vertex of type $(1, 1)$. The same reasoning applies to X_- and a disc of type $+1_d$. (In this regard, it is important to notice that we are looking at the *sum* $b(X_-) + b(X_+)$). Thus the two ‘end’ vertices of type $(1, 1)$ on a disc region of type $\pm 1_d$ contribute at least 1 to $b(X_+) + b(X_-)$. Of course they could also contribute much more, because there is no reason why the subarcs of X_- or X_+ which are in the boundary of a disc region cannot encircle the braid axis many times, but the point is that they contribute at least 1.

Now observe: A region of type 0_d has a unique vertex of type $(1, 1)$. Since we were only counting instances of ‘consecutive pairs’ in our earlier analysis, these vertices of type $(1, 1)$ were not counted. There are $E(s)$ regions total, and therefore at most $E(s)$ regions of type 0_d , so the vertex count must be reduced by $E(s)$ if we are only interested in the ones that drive up the braid index. Finally, vertices of type $(1, \beta), \beta \geq 3$ occur when ‘inside corners’ are created by the stringing together of regions of type 0_d . See Figure 58(b). Everything is now clear except for the factor 2 on the RHS. It is needed because, suppose for a moment that $E(s)$ and $V(1, \beta), \beta \geq 3$ are both zero. Then we will have counted twice as many vertices of type $(1, 1)$ as there are regions where the braid index changes. The inequality in (6) follows.

Proof of (7): We study Equation 7 and ask which terms can grow without bound on both sides. By statements (1) and (6) of this Lemma we know that the terms $V(1, 0)$ and $V(1, 1)$ on the LHS cannot grow without bound for fixed m and n . By statement (3) of this Lemma we know that if $V(0, 2)$ and/or $V(0, 3)$ on the LHS grow without bound, then the growth must occur inside the union \mathcal{N} of all normal neighborhoods of clasp arcs.

Passing to the RHS, we know from statement (5) that $E(s)$ cannot grow without bound, for fixed m, n . By statement (2) we know that $V(2, 1)$ and $V(3, 0)$ are bounded. But then, the only terms which might not be bounded, on the RHS of Equation 7, are those in the double sum. However, of the terms in the double sum we know from statement (2) that $V(\alpha, v - \alpha)$ is bounded if $\alpha \geq 2$.

Suppose that β is bounded but that $V(1, \beta)$ increases without bound. This means that there is some fixed value of β for which there are arbitrarily many vertices of type $(1, \beta)$. An example is illustrated in Figure 59(a) for $\beta = 4$. We show two vertices that contribute to the count $V(1, 4)$. But then, by our construction of the thinly foliated annuli there must be an unbounded number of vertices contributing to the count of $V'(1, 2)$. But by statement (4) we know that $V'(1, 2)$ is bounded. Similarly, we can deal with $V(0, \beta)$ by showing if the number of vertices contributing to the count of $V(0, \beta)$ for a fixed β is unbounded then there will be an unbounded number of vertices contributing to $V'(0, 4)$. But by statement (4) we know that $V'(0, 4)$ is bounded. (Again, visualize a ‘patch’ like the one in Figure 59(a), but in the interior of $P(\mathcal{TA})$.) Thus, an increase in $V(0, 2)$ and/or $V(0, 3)$ can only be balanced by an increase in β for vertices of type $(1, \beta)$ and/or $(0, \beta)$. This completes the proof of Lemma 5.6. \parallel

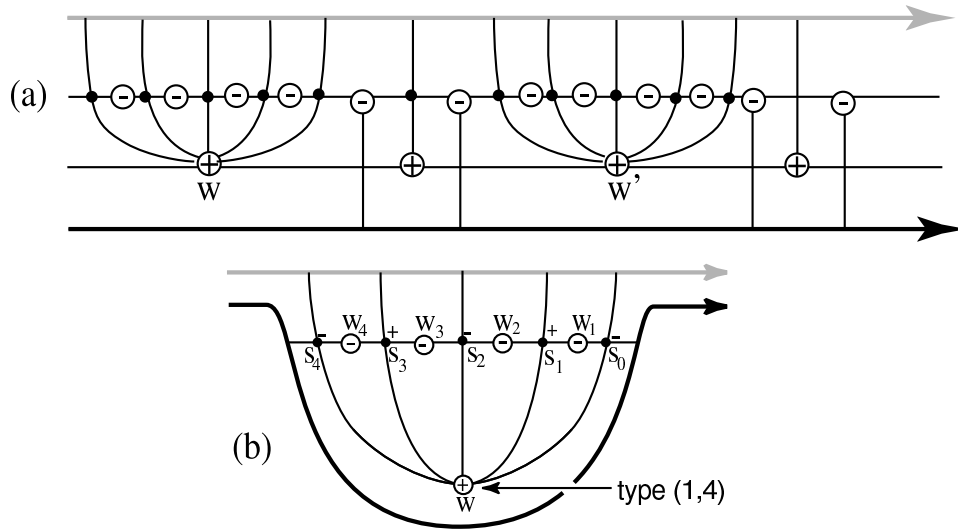


Figure 59: Patches

5.4.3 The boundary support \hat{S} of $X_- \sqcup X_+$, and the formation of moving blocks.

It should be clear from the work just done that the growth of vertices near the boundary of \mathcal{TA} is the key to understanding which aspects of \mathcal{TA} are finite. The *boundary support* of $X_- \sqcup X_+$ is a subset $\hat{S} \subset \mathcal{TA}$ which includes but is larger than the thinly foliated annuli constructed earlier. A b -arc in \mathcal{TA} is said to be *near* $X_- \sqcup X_+$ if it has a vertex endpoint that is also meets an a_ϵ arc. The foliation of \hat{S} is induced by the foliation on \mathcal{TA} and is determined by the following conditions:

- $\partial(\hat{\mathcal{S}})$ is a union of simple closed curves which are transverse to the foliation of \mathcal{TA} , with $X_+ \subset \partial(\hat{\mathcal{S}})$
- The self-intersection set of $\hat{\mathcal{S}}$ is a union of induced clasp arcs coming from \mathcal{TA} .
- Every singularity in the foliation of $\hat{\mathcal{S}}$ comes from either an $a_\epsilon a_\epsilon$ -singularity of \mathcal{TA} or a singularity that is associated with a b -arc that is near a_\pm , moreover there is a one-to-one correspondence between the b -arcs of $\hat{\mathcal{S}}$ and the b -arcs of \mathcal{TA} that are near $X_- \sqcup X_+$.
- There is a one-to-one correspondence between the s -arcs of $\hat{\mathcal{S}}$ and the s -arcs of \mathcal{TA}

Several remarks are in order. The first is that $\hat{\mathcal{S}}$ may not be a union of annuli. If the foliation of \mathcal{TA} contains $a_\epsilon a_\epsilon$ -singularities it is possible that $\partial(\hat{\mathcal{S}})$ contains components that are in the portion of the foliation of \mathcal{TA} that is split off by the separating arc in an $a_\epsilon a_\epsilon$ -singularity. Second, we note that it does not make sense to use the parity subscript for a -arcs when we talk about the induced foliation on $\hat{\mathcal{S}}$. Next, observe that there are no bb -tiles in $(\hat{\mathcal{S}})$ because all b -arcs in $\hat{\mathcal{S}}$ come from b -arcs in \mathcal{TA} that are near $X_- \sqcup X_+$. Therefore the tiling of $\hat{\mathcal{S}}$ contains aa -tiles, ab -tiles, as -tiles and sb -tiles (see Figure 28). Finally, the number of s -arc bands in the foliation of $\hat{\mathcal{S}}$ is exactly the same as the number of such bands in the foliation of \mathcal{TA} .

A clasp arc pair $\{\gamma_-, \gamma_+\} \subset \mathcal{TA}$ induces clasp arc pairs in $\hat{\mathcal{S}}$. We use the notation $\hat{\gamma}$ for clasp arcs in $\hat{\mathcal{S}}$. Let $\mathcal{N} \subset \mathcal{TA}$ be the union of all of the normal neighborhoods of clasp arcs in \mathcal{TA} . The foliation of $\hat{\mathcal{S}}$ can be broken down into three parts:

1. $\hat{\mathcal{S}}_s \subset \hat{\mathcal{S}}$ is the subset that is foliated by s -arcs.
2. $\mathcal{N}_{\hat{\mathcal{S}}} = \mathcal{N} \cap \hat{\mathcal{S}}$.
3. $\hat{\mathcal{S}}' = \hat{\mathcal{S}} - (\hat{\mathcal{S}}_s \cup \mathcal{N}_{\hat{\mathcal{S}}})$

We focus on $\hat{\mathcal{S}}'$. From the work that we have already done, it should be clear that the arcs in $X_- \cap \hat{\mathcal{S}}'$ are the strands of X_- which join up the blocks (fixed and moving) in the initial block-strand diagram of our template, whereas the arcs in $X_+ \cap \hat{\mathcal{S}}'$ are the strands of X_+ which join up the blocks (fixed and moving) in the final block-strand diagram of our template. Notice that $\hat{\mathcal{S}}'$ is embedded, because it is away from the double point set of \mathcal{TA} . By Lemma 3.2 it then follows that the combinatorial data in the boundary tiles of $\hat{\mathcal{S}}'$ will determine the embedding of these strands of X_- and X_+ . This fact will be used in the proof of Lemma 5.5, in the next section.

Our next task is to describe how $\mathcal{N}_{\hat{\mathcal{S}}} \subset \hat{\mathcal{S}}$ can be used to construct the moving blocks that we need for our templates. The methods are very similar to those used in Section 5.1, the main difference being that in Section 5.1 we were constructing maximal blocks for the motion of X_- across a thinly foliated annulus \mathcal{S} to curve which (by an abuse of notation) we called X_+ , whereas now we are constructing maximal blocks for the motion of X_- across \mathcal{TA} to the opposite boundary of \mathcal{TA} , i.e. the given link X_+ . The key point to notice is that by hypothesis all of our clasp arcs are doubly long.

Our concept of a *microstrand* is unchanged. See Figure 51. As before we can amalgamate pairs of microstrands that are near X_- (or X_+) into a microblock. The definition of an amalgamating block is unchanged (see Definition 14). The definition of connected subarcs of \mathbf{X} is unchanged. Similarly for a maximal connected collection of microstrands of uniform length, and for a (bg)-admissible collection of microstrands. The only new feature is that now we are working with $\hat{\mathcal{S}} \subset \mathcal{TA}$ rather than with the thinly foliated subset $\mathcal{S} \subset \hat{\mathcal{S}} \subset \mathcal{TA}$. The concept of a (bg)-top and a (bg)-bottom is replaced with the concept of a \pm -top and a \pm -bottom (because we are now back to working with X_- and X_+ , rather than with X_- and a curve which is transverse to the foliation \mathbf{H} and possibly in the interior of $P(\mathcal{TA})$).

Lemma 5.7 *Suppose that $X_+ \sqcup X_-$ is non-split. Let B^+ be a block that amalgamates the atomic blocks $\{B_1^+, \dots, B_r^+, B_{r+1}^+, \dots, B_p^+\}$ that are near X_+ , and B^- be a block that amalgamates the atomic blocks $\{B_1^-, \dots, B_r^-, B_{r+1}^-, \dots, B_q^-\}$. Suppose $\{N_1, \dots, N_r\}$ is a maximal connected collection with respect to B^+ and B^- of uniform length such that the atomic blocks B_i^\pm are associated with the long normal neighborhood N_i , for $1 \leq i \leq r$. Then we can amalgamate just the blocks $\{B_1^-, \dots, B_r^-\}$ near X_- into a new block, \hat{B}^- , and $\{B_1^+, \dots, B_r^+\}$ near X_+ into a new block \hat{B}^+ . Moreover, the isotopy carries \hat{B}^- to \hat{B}^+ .*

Proof: Clearly the blocks $\{B_1^+, \dots, B_r^+\}$ can be amalgamated near X_+ into a single amalgamating block \hat{B}^+ , and, similarly, the blocks $\{B_1^-, \dots, B_r^-\}$ can be amalgamated near X_- into a single amalgamating block \hat{B}^- . We can first take as a sub-block of B^- the truncated block that corresponds to B^- restricted to the disc fibers of \mathbf{H} that support $X_- \cap (\cup_{1 \leq i \leq p} N_i)$ which we call B_{trun}^- . Since $\{N_1, \dots, N_r\}$ is a maximal connected collection we will have $\partial B_{trun}^- \cap (\cup_{1 \leq i \leq p} N_i)$ a connected 4-valent graph having endpoints at $X_- \cap \partial B_{trun}^-$ (because our collection of normal neighborhoods is of uniform length). Then we take $\hat{B}^- \subset B_{trun}^-$ to be the sub-block that has $\partial \hat{B}^- \cap \mathcal{TA} \equiv \partial \hat{B}^- \cap (\cup_{1 \leq i \leq p} N_i)$.

What is needed to establish our result is that there is an isotopy of \hat{B}^- to \hat{B}^+ as we move X_- across. We want to use $\cup_{1 \leq i \leq p} N_i$ to drag \hat{B}^- to \hat{B}^+ . In fact what we need to know is that there is a 3-ball that contains $\hat{B}^- \cup \hat{B}^+ \cup (\cup_{1 \leq i \leq p} N_i)$ whose intersection with $X_+ \sqcup X_-$ is exactly equal to $(X_+ \cap \hat{B}^+) \cup (X_- \cap \hat{B}^-)$. If we take the boundary regular neighborhood of $\hat{B}^- \cup \hat{B}^+ \cup (\cup_{1 \leq i \leq p} N_i)$ we will end up with a collection of 2-spheres: one of which is punctured by $X_+ \sqcup X_-$ some number of times since it will be parallel to the “top” and “bottom” of \hat{B}^- and \hat{B}^+ ; and the remaining 2-spheres will be in the complement of $X_+ \sqcup X_-$. Since we are assuming that $X_+ \sqcup X_-$ is non-split, these 2-spheres bound 3-ball. the union of these 3-balls will give us the needed 3-ball for the isotopy of \hat{B}^- to \hat{B}^+ . \parallel

The proof of the following two lemmas is identical with that of Lemma 5.3:

Lemma 5.8 *Suppose $\{N_1, \dots, N_p\} \subset \mathcal{N}_S$ is a maximal connected collection between disc fibers $H_{t_1}, H_{t_2} \subset \mathbf{H}$. If this collection has a \pm -top and \pm -bottom then near X_\pm there exists a block B that is an amalgamation of all of the micro block of the collection near X_\pm .*

Lemma 5.9 *Let $\{N_1, \dots, N_p\}, \{N'_1, \dots, N'_q\} \subset \mathcal{N}_S$ be two maximal connected collections of normal neighborhoods whose microblocks near X_\pm can be amalgamated into blocks B and B' respectively. Suppose that the \pm -bottom for $\{N_1, \dots, N_p\}$ is equal to the \pm -top for $\{N'_1, \dots, N'_q\}$. Then we can amalgamate B and B' .*

Proof: Straightforward from the proof of 5.8. We simply combine the stratifications of $\{N_1, \dots, N_p\}$ and $\{N'_1, \dots, N'_q\}$. \parallel

5.4.4 Proof of Lemma 5.5 (the Finiteness Lemma):

We fix the integers m and n , with $m \geq n$. We are given the set $\mathbf{X}_{m,n}$ of all pairs of closed braid representatives of braid index m of all knots and links \mathcal{X} of braid index n . For each pair $(X_-, X_+) \in \mathbf{X}_{m,n}$ let \mathcal{TA} be the foliated total annulus whose boundary is $X_- - X_+$. Assume that the triplet (X_-, X_+, \mathcal{TA}) has minimum complexity. Assume that $P(\mathcal{TA})$ has $0 \leq c < \infty$ doubly long clasp arcs. With these assumptions we will prove parts (i) and (ii), and after that part (iii) of Lemma 5.5.

Define the subset $\hat{\mathcal{S}}'$ of \mathcal{TA} as before. Combinatorially there are only finitely many foliated annuli $\hat{\mathcal{S}}'$. Choose one (i.e. fix the tiling and parity assignments of $\hat{\mathcal{S}}'$) and consider a sequence of foliations

of $\hat{\mathcal{S}}'$ containing this fixed $\hat{\mathcal{S}}'$ subtiling. By assertion (5) of Lemma 5.6 we know that the number of s -arc bands is bounded. Since $E(s)$ is bounded there are only finitely many sb -singularities and they occur in pairs. Let $\mathcal{H} = \{H_{t_1}, H_{t_2}, \dots, H_{t_k}\} \subset \mathbf{H}$ be a complete cyclic listing of all disc fibers that have either a singularity of $\hat{\mathcal{S}}'$, or an sb -singularity, or an $a_\epsilon a_\epsilon$ -singularity. By the finiteness of $\hat{\mathcal{S}}'$ and the boundedness of sb - and $a_\epsilon a_\epsilon$ -singularities, there are only finitely many choices for such a cyclic listing of disc fibers. We fix on one such choice \mathcal{H}_0 .

Let $\{\mathcal{S}'_1, \dots, \mathcal{S}'_i, \dots\}$ be a sequence of tilings such that: 1) when we restrict our attention to $\hat{\mathcal{S}}'$ and the sb - and $a_\epsilon a_\epsilon$ -singularities we have the same \mathcal{H}_0 for each \mathcal{S}'_i in our sequence. Moreover, let $V_i(\alpha, v - \alpha)$ be the vertex count corresponding to the associated total annulus $\mathcal{S}'_i \subset \mathcal{TA}_i$ of our sequence. By (4) of Lemma 5.6 and Equation 7 we assume that the following sum increases as the index i increases.

$$(8) \quad V_i = \sum_{\beta=1} \inf V_i(1, \beta)$$

Thus, the only way V_i of Equation 8 can increase is if there exists $H_{t_i}, H_{t_{i+1}} \in \mathcal{H}_0$ such that the number of tiles in the $\mathcal{N}_{\mathcal{S}'_i} \subset \mathcal{S}'_i$ increases. In fact, between any two consecutive disc fibers of \mathcal{H}_0 we have an opportunity to have a growth in the V_i and, thus, the number of tiles in $\mathcal{N}_{\mathcal{S}'_i}$.

Concentrating on the growth of normal neighborhoods between H_{t_i} and $H_{t_{i+1}}$, we consider the components of $(\cup_{t \in [t_i, t_{i+1}]} H_t - \mathcal{S}')$ (where recall that $\hat{\mathcal{S}}'$ is fixed for our sequence). Since there are no singularities of $\hat{\mathcal{S}}'$ and no sb -, $a_\epsilon a_\epsilon$ -singularities between H_{t_i} and $H_{t_{i+1}}$ each component of $(\cup_{t \in [t_i, t_{i+1}]} H_t - \mathcal{S}')$ contains only normal neighborhoods of clasp arcs or s -arc bands. If \mathcal{C} is such a component then \mathcal{C} is a 3-ball having a product structure $\{D^2 \times [t_i, t_{i+1}]\}$. Having $b(X_-) + b(X_+)$ fixed means that there are a fixed number of components of $\mathcal{C} \cap (X_- \sqcup X_+)$. Let $\{x_1^\pm, \dots, x_{l_\pm}^\pm\} = \mathcal{C} \cap X_\pm$ be a listing of the components, each of which is an arc.

Now as V_i grows the number of normal neighborhoods having boundary in common with $\{x_1^\pm, \dots, x_{l_\pm}^\pm\}$ will increase. So the number of \pm -level paths in \mathcal{C} will increase and the number of \pm -decreasing paths will increase. The length (the number of neighborhoods) in a \pm -level path is at most $2l_\pm$, and the number of \pm -decreasing paths between two \pm -level paths is also bounded by $2l_\pm$. So as V_i grows \mathcal{C} becomes ‘‘saturated’’, forcing the formation of blocks (see Lemmas 5.8 and 5.9). Depending on how V_i grows respect the tiling attached the individual x_j components. There will be at most finitely many possible blocks formed in \mathcal{C} . Since there are only finitely many components of $(\cup_{t \in [t_i, t_{i+1}]} H_t - \mathcal{S}')$ we have only finitely many blocks that can be initial formed in $\cup_{t \in [t_i, t_{i+1}]} H_t$.

In a similar fashion we may consider the braiding of the s -arc bands in \mathcal{C} , away from $\mathcal{N}_{\mathcal{S}'_i}$. Since $m + n$ is fixed, this means that there are a fixed number of components of $\mathcal{C} \cap (X_- \sqcup X_+)$. If these components intersect s -arcs we will have a pairing of components to form the boundary arcs of the s -arc bands. Thus, in each component \mathcal{C} we can have exactly one initial formation of an s -arc block. Since there are only finitely many disc fibers in \mathcal{H}_0 , overall we have only finitely many initial blocks formed.

Now that we have these initial block formations by amalgamation of microblocks and amalgamation of s -arc band braiding we consider these blocks in the full foliation and H_t -sequence of \mathcal{TA} . The addition of this foliation can possibly split our initial blocks ‘length-wise’, i.e. a block of braid index k might be subdivided into blocks of braid index k_1, k_2 with $k_1 + k_2 = k$. This splitting still gives us a finite number of blocks. We are now in a position now to apply Lemma 5.7 to further finitely sub-divide our initial block amalgamation of microblocks. This establishes parts (i) and (ii) of the Finiteness Lemma (Lemma 5.5).

We turn our attention to part (iii). As noted right after we defined $\hat{\mathcal{S}}'$, the arcs in $X_- \cap \hat{\mathcal{S}}'$ (resp. $X_+ \cap \hat{\mathcal{S}}'$) are the strands of X_- (resp. X_+) which join up the blocks (fixed and moving) in the initial (resp. final) block-strand diagram of our template. The subset $\hat{\mathcal{S}}'$ of \mathcal{TA} is embedded, because by definition it is away from \mathcal{N} and so also from the double point set of \mathcal{TA} . By Lemma 3.2 it then follows that the combinatorial data in the boundary tiles of $\hat{\mathcal{S}}'$ will determine the embedding of these strands of X_- and X_+ . Clearly there are only finitely many ways to associate combinatorial data

to a finite set of vertices and singularities, so our task is to show that the number of vertices and singularities in the boundary tiles of \hat{S}' is bounded, under the hypotheses of the Lemma.

Tiles which meet the boundary of \hat{S}' have type $(1, \beta)$ or have singularities which involve s -arcs (see Figure 28). By statements (1), (6) and (7) of Lemma 5.6 the number of vertices of type $(1, \beta)$ are bounded. By statement (5) the number of singularities involving s -arcs is bounded. Thus there are only finitely many such tiles and each has finitely many vertices and singularities. This completes the proof of part (iii) and so of Lemma 5.5.

We have proved that each fixed pair $(X_-, X_+) \in \mathbf{X}_{m,n}$ is carried by one of finitely many templates in $\mathcal{T}(m, n)$. To prove the assertion in part (d) of the MTWS we need to remove the dependence of our finite set of templates on n . For that, define $\mathcal{T}(m)$ by:

$$\mathcal{T}(m) = \mathcal{T}(m, m) \sqcup \mathcal{T}(m, m-1) \sqcup \cdots \sqcup \mathcal{T}(m, 1).$$

Since each set $\mathcal{T}(m, n)$ is finite, and the union of finitely many finite sets is finite, it follows that the set $\mathcal{T}(m)$ is finite. We have thus proved part (d) of the MTWS. We already established Parts (a), (b) and (c). The proof of the MTWS is complete. \parallel

6 Applications to transverse knots

In this section we will give an application of the MTWS and the associated foliation machinery on the total annulus \mathcal{TA} to the classification problem for transversal knots in the standard contact structure on \mathbb{R}^3 .

We begin with definitions and notation. The *standard tight contact structure* ξ in oriented 3-space \mathbb{R}^3 with cylindrical coordinates (ρ, θ, z) , is the kernel of the 1-form $\alpha = \rho^2 d\theta + dz$. An oriented knot K in contact \mathbb{R}^3 is said to be a *transversal* knot if it is transversal to the planes of this contact structure. If the knot K is parametrized by $(\rho(t), \theta(t), z(t))$, then K is transversal if and only if $z'(t) \neq -(\rho(t))^2 \theta'(t)$ for every t . We will assume throughout this section that $z'(t) > -(\rho(t))^2 \theta'(t)$ for all t . The *topological knot type* \mathcal{X} of a knot $X \subset \mathbb{R}^3$ is its equivalence class under isotopy of the pair (X, \mathbb{R}^3) . A sharper notion of equivalence is its *transversal knot type* \mathcal{TX} , which requires that $z'(t) > -(\rho(t))^2 \theta'(t)$ at every point of the deformed knot, during every stage of the isotopy. By definition, the topological type \mathcal{X} of a transversal knot X is an invariant of \mathcal{TX} .

A parametrized knot $X \subset \mathbb{R}^3$ is said to be represented as a closed braid if $\rho(t) > 0$ and $\theta'(t) > 0$ for all t . It is easy to see that every closed braid can be deformed to a transversal closed braid. It was proved by Bennequin in §23 of [2] that every transversal knot is transversally isotopic to a transversal closed braid. Bennequin's result allows us to apply results obtained in the study of closed braid representatives of topological links to the problem of understanding transversal isotopy. A well-known invariant $\beta(\mathcal{TX})$ of a transversal knot type \mathcal{TX} was discovered by Bennequin in [2]. It's an invariant of \mathcal{TX} , but not of \mathcal{X} , and it can be computed from any closed braid representative X as follows. Let $e(X)$ be the algebraic crossing number of the closed braid diagram for X and let $b(X)$ denote the braid index of X . Then the *Thurston-Bennequin invariant* of \mathcal{TX} is $\beta(\mathcal{TX}) = e(X) - b(X)$. Theorem 2 of this paper asserts that the transversal knot types $(\mathcal{TX}_-, \mathcal{TX}_+)$ which are defined by the pairs of closed 3-braids

$$(9) \quad TX_- = \sigma_1^{2p+1} \sigma_2^{2r} \sigma_1^{2q} \sigma_2^{-1}, \quad TX_+ = \sigma_1^{2p+1} \sigma_2^{-1} \sigma_1^{2q} \sigma_2^{2r}, \quad q \neq r, \quad p, q, r > 1$$

belong to the same topological knot type and have the same Thurston-Bennequin invariant, but do not represent the same transversal knot type.

Proof of Theorem 2. The pairs of closed braids which are defined in Equations (9) above are related by a negative 3-braid flype, so it is immediate that they determine the same topological

knot type. Since both have braid index 3 and algebraic crossing number $2p + 2r + 2q$, it is also immediate that they have the same Thurston-Bennequin invariant. Our task is to prove that there is no transversal isotopy from TX_- to TX_+ .

Our plan for the proof is to establish a very special version of the the TMTWS (the transverse MTWS), under the assumptions that (i) TX_- and TX_+ both have braid index 3, and (ii) the transverse knot type \mathcal{TX} which they determine also has braid index 3. We will then show that under these assumptions a transverse isotopy $TX_- \rightarrow TX_+$ can only be a product of exchange moves. We further show that it must be supported by the negative flype template. After that we show that if such an isotopy exists, there are other examples of pairs of closed 3-braid representatives of certain transverse 2-component links (carried by the same template) and that they too must be transversally equivalent. The final contradiction is that this cannot happen because the Thurston-Bennequin invariants of the link components are not preserved under the transverse isotopy which we have assumed exists. It follows that no such can isotopy exist, and therefore the transverse knots which are represented by TX_- and TX_+ cannot be transversally equivalent.

Our proof begins with a review of what is known about the topological classification of knots and links which are represented by closed 3-braids.

Lemma 6.1 [9] *A link which is determined by a closed 3-braid admits a unique braid isotopy class of closed 3-braid representatives, with the following exceptions:*

- (1) *The unknot has 3 braid isotopy classes of 3-braid representatives, namely the conjugacy classes in B_3 of $\sigma_1^\mu \sigma_2^\tau$, where $(\mu, \tau) \in \{(1, 1), (-1, -1), (1, -1)\}$.*
- (2) *Type $(2, k)$ torus links, $k \neq 1$ have two braid isotopy classes of 3-braid representatives, namely the conjugacy classes in B_3 of $\sigma_1^k \sigma_2^\mu$, where $\mu = \pm 1$.*
- (3) *A special class of links with braid index 3 which have 3-braid representatives admitting 3-braid flypes. These links have at most 2 braid isotopy classes of 3-braid representatives, namely the conjugacy classes of $\sigma_1^u \sigma_2^v \sigma_1^w \sigma_2^\epsilon$ and $\sigma_1^u \sigma_2^\epsilon \sigma_1^w \sigma_2^v$, where $\epsilon = \pm 1$. The sign of the flype is the sign of ϵ .*

We will need additional topological information about the examples in case (3).

Lemma 6.2 [23] *Let $\sigma_1^u \sigma_2^v \sigma_1^w \sigma_2^\epsilon$ and $\sigma_1^u \sigma_2^\epsilon \sigma_1^w \sigma_2^v$ be the closed 3-braids in (3) above. Then the following hold:*

- (3.1) *They determine knots if and only if (i) v is even, and (ii) u is even if and only if w is odd.*
- (3.2) *The two associated braid isotopy classes are distinct if and only if neither u nor w is equal to $0, \epsilon, 2\epsilon, v + \epsilon$, also $u \neq w$, also $|v| \geq 2$.*
- (3.3) *The closed braid $\sigma_1^u \sigma_2^v \sigma_1^w \sigma_2^\epsilon$ admits a flype of sign ϵ and also a flype of sign $-\epsilon$ if and only if $u = -\epsilon$ or $w = -\epsilon$ or $v = -2\epsilon$.*

Applying Lemmas 6.1 and 6.2 to the special case of the examples in Theorem 2 we have:

Lemma 6.3 *The pairs of topological links which are defined by the 3-braids $\sigma_1^{2p+1} \sigma_2^{2r} \sigma_1^{2q} \sigma_2^{-1}$ and $\sigma_1^{2p+1} \sigma_2^{-1} \sigma_1^{2q} \sigma_2^{2r}$ in Theorem 2 have the following properties:*

- (1) *The closed braids determine knots.*
- (2) *The members of each pair represent the same topological knot type \mathcal{X} , where $b(\mathcal{X}) = 3$, and have the same Bennequin number, but they belong to distinct braid isotopy classes.*

- (3) *The only closed 3-braid representatives of \mathcal{X} are the braid isotopy classes of $\sigma_1^{2p+1}\sigma_2^{2r}\sigma_1^{2q}\sigma_2^{-1}$ and $\sigma_1^{2p+1}\sigma_2^{-1}\sigma_1^{2q}\sigma_2^{2r}$. These classes are distinct, and are related by a negative 3-braid flype. They are not equivalent under a positive 3-braid flype. They are therefore carried by the initial and final block-strand diagrams in precisely 1 of the 4 templates of Lemma 6.4 below, namely the negative flype template.*

As a consequence of Lemmas 6.1 and 6.2, we are also able to give a complete list of the templates which are needed in the MTWS, in the special case when $b(X_-) = 3$:

Lemma 6.4 *Exactly 4 templates are needed to describe the moves of the MTWS, in the special case where X_- is a closed 3-braid and X_+ is a knot of braid index ≤ 3 : the two destabilization templates of Figure 1 and the two 3-braid flype templates of Figure 3. Moreover, every knot or link which is a closed 3-braid either has a closed braid representative which is unique up to braid isotopy, or it is carried by one of these 4 templates.*

We will also need one further result, established in [8], about minimum genus spanning surfaces for links which have braid index 3 and are represented by closed 3-braids:

Lemma 6.5 (Theorem 1 of [8]) *If \mathcal{X} is a knot of braid index 3, and if X is a closed 3-braid representative of \mathcal{X} , then X is the boundary of an incompressible spanning surface which is a union of 3 discs joined up by half-twisted bands. In the braid foliation of this surface each disc is pierced once, positively, by \mathbf{A} and is foliated radially, as in Figure 14(a). In particular, there are no negative vertices in the foliation. Each band is foliated as an aa-tile, as in Figure 17(a).*

We turn now to the classification of the same examples under transversal isotopy. We know that our X_- can be changed to X_+ by the non-transversal isotopy which is associated to a negative 3-braid flype. By (3.3) of Lemma 6.2, we know that X_- cannot be changed to X_+ by the transversal isotopy associated to a positive 3-braid flype. Our problem is to prove that there cannot be some other transversal isotopy which relates them.

To begin, refer back to the construction of the annulus \mathcal{TA} in Section 2, using the notation X_-, X_0, X_+ introduced there. We wish to adapt that construction to the given example, in the transverse setting.

Lemma 6.6 *Let X_- and X_+ be two closed 3-braids representing the same knot type \mathcal{X} , where $b(\mathcal{X}) = 3$. Assume that when considered as transversal knots in the standard contact structure for \mathbb{R}^3 , the same two closed braids (now called TX_- and TX_+) also represent the same transversal knot type \mathcal{TX} . Then the following hold for the closed braid X_0 which is constructed in Lemma 2.1 in Section 2 of this paper:*

- (1) X_0 may be assumed to be transversal, moreover it is also in \mathcal{TX} .
- (2) The transversal closed braid TX_0 of (1) is isotopic to TX_- through a sequence of transverse exchange moves.
- (3) TX_0 coincides with TX_+ . The annulus \mathcal{A}_+ is empty, also the braid index of TA_0 is 3.

Proof: The construction is a modification of the construction given in Section 2 of this paper to the transverse setting.

We establish (1) by adapting the proof of Lemma 2.1 to the transverse case, under the special assumptions that X_- and X_+ have the same braid index, and that this braid index is minimal for the transverse knot type \mathcal{TX} . As in the proof of Lemma 2.1, the work begins with the construction of an intermediate closed braid representative X'_+ of \mathcal{X} by pushing off a parallel copy of TX_+ along a Seifert surface \mathbf{F}_+ for TX_+ to a preferred longitude X'_+ for TX_+ . See Figure 11(a). By choosing X'_+ to be arbitrarily close to TX_+ and modifying the interior of \mathbf{F}_+ if necessary we may assume

that X'_+ is a transversal closed braid. Call it TX'_+ . By our special assumptions on the knot type \mathcal{TX} we know that TX_+ represents a non-trivial knot type, and so TX_+ and TX'_+ are geometrically linked.

We next construct the knot X''_+ of Figure 11(b) in the same way as in the proof of Lemma 2.1, by pushing each arc α_i across the disc D_i to the arc β_i . It will be helpful to think of D_i as a neighborhood of a ‘vertical’ arc η_i which runs from an interior point of α_i to an interior point of β_i . This neighborhood may be assumed to be arbitrarily small, so possibly after small changes we may assume that each β_i is transversal, and that the isotopy α_i to β_i is a transversal isotopy. Therefore X''_+ will be denoted TX''_+ from now on. Clearly TX''_+ also represents \mathcal{TX} .

The disc D_i is divided by \mathbb{R}^2 into subdiscs $D_{i,+} \subset \mathbb{R}^3_+$ and $D_{i,-} \subset \mathbb{R}^3_-$. We know that TX''_+ has the same transversal knot type as TX_- , and also that both TX''_+ and TX_- are in the lower half-space \mathbb{R}^3_- , so there is a transversal isotopy of \mathbb{R}^3_- that takes TX''_+ to TX_- . It takes $D_{i,+}$ to the disc we call r_i in Figure 11(c). Its vertical boundaries v_i and v'_i are the images of transversal subarcs of ∂D_- under a contactomorphism. Note that the disc r_i may be twisted, also there may be twisting of the vertical arcs v_i and v'_i . We define R_i , as before, to be $r_- \cup D_{-,+}$. We define X'_0 as before. It is a transversal representative of \mathcal{TX} as before.

Now, TX'_0 may not be a closed braid. Suppose δ is an arc that has a point of tangency with a H_{θ_0} at the point $q \in H_{\theta_0}$. Let $q = (\rho_0, \theta_0, z_0)$. Then q is on the Legendrian ray (ρ, θ_0, z_0) , $\rho > 0$. Without loss of generality we assume that this ray intersects no other δ -arc and does not intersect TX_- . We can then transversally isotop δ so as to eliminate a point of tangency with half-planes by positively stabilizing δ along the Legendrian ray. By [B-W] positive stabilizations are transversal isotopies. Iterating this procedure at every point of tangency with half-planes we obtain the transversal knot TX_0 . Since TX_0 is transverse to every H_{θ_0} , it is a closed braid. By construction TX_0 is the connect sum of TX_- and some number of copies of the unknot. By the transverse MTWS for the unknot, proved in [14] it follows that TX_- may be obtained from TX_0 by a sequence of exchange moves and positive destabilizations. This proves (1).

The argument now proceeds exactly as it did in Section 2. We show, as we did there, that TX_0 is a preferred longitude for TX_+ , and so TX_+ is a preferred longitude for TX_0 . We choose an incompressible Seifert surface \mathbf{F}_0 for TX_0 . We know that after an isotopy of \mathbf{F}_0 we may assume that TX_+ lies on \mathbf{F}_0 , cobounding with X_0 an embedded annulus $\mathcal{A}_+ \subset \mathbf{F}_0$. The isotopy (at this moment we cannot say that it’s transverse) from $TX_0 \rightarrow TX_+$ is a push across \mathcal{A}_+ .

The surface \mathbf{F}_0 supports a braid foliation. Since \mathcal{A}_+ is embedded, all possible subdiscs in \mathcal{A}_+ are good discs (see Definition 10). Thus Lemma 4.5 applies. Using it, we eliminate interior endpoints of $G_{\pm,\pm}$ by changes of foliation and exchange move. Changes of foliation leave the boundary TX_0 fixed. Exchange moves, as before, correspond to transversal isotopies. Thus, we may assume (in the transversal setting) that the graph $G_{\pm,\pm}$ has no interior endpoints. By the minimal braid index assumption on TX_+ we know that $G_{\pm,\pm}$ has no valence one vertices near TX_+ . If $G_{+,+}$ has a valence one vertex near TX_0 then we can positively destabilize TX_0 . Notice that $G_{-,-}$ cannot have a valence one vertex near TX_0 because such a vertex would force the difference in the Bennequin numbers $b(X_0) - b(X_+) = (s_+ - s_-) + (v_+ - v_-)$ to be nonzero, where s_{\pm} is the number of \pm -singularities in \mathcal{A}_+ and v_{\pm} is the number of \pm -vertices in \mathcal{A}_+ . Since TX_0 and TX_+ have the same transversal knot type these differences must be zero.

Combining these observations allows us to conclude that \mathcal{A}_+ is standardly tiled. See Definition 11, Figure 41 and Corollary 2. But if \mathcal{A}_+ is a standardly tiled annulus then TX_0 , like TX_- and TX_+ , is a 3-braid. Note that this shows that there are no destabilizations in the passage from TX_0 to TX_- , only exchange moves, so (1) is true. Even more, our Seifert surface \mathbf{F}_0 must be as described in Lemma 6.5. The foliation of such a surface has no negative vertices, so it cannot support a standardly tiled collar neighborhood of the boundary. That is, \mathcal{A}_+ must be empty and $TX_0 \equiv TX_+$. The proof of the Lemma is complete. ||

Completion of the proof of Theorem 2. The astute reader will have noticed that up to this

point we have not used the fact that, for our examples, the topological isotopy $X_- \rightarrow X_+$ can be realized by a negative flype, but not a positive flype. Yet the proof is almost done. We have learned that the transversal isotopy that we assumed exists takes TX_- to TX_+ and may be extended to a transversal template isotopy which takes blocks to blocks. That isotopy exists for any braiding assignment to the blocks, for example $\sigma_1^3 \sigma_2^4 \sigma_1^{-5} \sigma_2^{-1}$. By Lemma 6.1 this braiding assignment gives a 2-component link $L_1 \sqcup L_2$ which has two distinct isotopy classes of closed 3-braid representatives which are related by a negative flype, but not by a positive flype. If L_1 is the component associated to the left strand entering the sub-braid σ_1^3 , then $\beta(L_1) = -1$ and $\beta(L_2) = -3$ before the flype, but after the flype the representative will be $\sigma_1^3 \sigma_2^{-1} \sigma_1^{-5} \sigma_2^4$, with $\beta(L_1) = -3$ and $\beta(L_2) = -1$. By Proposition 2.1.2 of [16] a transversal isotopy of a knot/link extends to an ambient transversal isotopy of the 3-sphere. However, any transversal isotopy of $L_1 \sqcup L_2$ must preserve the Thurston-Bennequin invariants of the components. In this way we get the sought-for contradiction. Therefore the knots TX_- and TX_+ cannot represent the same transversal knot type, even though they have the same topological knot types and Thurston-Bennequin invariants. (Remark: On the other hand, if we modify the knots TX_-, TX_+ to $\sigma_1^{2p+1} \sigma_2^{2r} \sigma_1^{2q} \sigma_2^{-1}$, $\sigma_1^{2p+1} \sigma_2^{-1} \sigma_1^{2q} \sigma_2^{2r}$, $q \neq r$, $p, q, r > 1$ then the link we need for a contradiction changes to $\sigma_1^3 \sigma_2^4 \sigma_1^{-5} \sigma_2$. But then the flype is positive, and in fact the Bennequin numbers of L_1 and L_2 will be -1 and -1 and the contradiction vanishes.) ||

References

- [1] J. W. Alexander, *A lemma on systems of knotted curves*, Proc. Nat. Acad. Sci. USA. **9** (1923), 93-95.
- [2] D. Bennequin, *Entrelacements et equations de Pfaff*, Asterisque **107-108** (1983), 87-161.
- [3] J. S. Birman, *Braids, Links and Mapping Class Groups*, Annals of Math. Studies **82** (1974).
- [4] J. S. Birman and E. Finkelstein, *Studying surfaces via closed braids*, J. of Knot Theory and its Ramifications, **7**, No. 3 (1998), 267-334.
- [5] J.S. Birman, K.H. Ko and S.J.Lee, *A new approach to the word and conjugacy problems in the braid groups*, Advances in Mathematics **139** (1998), 322-353.
- [6] J.S. Birman and M. Hirsch, *A new algorithm for recognizing the unknot*, Geometry and Topology **2**, (1998), 175-220.
- [7] J. S. Birman & W. W. Menasco, *Studying Links Via Closed Braids I: A Finiteness Theorems*, Pacific J. Math., **154**, No. 1 (1992), 17-36.
- [8] J. S. Birman & W. W. Menasco, *Studying Links Via Closed Braids II: On a Theorem of Bennequin*, Topology and its Applications, **40** (1991), 71-82.
- [9] J. S. Birman & W. W. Menasco, *Studying Links Via Closed Braids III: Classifying Links which are Closed 3-Braids*, Pacific J. Math., **161**, No 1 (1993), 25-113.

- [10] J. S. Birman & W. W. Menaso, *Studying Links Via Closed Braids IV: Closed Braid Representatives of Split and Composite Links*, *Inventiones Math.*, **102** Fasc. 1 (1990), 115-139.
- [11] J. S. Birman & W. W. Menaso, *Studying Links Via Closed Braids V: Closed Braid Representatives of the Unlink*, *Trans AMS*, **329** No. 2 (1992) pp. 585-606.
- [12] J. S. Birman & W. W. Menaso, *Studying Links Via Closed Braids VI:A Non-Finiteness Theorem*, *Pacific J. Math.*, **156**, No. 2, 1992, p. 265-285.
- [13] J. S. Birman & W. W. Menaso, *On Markov's Theorem*, *Proceedings of KNOTS-2000, Journal of Knot Theory and its Ramifications*, to appear
- [14] J.S. Birman and N. Wrinkle, *On transversally simple knots*, *Journal of Differential Geometry* **55** (2000), 325-354.
- [15] G. Burde and H. Zieschang, *KNOTS*, de Gruyter 1985
- [16] Y. Eliashberg, *Legendrian and transversal knots in tight contact 3-manifolds*, *Topological methods in Modern Mathematics, Proceedings of a Symposium at SUNY Stonybrook in 1991*, Publish or Perish, Houston, Texas (1993)
- [17] T. Fiedler, *A small state sum for knots*, *Topology* **32** (1993), 281-294.
- [18] J. Franks and B. Williams, *Braids and the Jones-Conway polynomial*, *Trans. AMS* **303** (1987), No. 1, 97-108.
- [19] V. Guillemin and A. Pollack, *DIFFERENTIAL TOPOLOGY*, Prentice-Hall (1974).
- [20] J. Hempel, *3-Manifolds*, *Annals of Math Studies* **86** (1976), Princeton Univ. Press.
- [21] V.F.R. Jones, *Hecke algebra representations of braid groups and link polynomials*, *Annals of Math.* **126** (1987), 335-388.
- [22] R. Kirby, *A calculus for framed links in S^3* , *Invent. Math.* **45** (1978), 35-56.
- [23] K.Y.Ko and S.J.Lee, *Flypes of closed 3-braids in the standard contact space*, *J. Korean Math Soc.* **36** (1999), 51-71.
- [24] S. Lambropoulou & C. Rourke, *Markov's theorem in 3-manifolds*, *Topology and its Applications*, **78** (1997), 95-122.
- [25] A. A. Markov, *Über die freie Äquivalenz geschlossener Zöpfe*, *Recueil Mathematique Moscou*, **1** (1935), 73-78.

- [26] W. W. Menasco, *On iterated torus knots and transversal knots*, *Geometry and Topology* **5** (2001), 651-682.
- [27] W. W. Menasco, *Closed braids and Heegaard splittings*, in *AMS/IP Studies in Advanced Mathematics* **24**, Amer. Math Society and International Press, 2001.
- [28] W. W. Menasco & M. Thistlethwaite, *The classification of alternating links*, *Annals of Mathematics*, **138** (1993), 113-171.
- [29] H. Morton, *Infinitely many fibred knots having the same Alexander polynomial*, *Topology* **17** (1978), 101-104.
- [30] H. Morton, *An irreducible 4-braid with unknotted closure*, *Math. Proc. Cambridge Phil. Soc.*, **93** (1983), 259-261.
- [31] H. Morton, *Seifert circles and knot polynomials*, *Math Proc. Camb. Phil. Soc.* **99** (1986), 107-109.
- [32] H. Morton, *Threading knot diagrams*, *Math Proc. Camb. Phil. Soc.* **99**, 247-260.
- [33] K. Murasugi, *On closed 3-braids*, *Memoirs AMS* **151** (1974)
- [34] J. P. Otal, *Présentations en ponts du noeud trivial*, *C.R. Acad. Sc. Paris*, **294-I**, 553-556.
- [35] D. Rolfsen, *KNOTS*, Publish or Perish, first edition (1976)
- [36] M. Scharlemann and A. Thompson, *Thin Position and Heegaard Splittings of the 3-Sphere*, *Jour. Diff Geom.* 39 1994, pp. 343-357
- [37] J. Singer, *Three-dimensional manifolds and their Heegaard diagrams*, *Trans. Amer. Math. Soc.*, **35** (1933), 88-111.
- [38] P. Traczyk, *A new proof of Markov's braid theorem*, *KNOT THEORY: WARSAW, 1995*, p.409-419. *Banach Center Publ.* **42**, Polish Academy of Sciences, Warsaw (1998).
- [39] F. Waldhausen, , *Heegaard-Serlegungen der 3 Sphäre*, *Topology* **7**(1968), 195-203.
- [40] N. Wrinkle, *The Markov Theorem for Transverse Knots*, preprint, 2002.
- [41] S. Yamada, *The minimum number of Seifert circles equals the braid index of a link*, *Invent.math.*, **89** (1987), 347-356.
- [42] J. Zablow, PhD thesis, City University of New York (1999).

Abstract

The main result, Theorem 1, is Markov's Theorem Without Stabilization (MTWS) for links in 3-space. Choose any oriented link type \mathcal{X} and any closed braid representatives X_-, X_+ of \mathcal{X} , where X_+ has minimal braid index. The MTWS asserts that there is a complexity function and a finite set of 'templates' such that (possibly after initial complexity-reducing modifications in the choices of X_-, X_+ , which replace them with closed braids X'_-, X'_+ of the same braid index) there is a sequence of closed braid representatives $X'_- = X^1 \rightarrow X^2 \rightarrow \cdots \rightarrow X^r = X'_+$ such that each passage $X^i \rightarrow X^{i+1}$ is strictly complexity reducing and non-increasing on braid index. The templates which define the 'moves' of the MTWS include 3 familiar ones: the destabilization, exchange move and admissible flype templates, and in addition, for each braid index $m \geq 4$ a finite set $\mathcal{T}(m)$ of templates. The cardinality $|\mathcal{T}(m)|$ of $\mathcal{T}(m)$ is an increasing function of m for sufficiently large m . We give examples of members of $\mathcal{T}(m)$, but not a complete listing.

There are consequences for the classification of transversal knots, i.e. knots which are everywhere transverse to the standard tight contact structure in S^3 . Theorem 2 proves the existence of transversal knot types that are not determined by their topological knot type and Thurston-Bennequin invariant. The examples uncovered in the course of the proof give rise to several related conjectures about the complicated nature of transversal knot theory.